SHRP-H-346

Improved Cutting Edges for Ice Removal

Wilfrid A. Nixon

Iowa Institute of Hydraulic Research
University of Iowa, Iowa City

Strategic Highway Research Program
National Research Council
Washington, DC 1993

SHRP-H-346
Contract H-204A
ISBN 0-309-05605-5
Product Code 3022

Program Manager: *Don M. Harriott*
Project Manager: *L. David Minsk*
Program Area Secretary: *Francine A. Burgess*
Copy Editor: *Katharyn L. Bine Brosseau*

August 1993

key words:
chemical deicing
highway maintenance
snow and ice control
snow plow blades

Strategic Highway Research Program
2101 Constitution Avenue N.W.
Washington, DC 20418

(202) 334-3774

The publication of this report does not necessarily indicate approval or endorsement by the National Academy of Sciences, the United States Government, or the American Association of State Highway and Transportation Officials or its member states of the findings, opinions, conclusions, or recommendations either inferred or specifically expressed herein.

©1993 National Academy of Sciences

1.5M/NAP/893

Acknowledgments

The research described herein was supported by the Strategic Highway Research Program (SHRP). SHRP is a unit of the National Research Council that was authorized by section 128 of the Surface Transportation and Uniform Relocation Assistance Act of 1987.

The support of the Director of the Iowa Institute of Hydraulic Research (IIHR), Dr. Jack Kennedy, and of the Acting Director (from June 1991), Dr. Robert Ettema, is gratefully acknowledged. The shop staff at IIHR, led by Mr. Jim Goss, made these experiments possible with their aid and insight. The experiments were performed by Mr. Eric (Chung-Hua) Chung, Mr. Todd Frisbie, Mr. Larry Weber, Mr. Michael Pokorny, Mr. Wasif Alimuddin and Mr. William McCauley, under the guidance and direction of the Principal Investigator, Dr. Wilfrid Nixon.

The field tests were conducted using a truck provided by the Iowa Department of Transportation (IDoT), which also provided funding for the field work under their project HR 334. Permission was given to use the test site at the Coralville Reservoir by the US Army Corps of Engineers. The assistance of both these organizations, without whose support the tests could not have been conducted, is gratefully acknowledged.

Contents

Acknowledgments iii
Abstract 1
Executive Summary 3

1. Literature Review 5
   1.1. Introduction 5
   1.2. Ice Control 5
   1.3. Techniques of Ice Removal 6

2. Experimental Description 9
   2.1 Introduction 9
   2.2 Test Samples 9
      2.2.1 Concrete Blocks 10
      2.2.2 Sample Manufacture 10
   2.3 The Test Matrix 10
      2.3.1 Base Line Tests 11
      2.3.2 Clearance Angle and Blade Flat Width 11
      2.3.3 Attack Angle 12
      2.3.4 Blade Width 12
      2.3.5 Pre-treatment Tests 12
      2.3.6 Temperature and Scraping Velocity 13
   2.4 Data Reduction Scheme 13
      2.4.1 Obtaining Acceleration 14
      2.4.2 Developing Ice-Cutting Force 15

3. Results 23
   3.1 Introduction 23
   3.2 Baseline Tests 23
   3.3 Clearance Angle and Blade Flat Tests 24

3.4 Attack Angle Tests 26
3.5 Blade Width Tests 29
3.6 Pretreatment Tests 30
3.7 Temperature and Cutting Velocity Tests 32
3.8 Summary 32

4. Discussion of Results 48
4.1 Introduction 48
4.2 Base Line Tests 48
4.3 Clearance Angle and Blade Flat Tests 48
4.4 Attack Angle Tests 49
4.5 Blade Width Tests 49
4.6 Pretreatment Tests 50
4.7 Temperature and Cutting Velocity Tests 50
4.8 Ice Cutting Model 50
4.9 Summary 51

5. Field Tests of Prototype Blade 53
5.1 Blade Design Methodology 53
5.2 Field Test Apparatus 53
5.3 Experimental Method 55
5.4 Field Test Results 56

6. Conclusions 71

Appendix A The Ice Cutting Equipment 73
A.1 The Hydraulic Ice-cutting Machine 73
A.1.1 The Hydraulic System 73
A.1.2 Safety Features 74
A.1.3 Machine Instrumentation 75

Appendix B A Proof of the Validity of Ignoring Horizontal Translation During the Ice-Cutting Process 86

Appendix C Experimental Results 90

Bibliography 97

List of Figures

Figure 1.1. Geometry of the blade (side view) 7
Figure 1.2. Geometry of the blade (top view) 7
Figure 1.3. Pictorial representation of Huang's study 8
Figure 2.1. A pavement sample ready for testing 17
Figure 2.2. Pavement samples with neoprene rubber collars 17
Figure 2.3. Blades with various rake angles 18
Figure 2.4. Blades with various clearance angles 18
Figure 2.5. Blades with various attack angles 19
Figure 2.6. Blades with various widths 19
Figure 2.7. Blades with various flat widths 20
Figure 2.8. Free body diagram of the pavement sample 21
Figure 3.1. Data from top load cell 35
Figure 3.2. Data from bottom load cell 35
Figure 3.3. Position data for one test 36
Figure 3.4. Cutting forces on the blade (velocity = 10 mph) 37
Figure 3.5. Maximum cutting forces for various rake angles 38
Figure 3.6. Maximum cutting forces for various clearance angles 39
Figure 3.7. Maximum download forces for various clearance angles 40
Figure 3.8. Maximum cutting forces for three blade flat widths 41
Figure 3.9. Maximum download forces for three flat widths 42
Figure 3.10. Maximum cutting forces for two attack angles 43
Figure 3.11. Maximum cutting forces for two blade widths 44
Figure 3.12. Maximum cutting force for five quantities of salt 45
Figure 3.13. Maximum cutting force for four rake angles at two temperatures 46
Figure 3.14. Maximum cutting force for various levels of cutting velocity 47
Figure 4.1. A truck cutting ice 52
Figure 4.2. Tentative model of ice cutting 52
Figure 5.1. Design of prototype cutting edge 57
Figure 5.2. Prototype cutting edge 58
Figure 5.3. IDoT instrumented plowing truck 58
Figure 5.4. Definition of blade angle and cast angle 59
Figure 5.5. Attachment of cutting edge to blade support 60
Figure 5.6. Schematic representation of three cutting edges 61
Figure 5.7. Cutting edge instrumentation 61
Figure 5.8. Friction sled 62

Figure 5.9. Test truck data acquisition system 62
Figure 5.10. Test truck spray system 63
Figure 5.11. Raw data output from test of Jan 28, 1992 64
Figure 5.12. Horizontal and vertical force, cutting edge # 1, low pressure, 15° angle Test of Dec 4, 1991 65
Figure 5.13. Horizontal and vertical force, cutting edge # 2, low pressure, 15° angle Test of Jan 28, 1992 66
Figure 5.14. Horizontal and vertical force, cutting edge # 3, low pressure, 15° angle test of March 11, 1992 67
Figure 5.15. Horizontal and vertical force, cutting edge # 1, low pressure, 30° angle test of Dec 4, 1991 68
Figure 5.16. Horizontal and vertical force, cutting edge # 2, low pressure, 30° angle test of Jan 28, 1992 69
Figure 5.17. Horizontal and vertical force, cutting edge # 3, low pressure, 30° angle test of March 13, 1992 70
Figure A.1. Schematic of the ice-scraping machine 76
Figure A.2. Ice-scraping machine 76
Figure A.3. Sled of the ice-cutting machine 77
Figure A.4. Sled of the ice-scraping machine 78
Figure A.5. Pavement sample anchored to two fixed plates 78
Figure A.6. Schematic of the hydraulic system 79
Figure A.7. The three positions of the four-way valve 80
Figure A.8. Direction of fluid flow in slow speed mode when forward button was pushed 81
Figure A.9. Trigger on the ice-cutting machine 82
Figure A.10. Direction of fluid flow when retract button was pushed 82
Figure A.11. Direction of flow in high speed mode when forward button was pushed . . 83
Figure A.12. Shock absorber 84
Figure A.13. Switches on the doors for safety 84
Figure A.14. Position measuring device 85
Figure B.1. Geometry of the pavement sample 89

List of Tables

Table 2.1. Test matrix 11
Table 2.2. Quantities of sodium chloride in pretreatment tests 13
Table 3.1. Maximum cutting forces for various rake angles 24
Table 3.2. Maximum cutting forces for various clearance angles 25
Table 3.3. Maximum download for various clearance angles 26
Table 3.4. Maximum cutting forces for various flat widths 27
Table 3.5. Maximum download forces for various flat widths 28
Table 3.6. Maximum cutting forces and side loads with attack angles 29
Table 3.7. Maximum cutting forces for various blade widths 30
Table 3.8. Maximum scraping forces for five quantities of salt 31
Table 3.9. Maximum cutting force at two temperatures 33
Table 3.10. Maximum cutting force for various levels of cutting velocity 34
Table C.1. Experimental results 91

Abstract

Laboratory tests were performed with a hydraulic ice-cutting rig to determine the effects of the geometry of the cutting edge of a snow plow blade on the force required to remove ice from a highway pavement surface. Test results indicated that the most important parameter was the clearance angle, and the associated flat width. Using this information, a prototype cutting edge was designed and fabricated for field testing during the winter of 1991-92. Three different cutting edges were tested: the prototype cutting edge, and two commercially available cutting edges. The prototype cutting edge was shown to be clearly superior to the other two edges, cutting more ice with less downforce and thus resulting in greater vehicle control.

Executive Summary

The purpose of this study is to examine the effect of cutting edge geometry on the forces required to cut ice from the pavement, and thereby improve the ice removal capabilities of currently available plows, by providing them with improved cutting edges.

A hydraulic ram was designed and constructed to cut ice at speeds of up to 20 mph (8.94 m/s) in a cold room at the Iowa Institute of Hydraulic Research (IIHR). It was used to perform a series of studies of the effects of cutting edge geometry on the ice scraping force. Parameters included: rake angle, clearance angle, flat width, blade width, attack angle, cutter velocity and temperature. A brief series of tests was also conducted to investigate the effect of chemical pre-treatment on ice cutting forces. Between two and four conditions of each parameter were tested, and a minimum of three tests were conducted for each combination of parameters. Not all possible combinations were studied, since this would have required over 6,000 tests. Accordingly, a fractional factorial design was used.

The results of the tests indicated that the key parameter is the clearance angle. Very high downforces were experienced when this was zero, so much so that the test could not be completed successfully. However, even a small (in this case greater than 2°) clearance angle provided sufficient freedom for the blade to cut the ice successfully. Closely related to the clearance angle is the flat width. When this increased to about 3/8 in (0.9 cm), very high downforce was again observed, a result wholly consistent with the clearance angle results. No significant variation of force with rake angle or attack angle was found, though this may be due in part to the lack of any need for ice clearing in the laboratory tests (the samples were only 12 in (30.3 cm) long). Temperature also appears to have very little effect on scraping force within the range studied of 0°C to -20°C in this project. However, the force clearly decreased with increasing cutting velocity, which confirmed results found at slower speeds, and is consistent with current theories of ice fracture. There was a small effect associated with blade width, due to the fact that the wider blade overhung the edges of the sample, while the narrower blade did not. Even in the worst case, however, this effect is minimal. The results of the pre treatment tests were ambiguous at best. The quantity of deicer on the scraping force had no apparent effect in the laboratory. As this result was so much at odds with field experience. the samples must not have been representative.

On the basis of these laboratory results, a prototype cutting edge was designed and manufactured for field testing. This (shown in Fig. 5.2) has a non-zero clearance angle. The carbide insert was exposed on the leading face. Using a truck provided by the Iowa

Department of Transportation, a series of tests was performed to compare the prototype cutting edge with two standard cutting edges, one with a carbide insert, the other without. A test area, not accessible to the public, was sprayed with water at night, when weather conditions were appropriate, to give a test strip of ice up to 3/8 in (0.9 cm) thick and 180 ft (55 m) long. The results indicated that the prototype cutting edge cut more ice (i.e., took a deeper cut at a given velocity) and did so with less downforce than either of the other two blades. The field tests did not address the issues of blade wear or shock resistance. Further studies are required to determine this behavior.

Though cutting edge performance may benefit from further studies, it is clear from this study that fairly minor changes in cutting edge geometry result in substantially improved ice cutting.

1

Literature Review

1.1. Introduction

Each winter, more than half of the roads in the United States may become covered with ice from freezing rain, sleet, melting and refreezing of snow, or compaction of fresh snow. Often, chemicals are used on pavements to melt or break up ice. These chemicals, however, damage pavement, corrode automobiles, kill trees and grass, and pollute water supplies. If snowplows removed more ice from roads, smaller amounts of chemicals could be used--which would save money as well as trees.

This study examined several mechanical parameters involved in removing ice from pavement with a cutting edge. The parameters investigated were:

- velocity
- temperature
- blade geometry:
    - rake angle
    - clearance angle
    - blade width
    - flat width (Figure 1.1)
- attack angle (Figure 1.2)
- chemical pre-treatment

Figures 1.1 and 1.2 illustrate the terms used to describe blade geometry in this report.

The tests were performed under controlled laboratory conditions. Field testing of a newly designed cutting edge showed that the new design reduced the force necessary to cut ice.

1.2 Ice Control

Plowing, sanding, and salting are used to control ice. A snowplow removes lightly bonded

ice from the pavement. Sand improves traction. Deicing chemicals melt and break up ice on pavement. Other approaches have been tried, including crushing rollers, wobble wheels, spiral rollers, or serrated blades (Donald and Eigerman, 1972). Ice melting machines have also been proposed.

Ice crushing rollers can be effective. Proper operation is critical, however, to avoid pavement damage. Ice melting machines with forced-draft oil burners have also been tested at airports. The burners do not thoroughly deice, however, and can cause pavement damage. For these reasons, the primary means of mechanical ice control on roadways is by cutting.

1.3 Techniques of Ice Removal

The most commonly used methods to mechanically remove ice from pavement are shovels, chisels, spades, hammers, or snowplow blades. A study compared different methods for highway deicing and concluded that mechanical methods were the most feasible technically and operationally, and were most economically acceptable (Blackburn and St. John, 1977).

In practice, an ice-cutting blade is mounted on the front or under the body of a truck. The truck's hydraulic system pushes the blade down to cut the ice. As the truck proceeds, the broken ice is ejected in front of and behind the blade.

There are few reports about the techniques of ice removal. Nixon, DeJong and Chung (1993) found that the cutting force was dependent on both the blade geometry and the cutting velocity. In their study, however, blade velocity was less than 1 mph (1.6 kmph). Further research was required to increase the blade velocity to field requirements.

Huang (1981) studied how a layer of ice could be lifted from a flat surface by a sharp blade at the ice-surface interface (Figure 1.3). In Huang's study, the lifted ice (l) was treated as a Timoshenko beam (Shames and Dym, 1985) of the cantilever type with an increasing length. Huang derived the relationship between applied force (F) and the distance of separation at the interface (h). Huang also performed penetration experiments in a cold chamber at a controlled temperature. An aluminum alloy blade with a 10° angle (α) was used to penetrate ice and an initial crack was generated at the interface. It was found that as th thrust reached a maximum value, the crack propagated violently. and fracture of the ice followed. Two points, however, should be noted. First, all of Huang's tests were at speeds much less than 1 mph (1.6 kmph). Second, the geometry of the blade received minimal consideration. Only the angle α was considered as a variable, while the effects of the clearance angle, blade width, flat width (Figure 1.1), and the attack angle (Figure 1.2) were not considered.

It should be noted that it would be impractical to use a blade with an angle equal to 10°, the mean value used in Huang's tests. Such a blade would easily break and might also damage the road surface by digging into it. Ice is more effectively cut when this angle is between 45° and 90°.

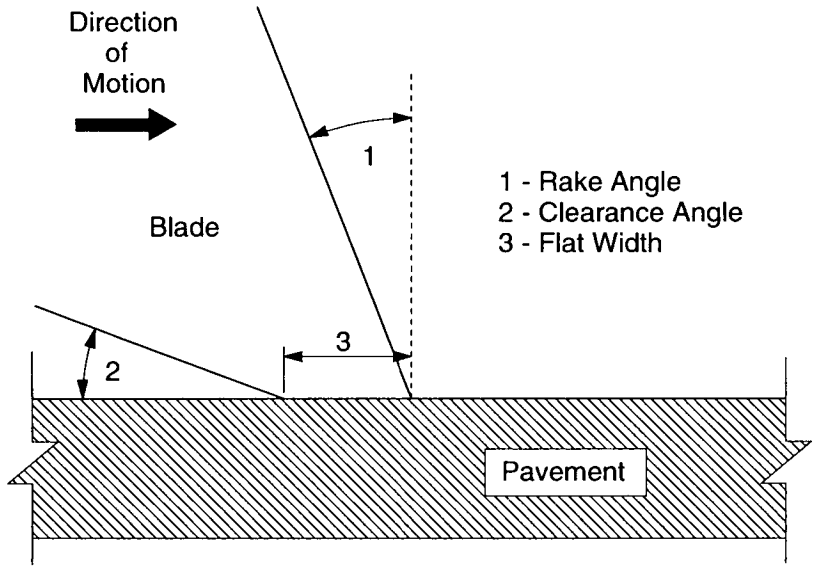

Figure 1.1 Geometry of the blade (side view)

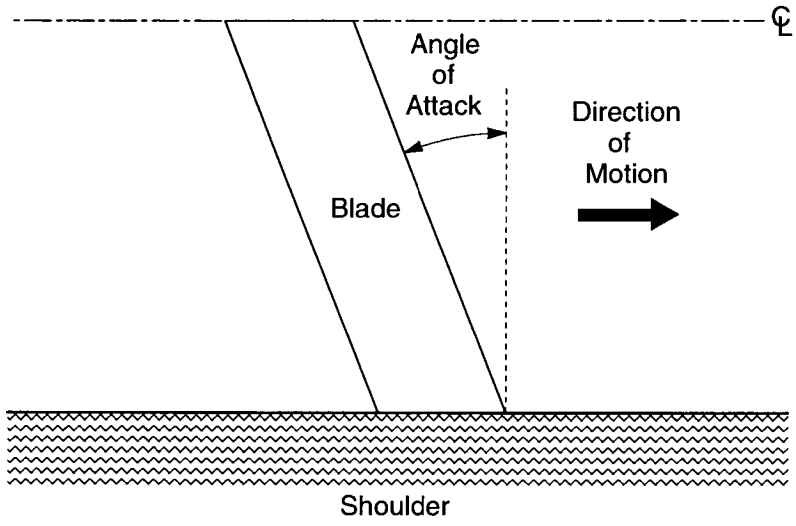

Figure 1.2 Geometry of the blade (top view)

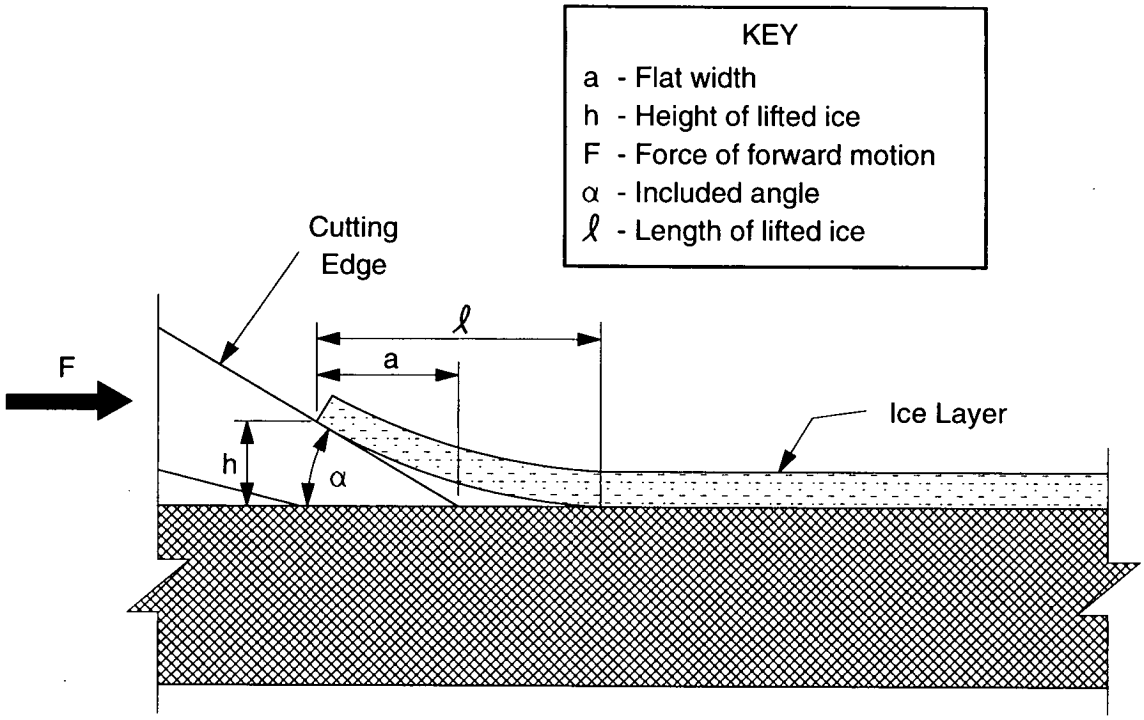

Source: N.C. Huang, "Mechanics of Ice-Lifing From a Flat Surface Through Penetration With a Sharp Blade," *Transaction of the ASME* (1981), Vol. 48

Figure 1.3 Pictorial representation of Huang's study

2

Experimental Description

2.1 Introduction

The objective of this study was to examine the relationship between the applied ice-cutting force and the geometry of the cutting edge. A prototype cutting edge was tested in the field and compared with existing cutting edges. An ice-cutting machine was built for laboratory studies. A prototype was designed, manufactured, and field tested.

Various parameters of the geometry of the cutting edge are considered in this study. These parameters include rake angles of 0°, 15°, 30°, and 45°, clearance angles of 0°, 2°, 5°, and 10°, attack angles of 0° and 35°, blade widths of 3 in. and 5 in. (7.62 cm and 12.7 cm), and blade flat widths of 0, 0.125, 0.25, and 0.375 in. (0, 0.318, 0.635, 0.952 cm). These variables are shown in Figures 1.1 and 1.2 and discussed more fully in chapter 1. Experiments were conducted at 5, 10, 15, and 20 mph (2.24, 4.97, 6.71, and 8.94 m/s) and at temperatures of 23°F and -4°F (-5°C and -20°C).

All the laboratory experiments conducted in this study were performed at the Iowa Institute of Hydraulic Research (IIHR) ice laboratory. The temperature in the ice lab was controlled and maintained to within ±0.54°F (±0.3°C). The experimental apparatus used for this study was a hydraulic ice-cutting machine. A digital interface was used for making high-resolution, low noise velocity and load measurements. A description of the apparatus is given in Appendix A.

2.2 Test Samples

The test samples were made of concrete. A 0.25 in. (0.6 cm) layer of ice was formed on each test sample (Figure 2.1).

2.2.1 Concrete Blocks

Fourteen portland cement concrete samples were used in the tests. The gradation for the structural concrete was Class C (mix No. C-4), described fully in the Iowa Standard Specifications for Highway and Bridge Construction (1984). Before the concrete became fully dry, the top surface of the pavement sample was roughened with a broom to increase the bond between the pavement and ice. The samples were 12 in. long by 4 in. wide by 8 in. high (30 cm by 10 cm by 20 cm).

2.2.2 Sample Manufacture

The required ice thickness was obtained by ponding water on top of the refrigerated concrete samples by using a neoprene collar. The water was between 1/16 and 1/8 in. (0.16 to 0.32 cm) deep. The concrete samples were cold soaked at 23°F (-5°C) for 24 hr prior to ice formation. The water was cooled to 32°F (0°C) prior to being placed on the sample. After this initial layer of ice was frozen, two more layers were added at intervals of two hours, bringing the total thickness to 0.25 in ±0.125 in. (0.63 cm ±0.32 cm). Figure 2.2 shows pavement samples with neoprene rubber collars in place. A fully prepared sample is shown in Figure 2.1.

The Test Matrix

A series of ice-cutting tests was performed using the high-speed test machine. This study was concerned primarily with discovering the effects of blade geometry on cutting force. Four rake angles (0°, 15°, 30°, and 45°), four clearance angles (0°, 2°, 5°, and 10°), two attack angles (0° and 35°), four blade flat widths (0, 0.125, 0.25, and 0.375 in., 0, 0.32, 0.64, and 0.95 cm) and two blade widths, 3 in. and 5 in. (7.62 cm and 12.7 cm), were considered. The geometry of the blade is shown in Figures 1.1 and 1.2. The actual blades used are shown in Figures 2.3 through 2.7.

Experiments were conducted at four speeds (5, 10, 15, and 20 mph; 2.24, 4.97, 6.71, and 8.94 m/s), and at two temperatures (23°F and -4°F; -5°C and -20°C). Table 2.1 lists the test parameters in this study. The pretreatment tests are described in further detail below. The gram/sample values refer to the quantity of salt used in each test.

Not all the possible combinations of variables were tested. This would involve over 2,000 test conditions, which with three tests at each condition (a minimum for assessment of repeatability) would result in over 6,000 tests. Rather, a fractional factorial approach (Montgomery, 1984) was taken. In a fractional factorial approach, only some of the combinations of the variables are tested. The variables can then be ranked according to their importance. The research effort can then be applied in these key areas.

Table 2.1. Test matrix

RAKE ANGLE	0°	15°	30°	45°	
CLEARANCE ANGLE	0°	2°	5°	10°	
ATTACK ANGLE	0°	35°			
SPEED (mph)	5	10	15	20	
BLADE WIDTH (in.)	3	5			
FLAT WIDTH (in.)	0	1/8	1/4	3/8	
TEMPERATURE (°C)	-5	-20			
PRE-TREATMENT (g/sample)	0.06	0.12	0.24	0.48	0.96

1 in.=2.54 cm: 1 mph=0.45 m/s: 1°C=1.8°F:

1 g=0.035 oz.

underlines indicate baseline test values

2.3.1 Base Line Tests

Base line tests were conducted at four rake angles with fixed 5° clearance angle, 0° attack angle, 5 in. (12.7 cm) blade width, and 0 in. blade flat width. At least three tests were run for each case. This allowed an estimate of test-to-test variability to be made. Tests were conducted at a temperature of 23°F (-5°C). Parameters for base line tests are double underlined in Table 2.1.

2.3.2 Clearance Angle and Blade Flat Width

In reality, if a cutting edge were manufactured with a sharp edge having some non-zero clearance angle, this sharp edge would wear down rapidly and create a flat area before the clearance angle. The extent to which this flat area affected cutting loads was of vital

importance, since it would determine the useful lifetime of the cutting edge. In order to get more information about the effect of the blade flat width, two load cells (base-load cells) were installed to measure the downloads during cutting. Additionally, a series of experiments was planned in which this blade flat width increased from 0 to 0.375 in. (0.95 cm).

As mentioned previously, four clearance angles and blade flat widths were considered in the study. For this part of the study, blades with a rake angle of 30° and an attack angle of 0° were used. The clearance angle after the flat width was 5°. Tests were executed at 10 and 15 mph (4.97 and 6.71 m/s). The width of the blade was 5 in. (12.7 cm) and the temperature was 23°F (-5°C).

2.3.3 Attack Angle

Only two angles of attack were used in the study, 0° and 35°. The latter was chosen to reflect common ice removal practice. In order to obtain full information on cutting forces, one load cell was incorporated to measure the side load. For both angles of attack, tests were done with 30° rake angle and 5° clearance angle. Tests were executed at 10 mph (4.97 m/s) and the temperature was 23°F (-5°C).

2.3.4 Blade Width

To determine edge effects on the blades, blades 3 in. and 5 in. (7.6 and 12.7 cm) wide were used in the experiment. The blade 5 in. (12.7 cm) wide overhung the sample. The blade 3 in. (7.6 cm) wide did not overhang the sample but cut a path through the ice, leaving unfractured ice on either side. This latter case is perhaps more representative of reality. These tests were performed with a 30° rake angle, a 5° clearance angle, a 0° attack angle, and a 0 blade flat width. Tests were conducted at 10 and 15 mph (4.97 and 6.71 m/s), and at 23°F (-5°C).

2.3.5 Pre-treatment Tests

One of the more promising methods of ice control consists of applying a chemical prior to a storm, in order to prevent the formation of a strong ice-pavement bond. In the pre-treatment tests conducted as part of this study, salt (sodium chloride) was placed on the sample prior to freezing the pavement sample in the cold room. Table 2.2 shows the quantities used in the tests, in pounds of salt per lane mile (the standard application rate is between 100 and 400 lb/LM) and grams of salt per sample. A modified sample preparation technique was required for these tests. The requisite amount of salt was dissolved in 30 cm^3 of water, and the solution was poured onto the sample surface, giving a layer approximately 0.039 in. (1 mm)

thick. This layer was allowed to evaporate, leaving a salt film behind. Then the sample was prepared in the standard way, which included cold soaking the sample, and adding water in approximately 1/16 in. (0.16 cm) increments to build to the desired thickness of 1/4 in. (0.635 cm). Tests were executed at both 23°F and -4°F (-5°C and -20°C) using a cutting edge with a 30° rake angle, a 5° clearance angle, and a 0° attack angle.

Table 2.2. Quantities of sodium chloride in pretreatment tests

Quantity per lane mile	Quantity per sample
25 lb/LM (7.03 kg/km)	0.002 oz. (0.06 g)
50 lb/LM (14.1 kg/km)	0.004 oz. (0.12 g)
100 lb/LM (28.2 kg/km)	0.008 oz. (0.24 g)
200 lb/LM (56.4 kg/km)	0.017 oz. (0.48 g)
400 lb/LM (113 kg/km)	0.034 oz. (0.96 g)

2.3.6 Temperature and Scraping Velocity

Tests were conducted at cutting velocities between 5 and 20 mph (2.24 and 8.94 m/s) and at temperatures of 23°F and -4°F (-5°C and -20°C). Most of the tests were conducted at a temperature of 23°F (-5°C). Only base line tests and pre-treatment tests were executed at both 23°F and -4°F (-5°C and -20°C). Four velocity levels (5, 10, 15, 20 mph (2.24, 4.97, 6.71, and 8.94 m/s)) were considered in the study, though for simplicity only two levels of velocity (10 and 15 mph) were used in most cases.

2.4 Data Reduction Scheme

As discussed in Appendix A, the load cell voltage is readily transformed into force (lb or N). Similarly, the voltage from the distance-measuring device is transformed into distance. Using these data, the velocity of the blade and the cutting force applied by the blade is obtained by means of the dynamic analysis discussed below.

2.4.1 Obtaining Acceleration

One fact became immediately apparent. The load, as recorded by both top and bottom load cells, continued to increase after the blade had finished cutting. When the blade hit the ice, it caused the whole concrete block to rotate about the rear load support. Thus, the load recorded by the top load cell was in fact a measure of the block displacement (similarly with the bottom load cell). A complete analysis required that the dynamic aspects of the blade-ice interaction be considered. An appropriate free-body diagram for this analysis is shown in Figure 2.8. The two unknown forces (F_S and F_D) are found by a simple force balance process given below.

Because the displacement of point A (Figure 2.8) during the ice-cutting process was very small (about 0.001 in. (0.0025 cm)), the displacement of point B was ignored (this is justified in Appendix B). By applying the known stiffness of the load cell to the load voltage data, the deflection at the top load cell was obtained. The acceleration, a, of point A was obtained by differentiation twice of the displacement function of the top load cell and the angular acceleration α of the pavement sample was obtained:

$$\alpha = \left(\frac{a}{\sin\theta}\right)\left(\frac{1}{d1}\right) \tag{2.1}$$

where Θ is the angle between AB and the horizontal line, and $d1$ the distance from A to B. The accelerations of central point G at X and Y (horizontal and vertical) directions are:

$$(a_G)_x = \frac{a\sin\phi}{\sin\theta}\frac{d2}{d1} \tag{2.2}$$

$$(a_G)_y = \frac{a\cos\phi}{\sin\theta}\frac{d2}{d1} \tag{2.3}$$

where:

$$\theta = \arctan\frac{5.25}{1.875} \tag{2.4}$$

$$\phi = \arctan\frac{4}{4.125} \tag{2.5}$$

$$d1 = \sqrt{5.25^2 + 1.875^2} \tag{2.6}$$

$$d2 = \sqrt{4.125^2 + 4^2} \tag{2.7}$$

and where ϕ is the angle between BG and the horizontal, and $d2$ the distance from B to G (Figure 2.8).

2.4.2 Developing Ice-Cutting Force

Given the accelerations of the centroid G, the equilibrium equations of the pavement sample can be written as follows:

$$\sum F_x = m(a_G)_x$$

$$F_S + F_B - F_T - F_F = m(a_G)_x \tag{2.8}$$

$$\sum F_y = m(a_G)_y$$

$$F_N - F_W - F_D = m(a_G)_y \tag{2.9}$$

$$\sum M_G = I_G \alpha$$

$$4F_S + 4F_F - 2.625F_B - 1.25F_T - 4.125F_N - (x-6)F_D = I_G \alpha \tag{2.10}$$

where F_S is the horizontal ice-scraping force, F_D is the vertical scraping force (the downforce), F_W the gravity force (i.e., weight) of the concrete sample, F_F the friction force of the roller, and F_T, F_B, and F_N are reactions from the top and bottom load cells and the roller load cell, respectively. M is the mass of the concrete block. $(a_G)_x$ and $(a_G)_y$ are accelerations of the concrete sample in x and y directions, and α is the angular acceleration as defined in Equation 2.1. The distance of the cutting edge from the left hand end of the sample is x, and thus ranges from 12 in. at the start of cutting to 0 in. at the end (30.5 to 0 cm).

From Equations 2.8, 2.9, and 2.10 there are three equations and three unknowns (F_F, F_D, and F_S). These can be solved simultaneously to give the following solutions for the two unknowns of interest (F_D, and F_S):

$$F_D = F_N - F_W - m(a_G)_y \tag{2.11}$$

$$F_S = \frac{1}{8}(I_G \alpha + 5.25F_T - 1.375F_B + 4m(a_G)_x + 4.125F_N - (x-6)(F_N - F_W - m(a_G)_y)) \tag{2.12}$$

Using these equations, data from each test were reduced to give a simple force-time plot for the ice cutting force. From this plot, the maximum cutting force for the test was readily determined.

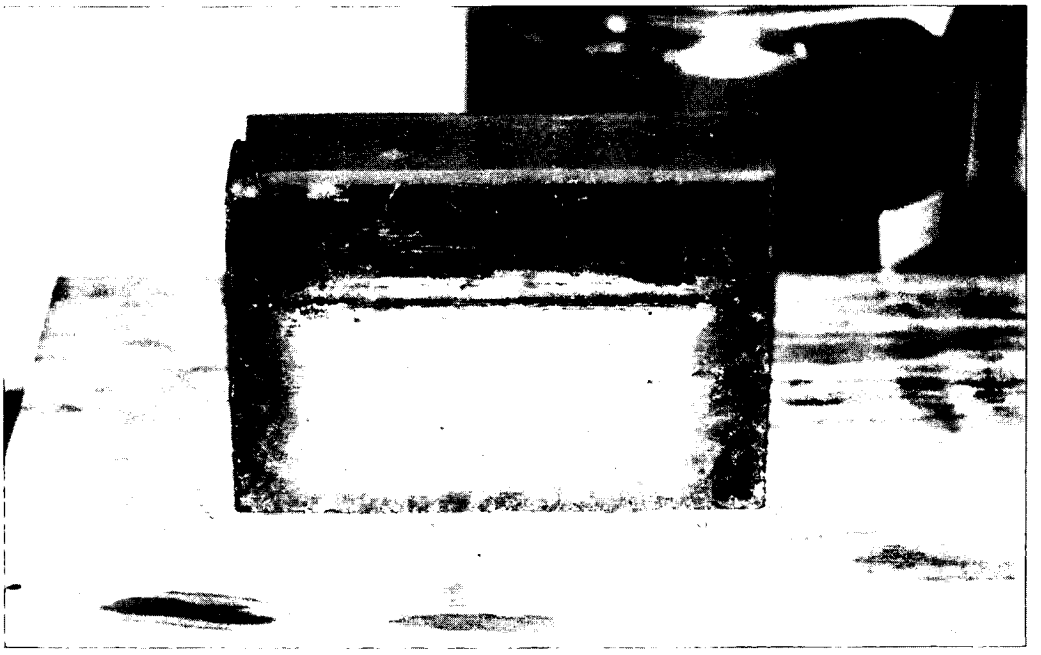

Figure 2.1. A pavement sample ready for testing

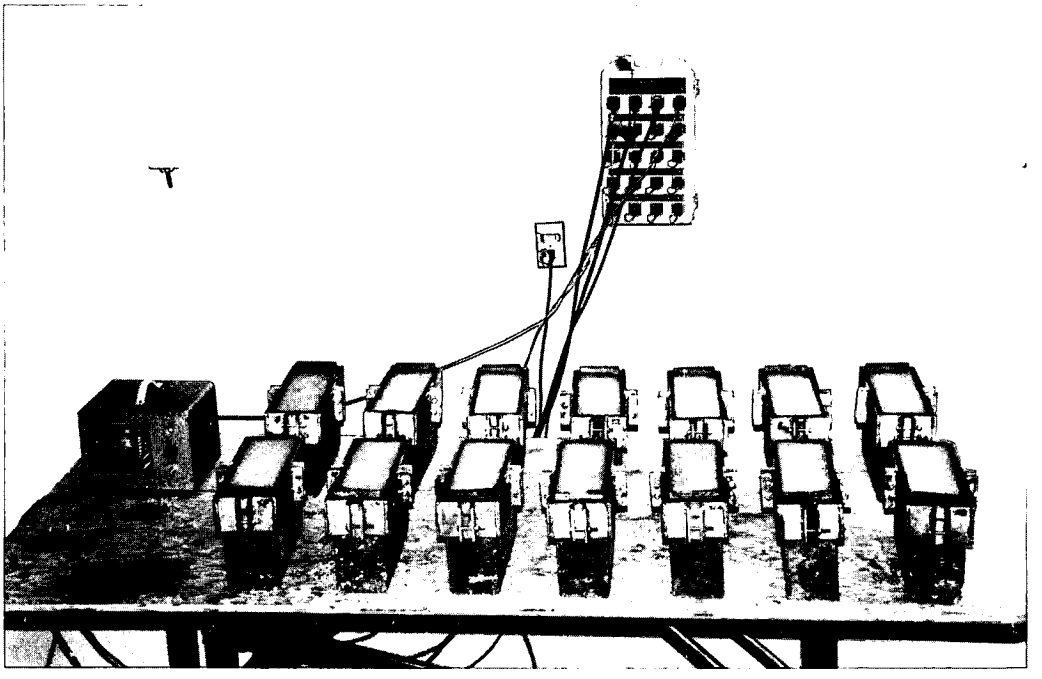

Figure 2.2. Pavement samples with neoprene rubber collars

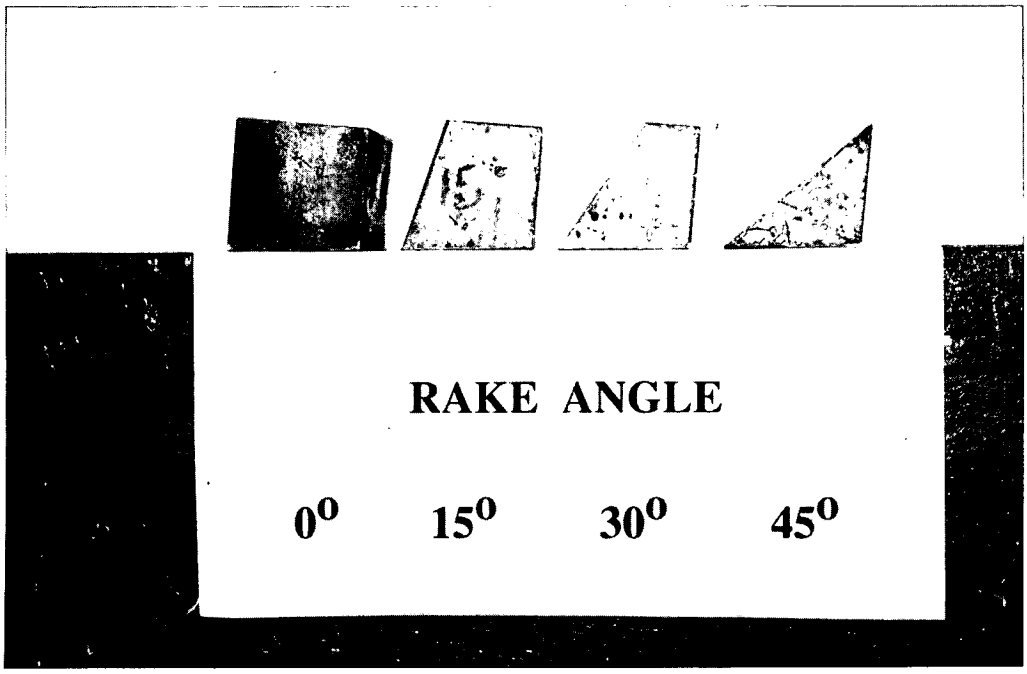

Figure 2.3. Blades with various rake angles

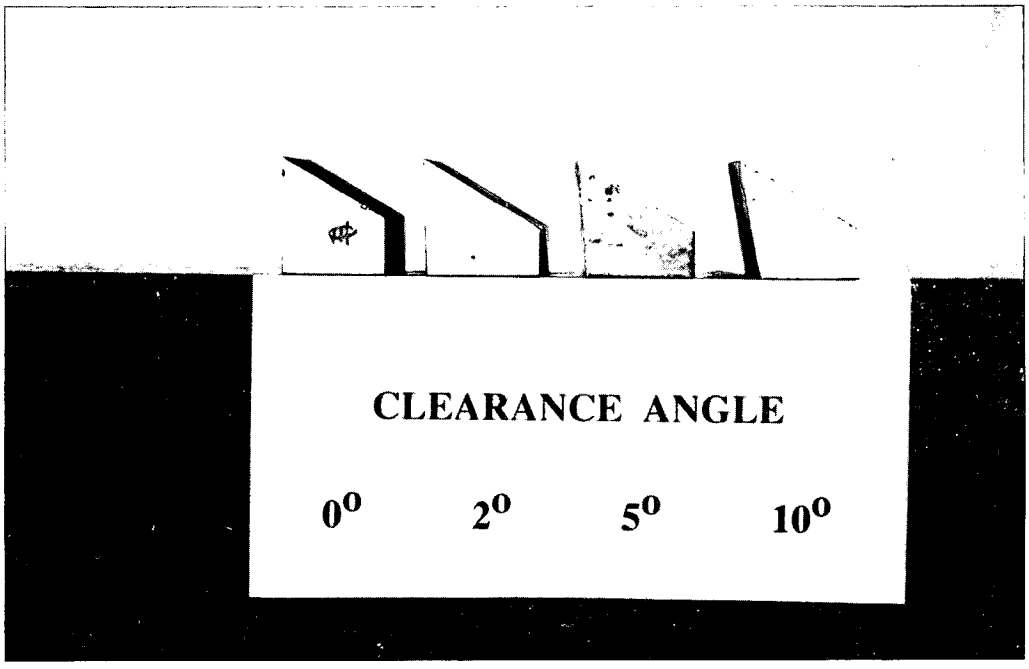

Figure 2.4. Blades with various clearance angles

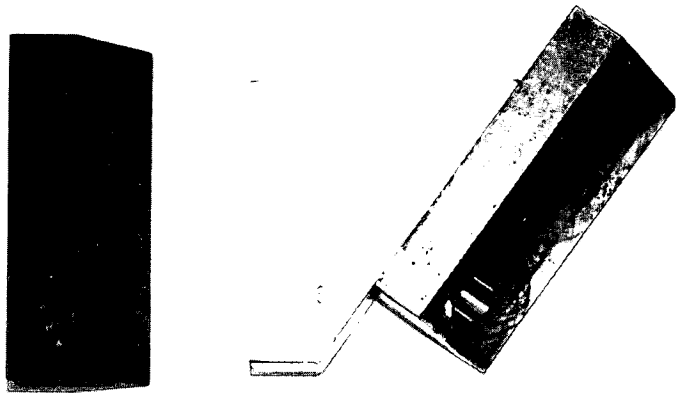

ATTACK ANGLE

0° 35°

Figure 2.5. Blades with various attack angles

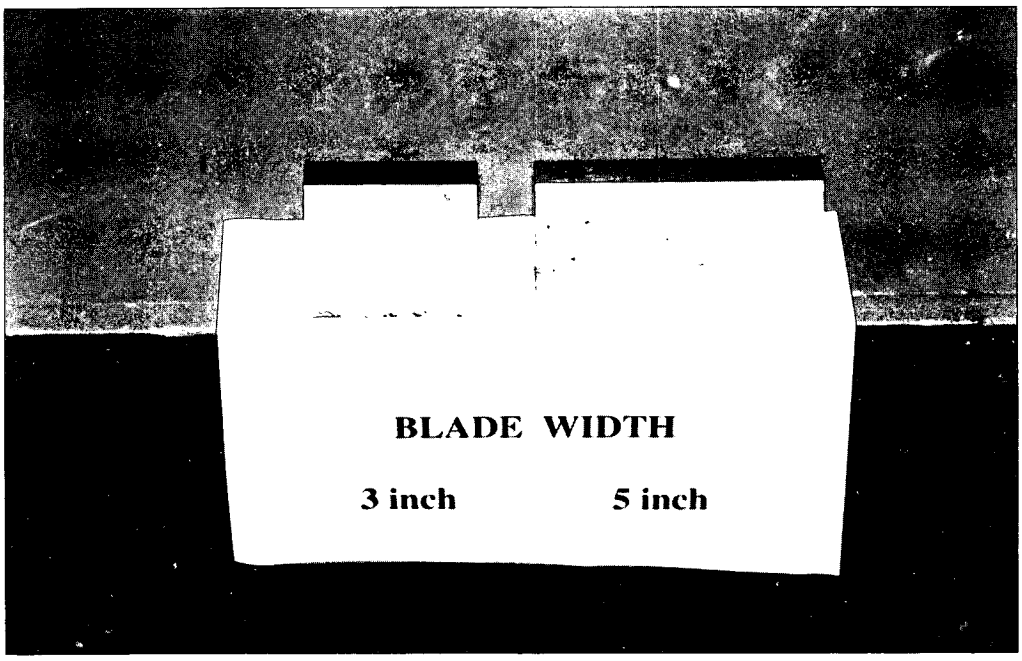

Figure 2.6. Blades with various widths

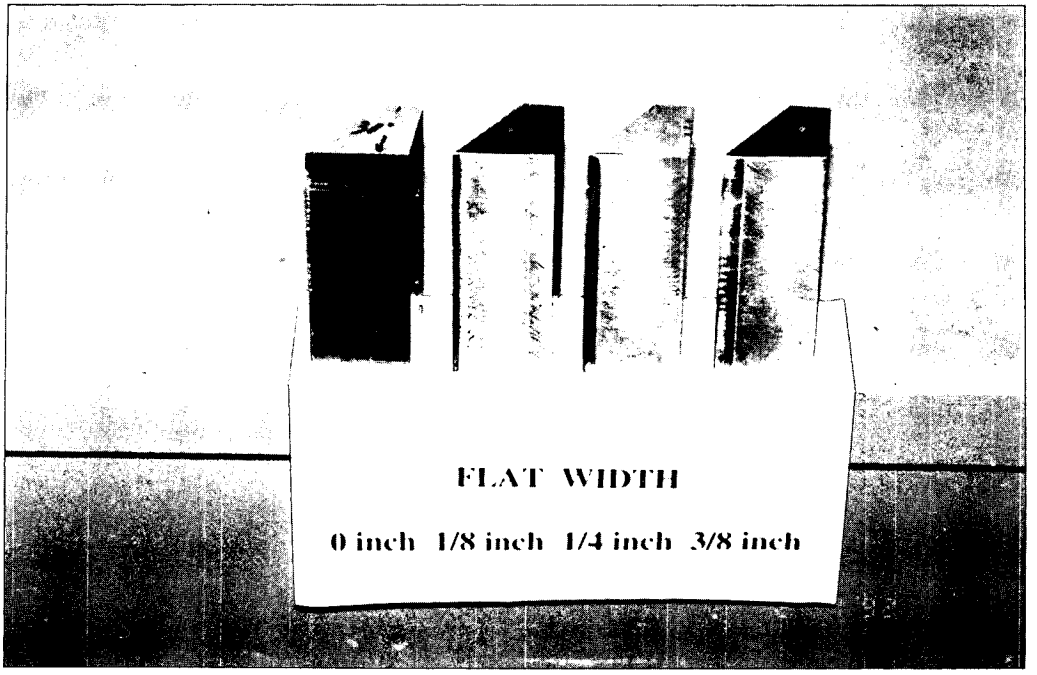

Figure 2.7. Blades with various flat widths

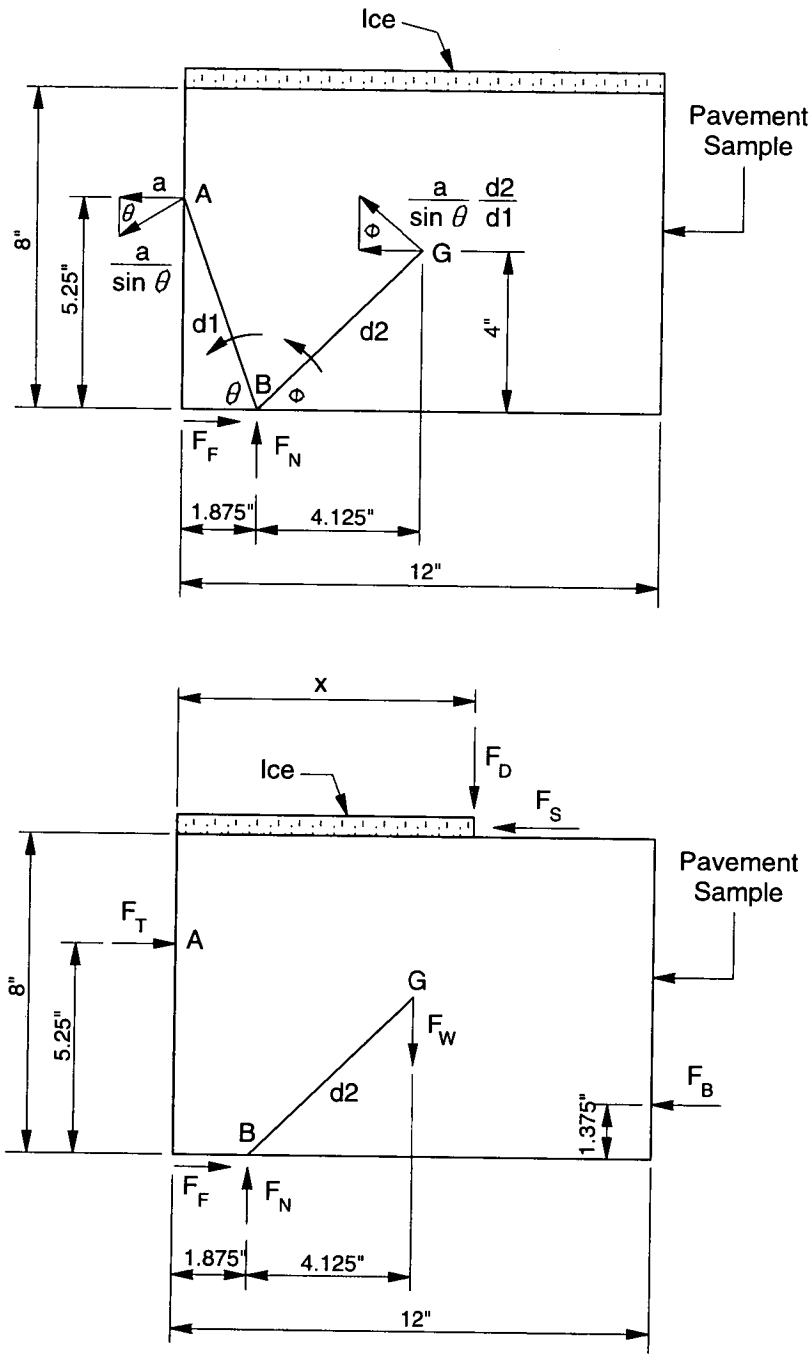

Figure 2.8. Free body diagram of the pavement sample

3

Results

3.1 Introduction

Original data from one test (using a blade with a 45° rake angle, a 5° clearance angle, a 0° attack angle, and no flat width) are shown in Figures 3.1 and 3.2. As can be seen, the load cell reading continues to rise even after the blade has passed over the sample, and is no longer cutting ice. This characteristic of increasing voltage after the blade had left the end of the sample was due to the inertia of the pavement sample. Although it appears that there were relatively few datapoints obtained during the cutting itself (when the blade was in contact with the ice), the data acquisition rate was set sufficiently high that at least one hundred datapoints were collected during the cutting process. The velocity data for this test are given in Figure 3.3.

Using Equation 2.12, the force experienced by the blade during the cutting was found. Figure 3.4 shows this force for the test in question. The force rose somewhat during the test. This may be due to a number of factors. Particles of broken ice trapped under the cutting edge may increase resistance, or the blade may be forced upward as it passes over the sample, thus increasing friction with the sled rails. Nonetheless, the force obtained in this manner was considered a satisfactory record of the force required to cut the ice from the pavement sample. It should be noted that not all tests showed such an increase in force during the test, but the majority showed some slight increase.

3.2 Baseline Tests

The baseline tests have been described in Section 2.3.1. The maximum cutting forces measured for various rake angles are listed in Table 3.1. Figure 3.5 shows the result of the maximum cutting force as a function of rake angle. In Figure 3.5, the error bars and the center of the circle represent, respectively, the standard deviation and the mean of the maximum cutting forces for each set of rake angle tests. A similar notation is used in all figures.

Table 3.1. Maximum cutting forces for various rake angles

	Force (lb)			
Test Number	0°	15°	30°	45°
1	19.90	17.46	18.88	20.37
2	21.71	17.09	18.40	20.47
3	22.72	17.27	18.31	20.09
4	22.69	20.20	17.84	22.53
5	20.28	17.46	19.23	23.66
6	18.97	17.46	18.72	24.33
7		17.27	17.86	24.01
8		17.09		21.94
9		19.36		22.11
10		17.39		
Mean Cutting Force	21.05	17.81	18.46	22.17
Standard Deviation	1.56	1.07	0.52	1.62
95% Confidence Interval	1.64	0.76	0.48	1.24
99% Confidence Interval	2.57	1.10	0.73	1.81

3.3 Clearance Angle and Blade Flat Tests

Four different clearance angles (0°, 2°, 5°, and 10°) and four flat widths (0, 1/8, 1/4, and 3/8 in. (0, 0.32, 0.64, and 0.95 cm)) were tested. The results of maximum scraping forces and download forces for various clearance angles are listed in Tables 3.2 and 3.3, respectively. Plots for maximum cutting forces and download forces versus various clearance angles are shown in Figures 3.6 and 3.7, respectively. It should be noted that, for 0° clearance angle tests, the blade could not go through the ice on the pavement sample in any of the tests. This special case is discussed in detail in Section 4.3.

Table 3.2. Maximum cutting forces for various clearance angles

Force (lb)			
	Clearance Angle		
Test Number	2°	5°	10°
1	17.16	18.88	18.81
2	17.21	18.40	18.02
3	17.27	18.31	18.86
4		17.84	
5		19.23	
6		18.72	
7		17.86	
Mean Scraping Force	17.21	18.46	18.56
Standard Deviation	0.06	0.52	0.47
95% Confidence Interval	0.14	0.48	1.17
99% Confidence Interval	0.31	0.73	2.66

For the results of the blade flat tests, Tables 3.4 and 3.5 list the maximum cutting forces and download forces respectively. The variation of cutting forces and download forces with flat widths are shown in Figures 3.8 and 3.9. The standard deviations (error bars) for 1/8 in. and 1/4 in. (0.32 and 0.64 cm) flat widths are too small to be seen in Figures 3.8 and 3.9.

Table 3.3. Maximum download for various clearance angles

Force (lb)				
	Clearance Angle			
Test Number	0°	2°	5°	10°
1	289.99	5.55	0.51	0.52
2	348.25	6.41	6.50	1.03
3	341.50	5.48	4.02	0.51
Mean Download	326.58	5.85	3.68	0.69
Standard Deviation	31.87	0.58	3.01	0.30
95% Confidence Interval	79.00	1.43	7.46	0.74
99% Confidence Interval	179.95	3.25	17.00	1.68

3.4 Attack Angle Tests

Blades with two attack angles (0° and 35°) were tested. Table 3.6 lists the maximum cutting forces and side loads for the two attack angles. It should be noted that the net cutting force for the 35° attack angle might be larger by vector addition of the cutting force and side load. A plot of cutting force against attack angle is shown in Figure 3.10.

	Force (lb)							
	Flat Width							
Test Number	0 in.		1/8 in.		1/4 in.		3/8 in.	
	10 mph	15 mph	10 mph	15 mph	10 mph	15 mph	10 mph	15 mph
1	18.88	19.10	18.27	17.13	17.24	17.37	17.46	17.59
2	18.40	18.90	17.28	17.31	17.29	17.59	17.43	17.31
3	18.31	18.74	17.55	17.26	17.24	17.21	17.37	17.98
4	17.84	17.10	17.27	17.55		17.29	17.62	17.14
5	19.23	17.39		17.44		17.81	17.15	
6	18.72	17.44		17.14		17.30		
7	17.86							
Mean Cutting Force	18.46	18.11	17.59	17.31	17.26	17.43	17.41	17.51
Standard Deviation	0.52	0.89	0.47	0.17	0.03	0.23	0.17	0.37
95% Confidence Level	0.48	0.94	0.75	0.17	0.07	0.24	0.21	0.58
99% Confidence Level	0.73	1.47	1.37	0.27	0.16	0.37	0.35	1.07

Table 3.4 Maximum cutting forces for various flat widths

Table 3.5. Maximum download forces for various flat widths

Force (lb)			
	Flat Width		
Test Number	1/8 in.	1/4 in.	3/8 in.
1	27.12	37.3	536.53
2	24.66	22.16	289.20
3	10.54	34.24	191.35
Mean Download Force	20.77	31.23	339.03
Standard Deviation	8.95	8.01	177.9
95% Confidence Interval	22.18	19.85	441.01
99% Confidence Interval	50.53	45.21	1000.0

Table 3.6. Maximum cutting forces and side loads with attack angles

	Force (lb)		
	0°	35°	
Test Number	Cutting Force	Cutting Force	Side Loads
1	18.88	18.07	
2	18.40	18.31	
3	18.31	17.42	
4	17.84	18.51	
5	19.23	17.12	1.58
6	18.72	17.16	0.78
7	17.86	17.32	
8		17.41	
9		18.04	0.94
10		18.43	
Mean Cutting Force	18.46	17.78	1.1
Standard Deviation	0.52	0.55	0.42
95% Confidence Interval	0.48	0.39	1.05
99% Confidence Interval	0.73	0.56	2.39

3.5 Blade Width Tests

Tests with blade widths of 3 in. and 5 in. (7.62 and 12.7 cm) were conducted. Results for maximum cutting force with various blade widths are listed in Table 3.7. Figure 3.11 shows a plot of maximum cutting force against blade width at two speeds, 10 and 15 mph (4.97 and 6.71 m/s).

Table 3.7. Maximum cutting forces for various blade widths

	Force (lb)			
	Blade Width			
	3 in		5 in	
Test Number	10 mph	15 mph	10 mph	15 mph
1	18.32	17.83	18.88	19.10
2	17.64	17.98	18.40	18.90
3	18.11	18.08	18.31	18.74
4		18.26	17.84	17.10
5		17.55	19.23	17.39
6		18.07	18.72	17.44
7			17.86	
Mean Cutting Force	18.02	17.96	18.46	18.11
Standard Deviation	0.35	0.25	0.52	0.89
95% Confidence Interval	0.86	0.26	0.48	0.94
99% Confidence Interval	1.97	0.40	0.73	1.47

3.6 Pretreatment Tests

Pretreatment tests were performed at 23°F and -4°F (-5°C and -20°C), using a cutting edge with a 30° rake angle, a 5° clearance angle, and a 0° attack angle. Five quantities of salt (sodium chloride) were used to run the tests. Results of maximum cutting forces for various quantities of salt used are listed in Table 3.8. Figure 3.12 shows the maximum cutting forces as a function of the various quantities of salt used at two temperatures. Details of how the salt was applied in the pretreatment tests are given in Section 2.3.5.

	Force (lb) at -5°C					Force (lb) at -20°C				
Salt Concentrations (g)	0.06	0.12	0.24	0.48	0.96	0.06	0.12	0.24	0.48	0.96
Test #1	17.40	17.10	17.59	17.61	17.12	17.37	17.94	19.37	17.90	17.77
Test #2	18.44	17.23	17.62	18.01	17.75	17.68	17.94	19.37	18.15	18.10
Test #3	17.90	19.58	17.79	18.55	18.86	17.80	18.48	19.39	18.36	18.11
Mean Cutting Force	17.92	17.97	17.67	18.06	17.91	17.62	18.12	19.38	18.14	17.99
Standard Deviation	0.52	1.40	0.11	0.47	0.88	0.22	0.31	0.01	0.23	0.19
95% Confidence Interval	1.29	3.46	0.27	1.17	2.18	0.55	0.77	0.03	0.57	0.48
99% Confidence Interval	2.94	7.88	0.61	2.66	4.98	1.25	1.76	0.07	1.30	1.09

Table 3.8 Maximum scraping forces for five quantities of salt

3.7 Temperature and Cutting Velocity Tests

As discussed in Section 2.3.5, only baseline and pretreatment tests were conducted at 23°F and -4°F (-5° and -20°C). Table 3.9 lists results for baseline tests at -5° and -20°C. The maximum cutting force as a function of rake angles is shown in Figure 3.13.
Table 3.10 lists the results of maximum scraping force at four velocity levels for various rake angles. The pictorial representation of these results is shown in Figure 3.14.

3.8 Summary

Results of all the scraping tests are tabulated in accordance with the different parameters being studied. Appropriate plots have been shown. A complete list of experimental results with detailed parameters is given in Appendix C. As discussed in Chapter 2, only some of the possible tests were run, since the complete factorial matrix would be unmanageable. Almost all tests were successful. Unsuccessful tests are noted.

		Force (lb)							
Rake Angle		0°		15°		30°		45°	
Test Number	Temperature	-5°C	-20°C	-5°C	-20°C	-5°C	-20°C	-5°C	-20°C
1		19.90	17.11	17.46	16.92	18.88	17.10	20.37	17.01
2		21.71	17.16	17.09	17.04	18.40	17.15	20.47	17.18
3		22.72	17.47	17.27	17.50	18.31	17.18	20.09	20.18
4		22.69		20.20		17.84		22.53	
5		20.28		17.46		19.23		23.66	
6		18.97		17.46		18.72		24.33	
7				17.27		17.86		24.01	
8				17.09				21.94	
9				19.36				22.11	
10				17.39					
Mean Cutting Force		21.05	17.25	17.81	17.15	18.46	17.14	22.17	18.12
Standard Deviation		1.56	0.20	1.07	0.31	0.52	0.04	1.62	1.78
95% Confidence Level		1.64	0.48	0.76	0.76	0.48	0.10	1.24	4.42
99% Confidence Level		2.57	1.10	1.10	1.73	0.73	0.23	1.81	10.07

Table 3.9 Maximum cutting force at two temperatures

Rake Angle		0°			15°			30°			45°	
Test Number	Speed (mph)	5	10	20	5	10	20	5	10	20	5	10	20
1		26.74	19.90	17.10		17.46	17.30	27.63	18.88	17.10	26.87	20.37	17.16
2		31.72	21.71	17.20		17.09	17.33	26.46	18.40	17.19	29.17	20.47	17.59
3		36.20	22.72	17.95		17.27	17.75		18.31	17.23	24.59	20.09	18.12
4		25.53	22.69			20.20			17.84		26.97	22.53	
5			20.28			17.46			19.23		25.05	23.66	
6			18.97			17.46			18.72		25.38	24.33	
7						17.27			17.86			24.01	
8						17.09						21.94	
9						19.36						22.11	
10						17.39							
Mean Cutting Force		30.05	21.05	17.42		17.81	17.46	27.05	18.46	17.17	26.34	22.17	17.62
Standard Deviation		4.90	1.56	0.47		1.07	0.25	0.83	0.52	0.07	1.69	1.62	0.48
95% Confidence Level		7.79	1.64	1.15		0.76	0.62	7.04	0.48	0.17	1.78	1.24	1.19
99% Confidence Level		14.28	2.57	2.62		1.10	1.42	28.67	0.73	0.38	2.79	1.81	2.72

Table 3.10 Maximum cutting force for various levels of cutting velocity

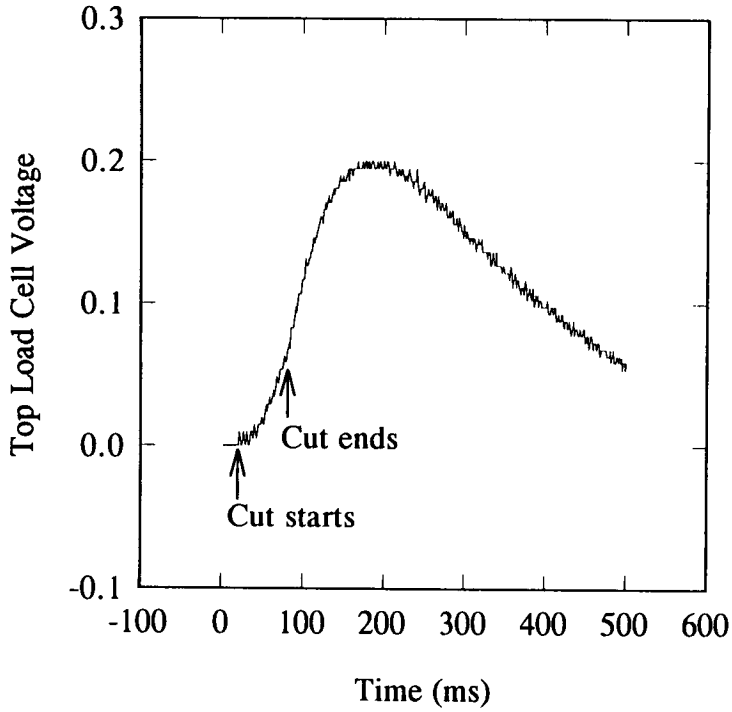

Figure 3.1. Data from top load cell

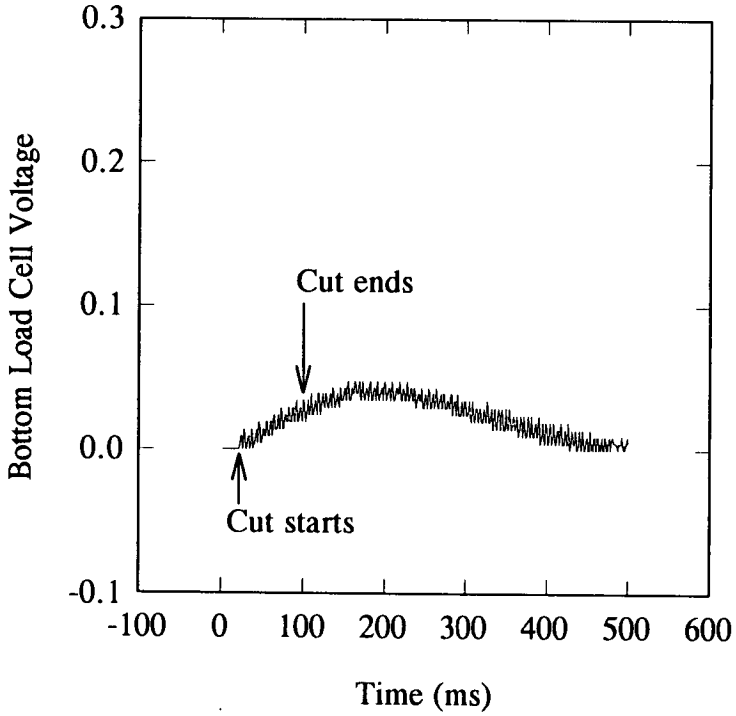

Figure 3.2. Data from bottom load cell

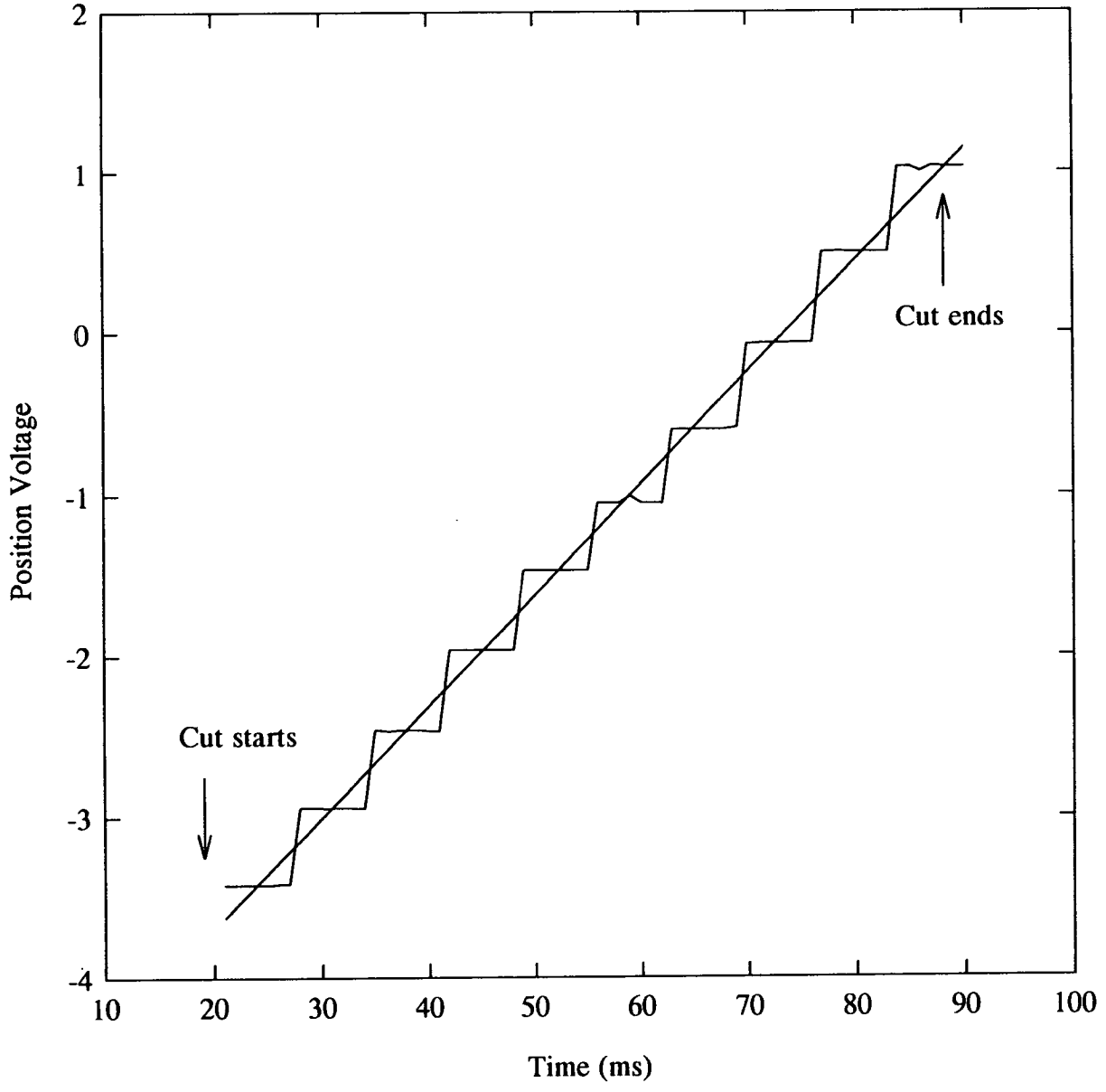

Figure 3.3. Position data for one test

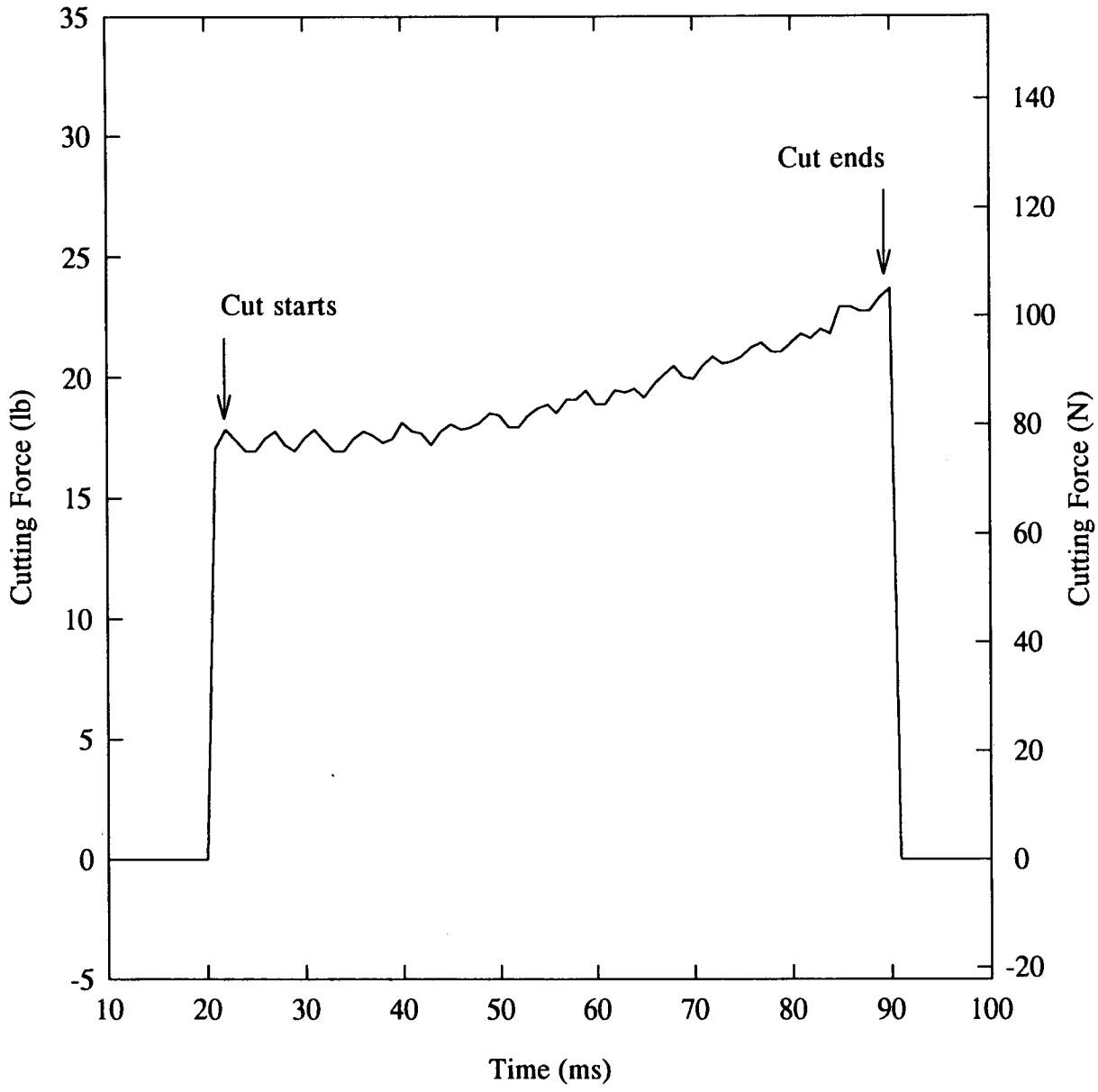

Figure 3.4. Cutting forces on the blade (velocity = 10 mph)

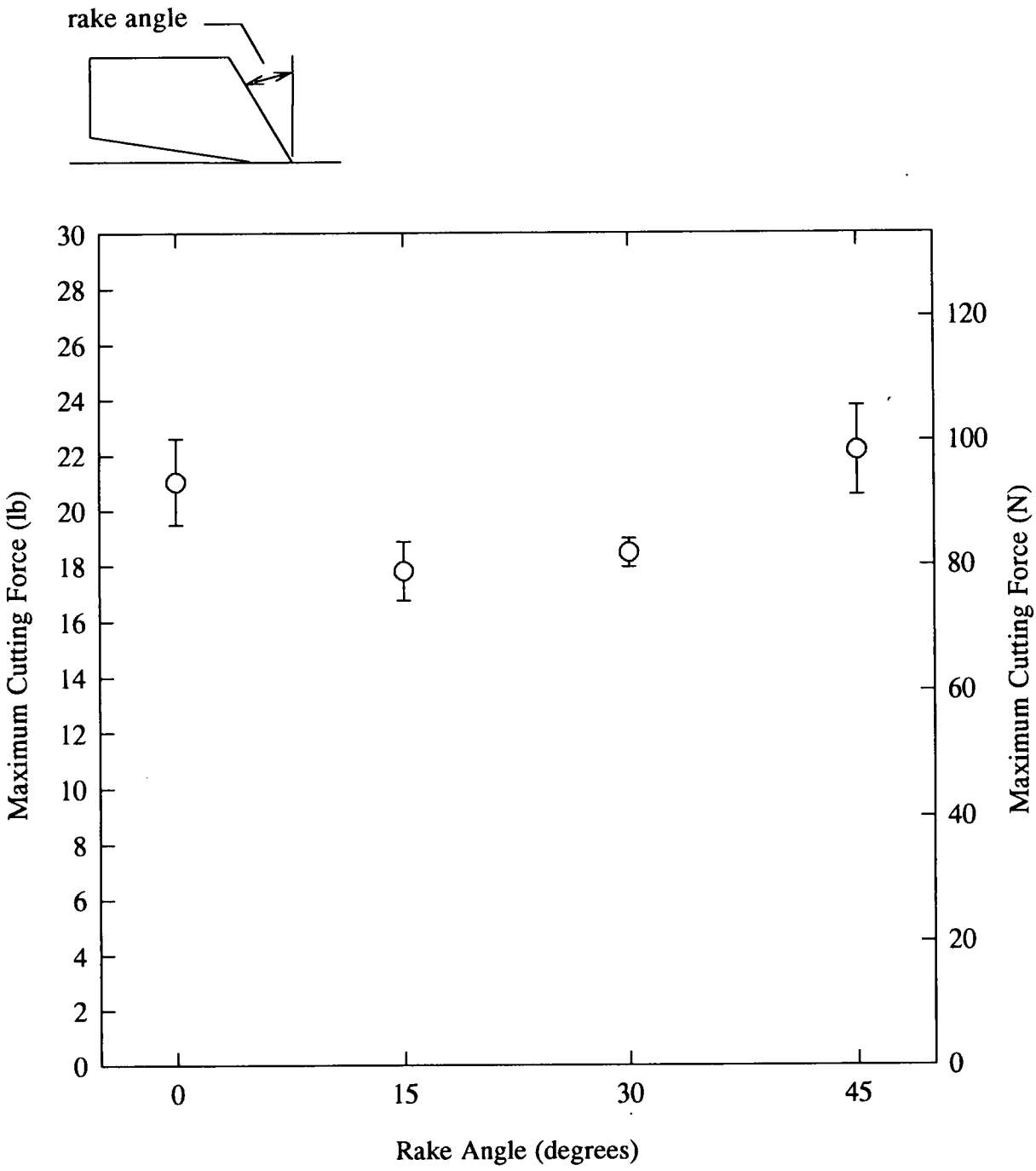

Figure 3.5. Maximum cutting forces for various rake angles

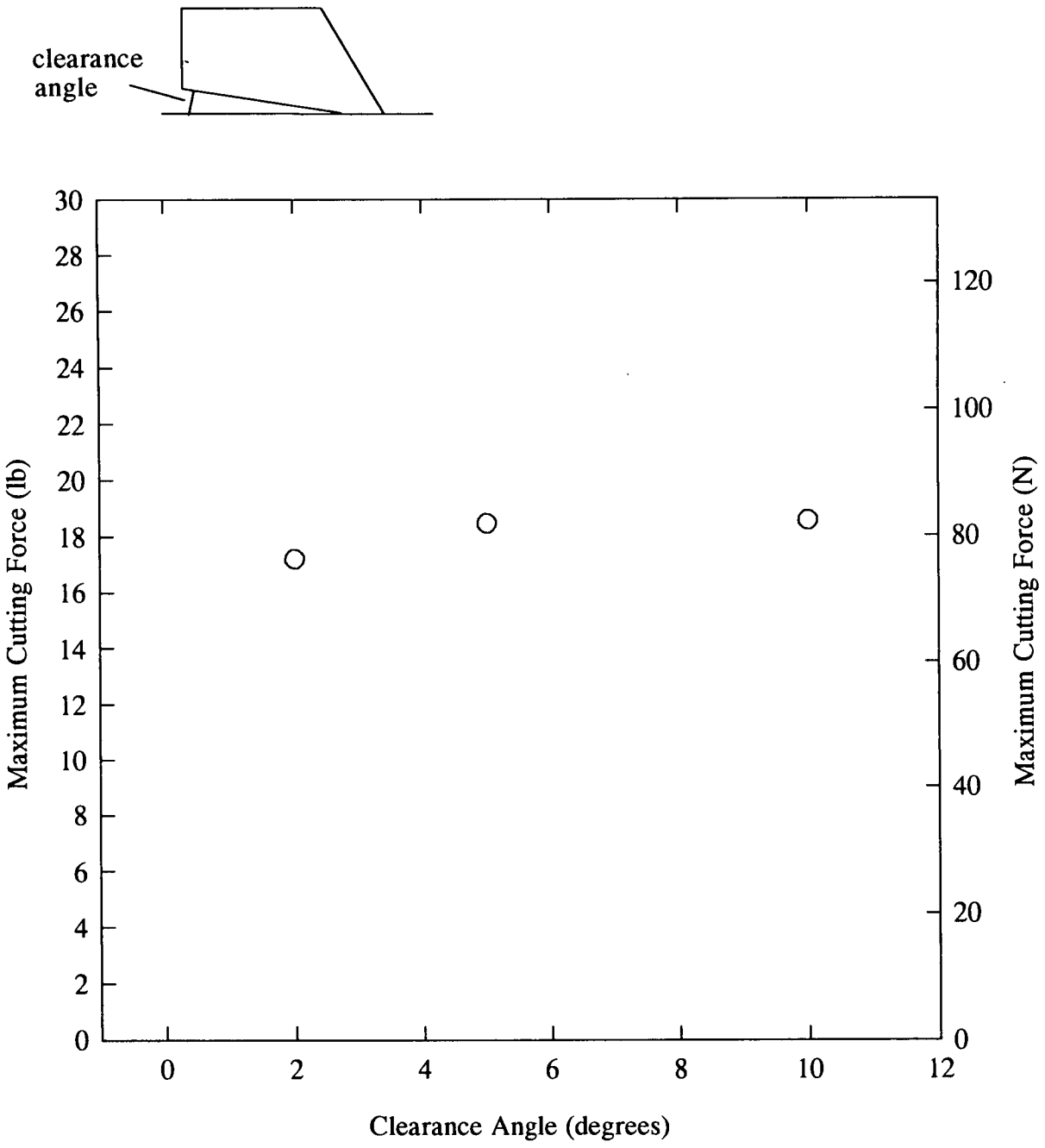

Figure 3.6. Maximum cutting forces for various clearance angles

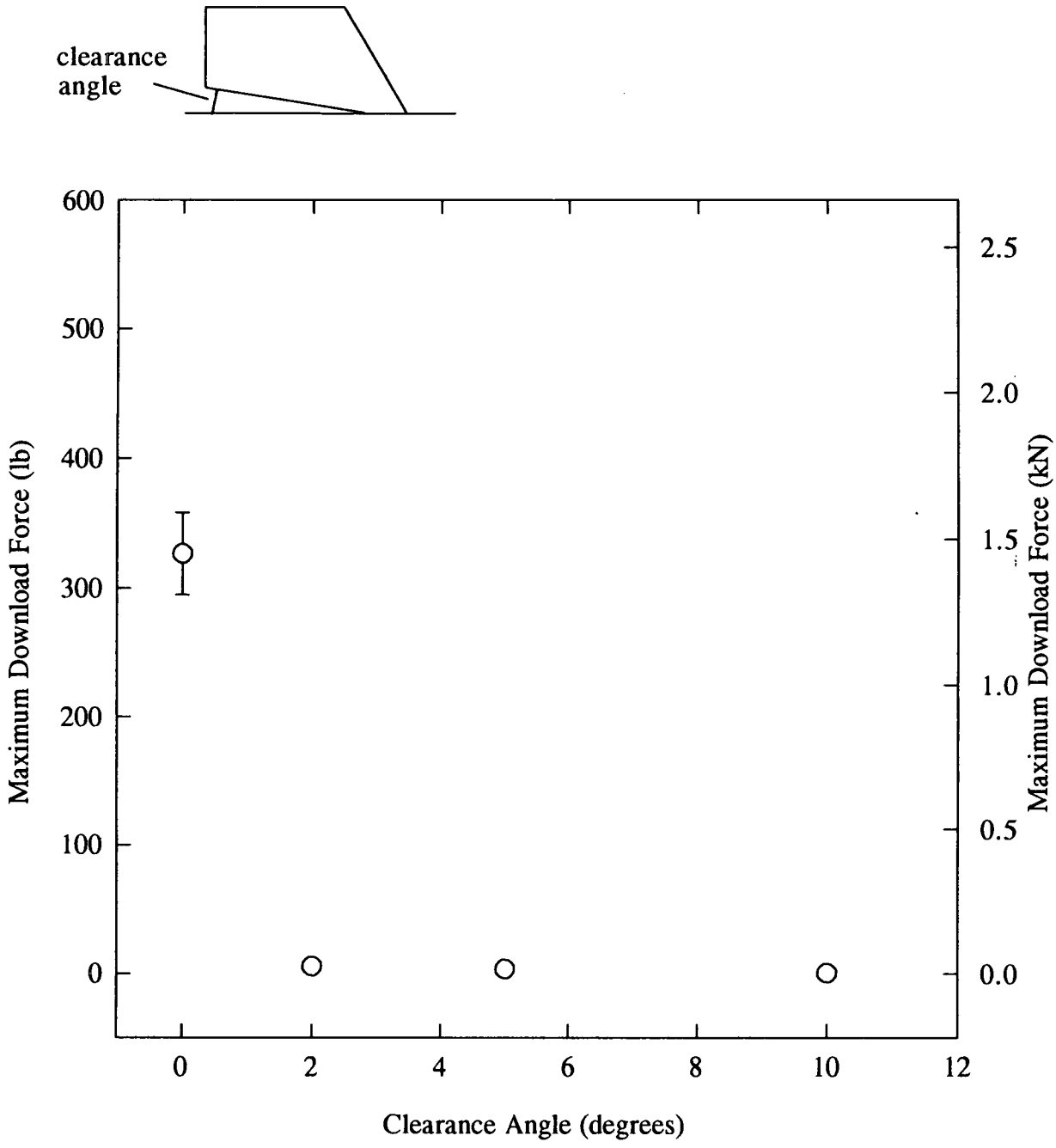

Figure 3.7. Maximum download forces for various clearance angles

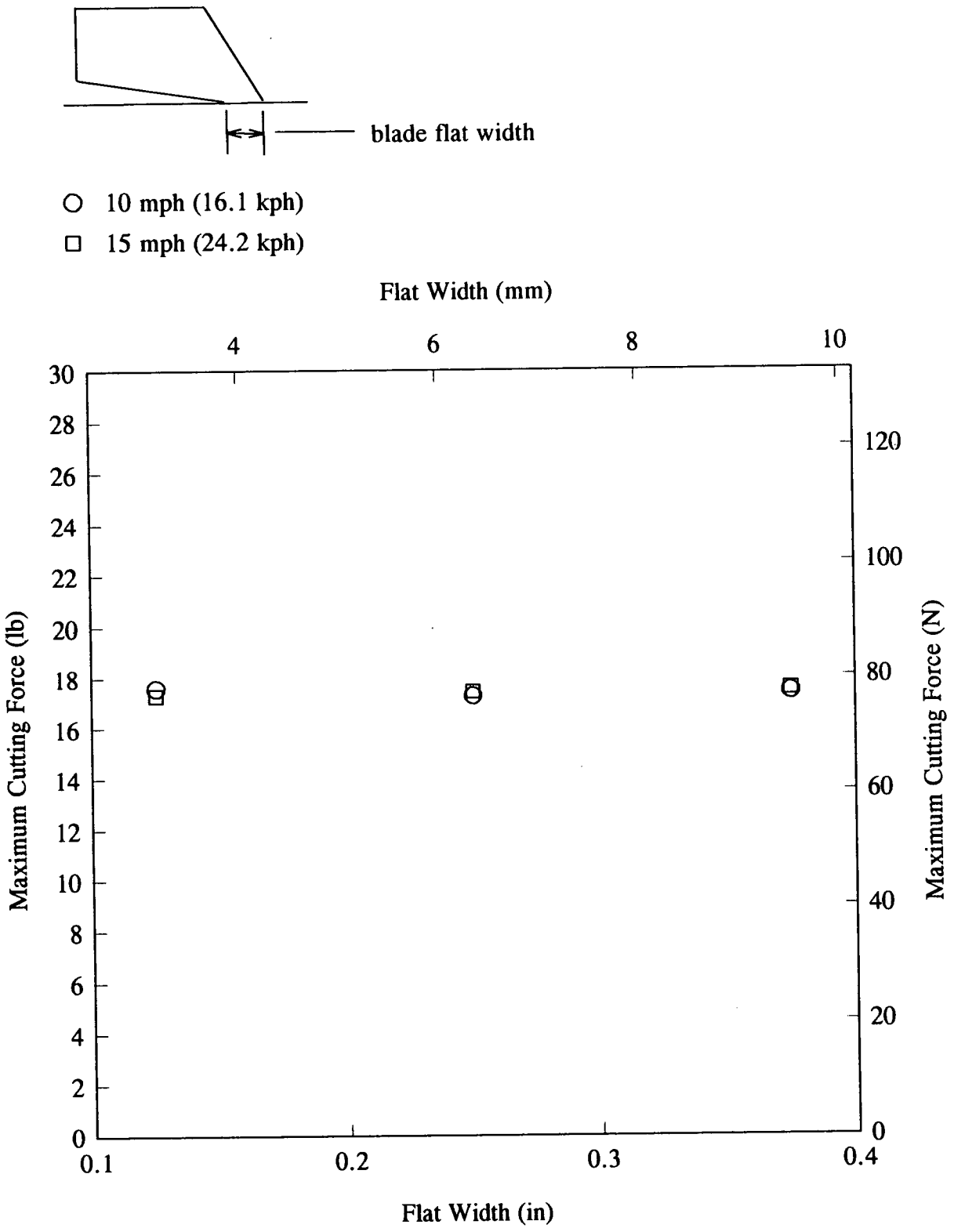

Figure 3.8. Maximum cutting forces for three blade flat widths

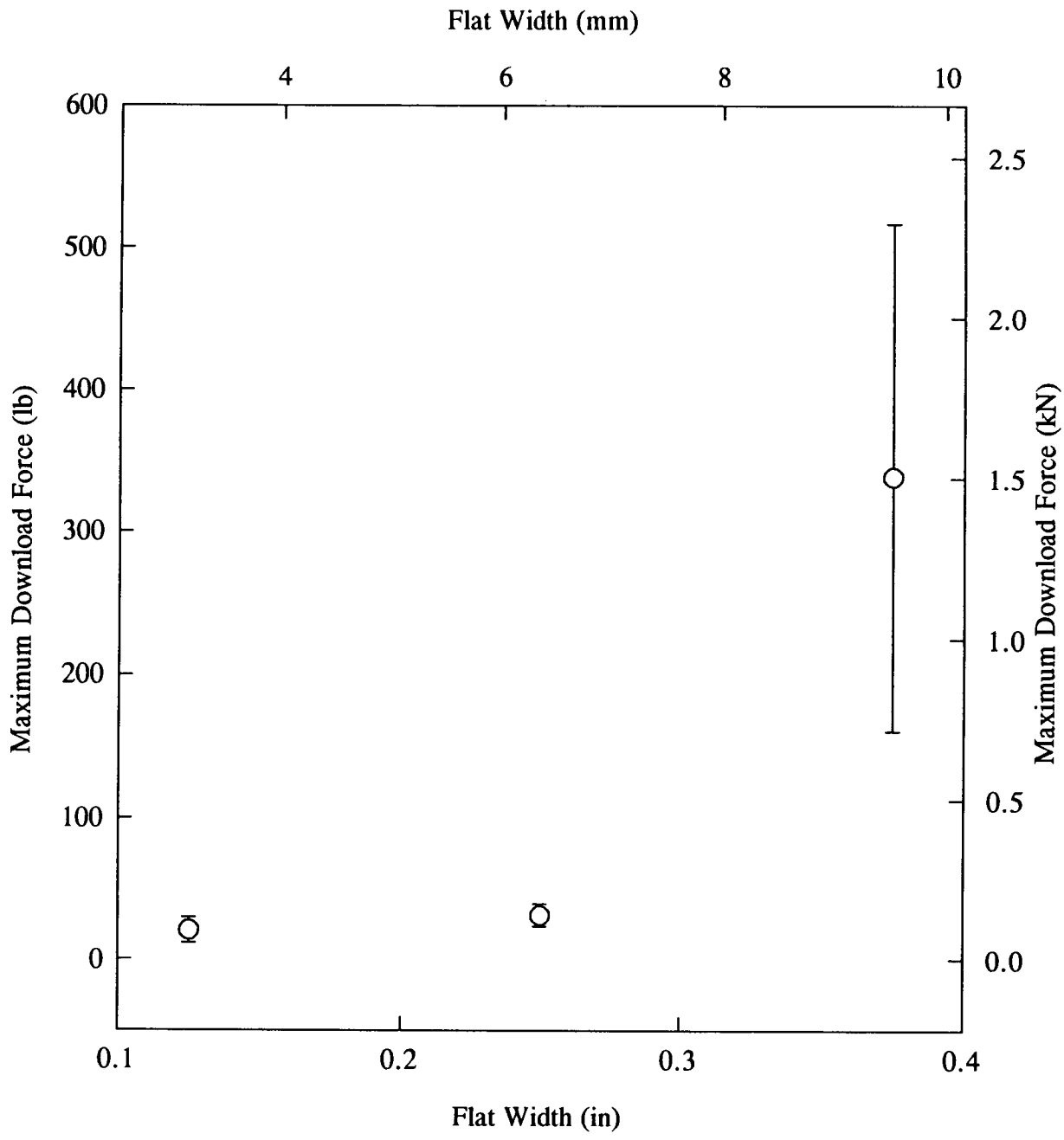

Figure 3.9. Maximum download forces for three flat widths

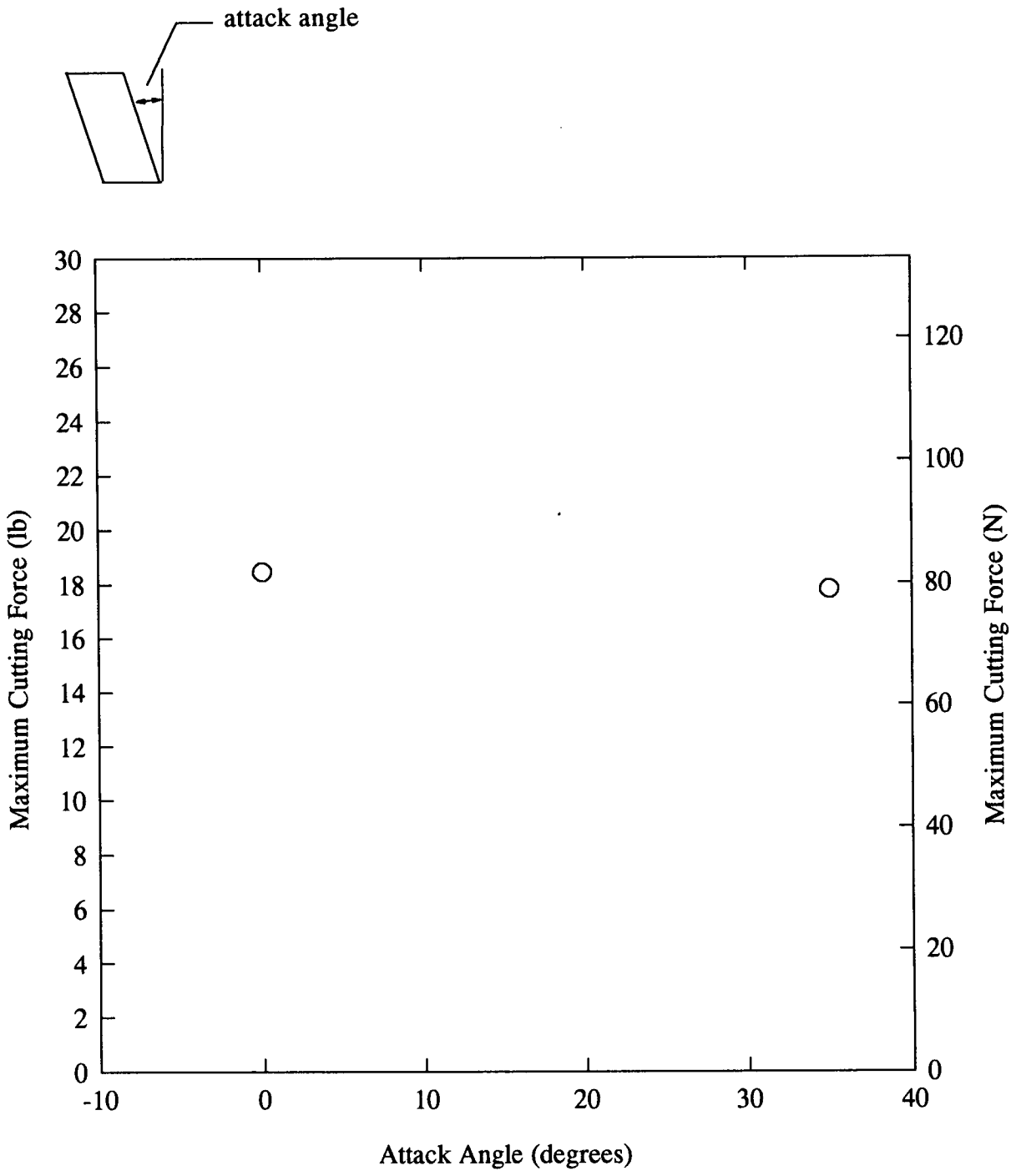

Figure 3.10. Maximum cutting forces for two attack angles

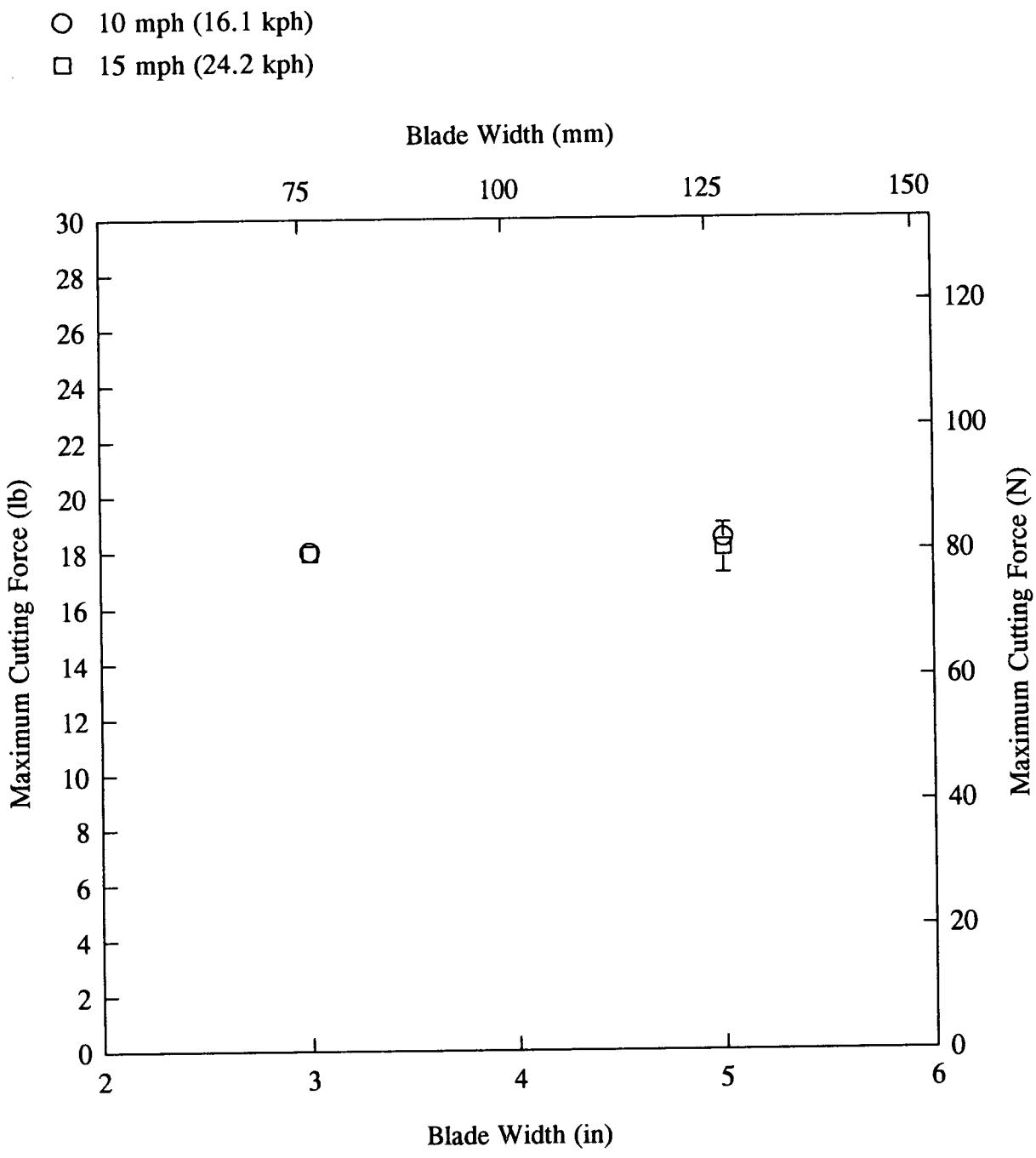

Figure 3.11. Maximum cutting forces for two blade widths

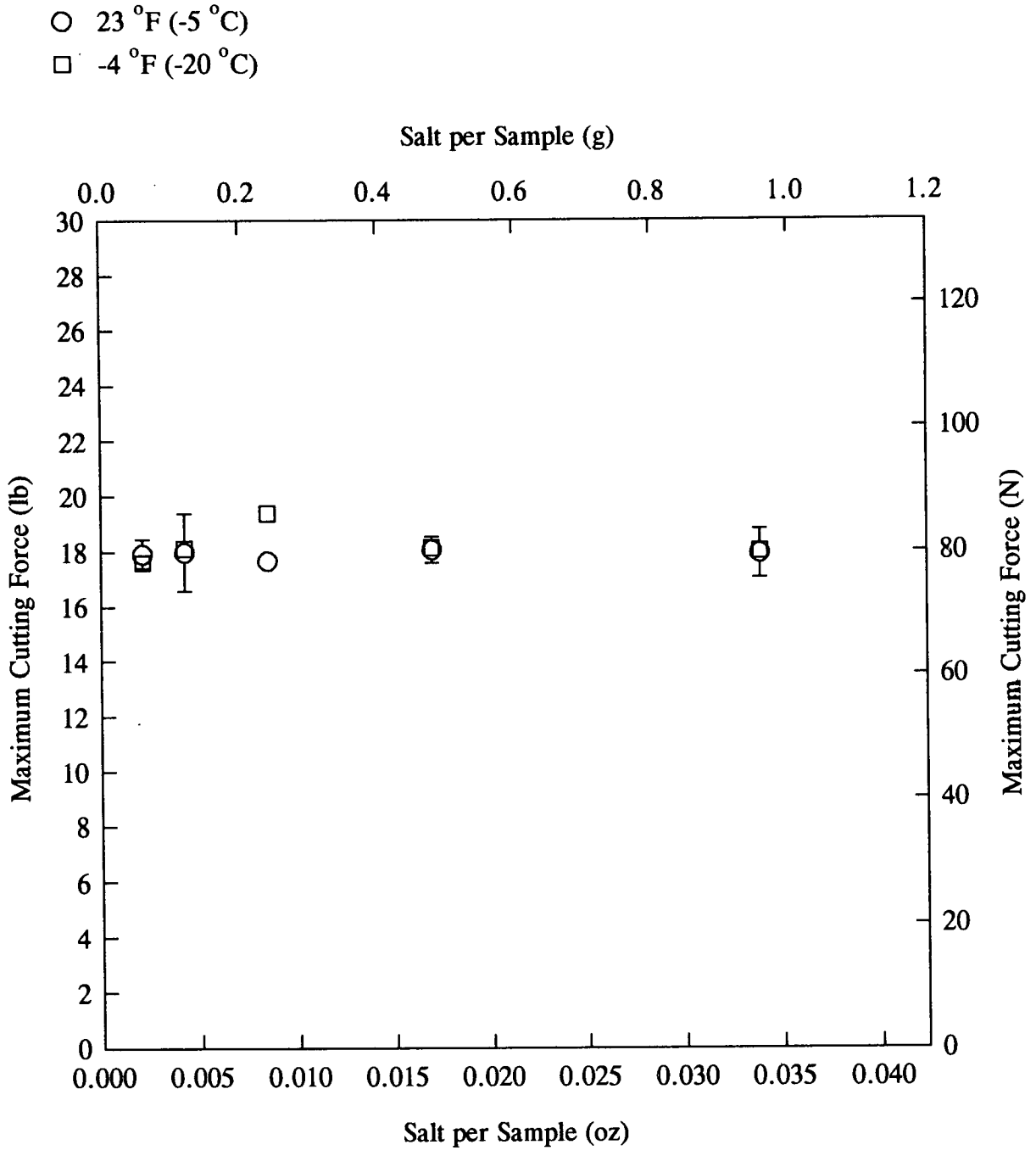

Figure 3.12. Maximum cutting force for five quantities of salt

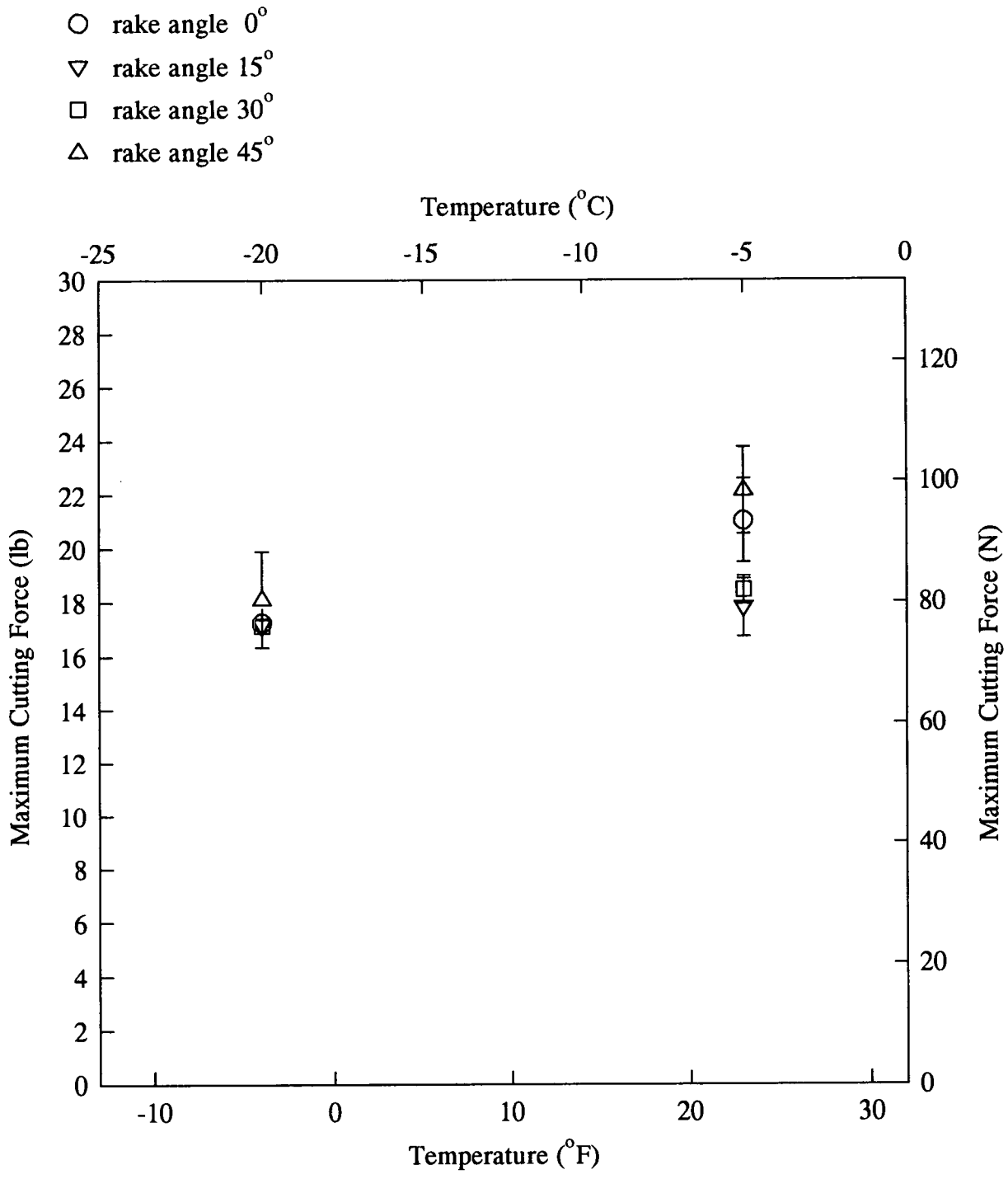

Figure 3.13. Maximum cutting force for four rake angles at two temperatures

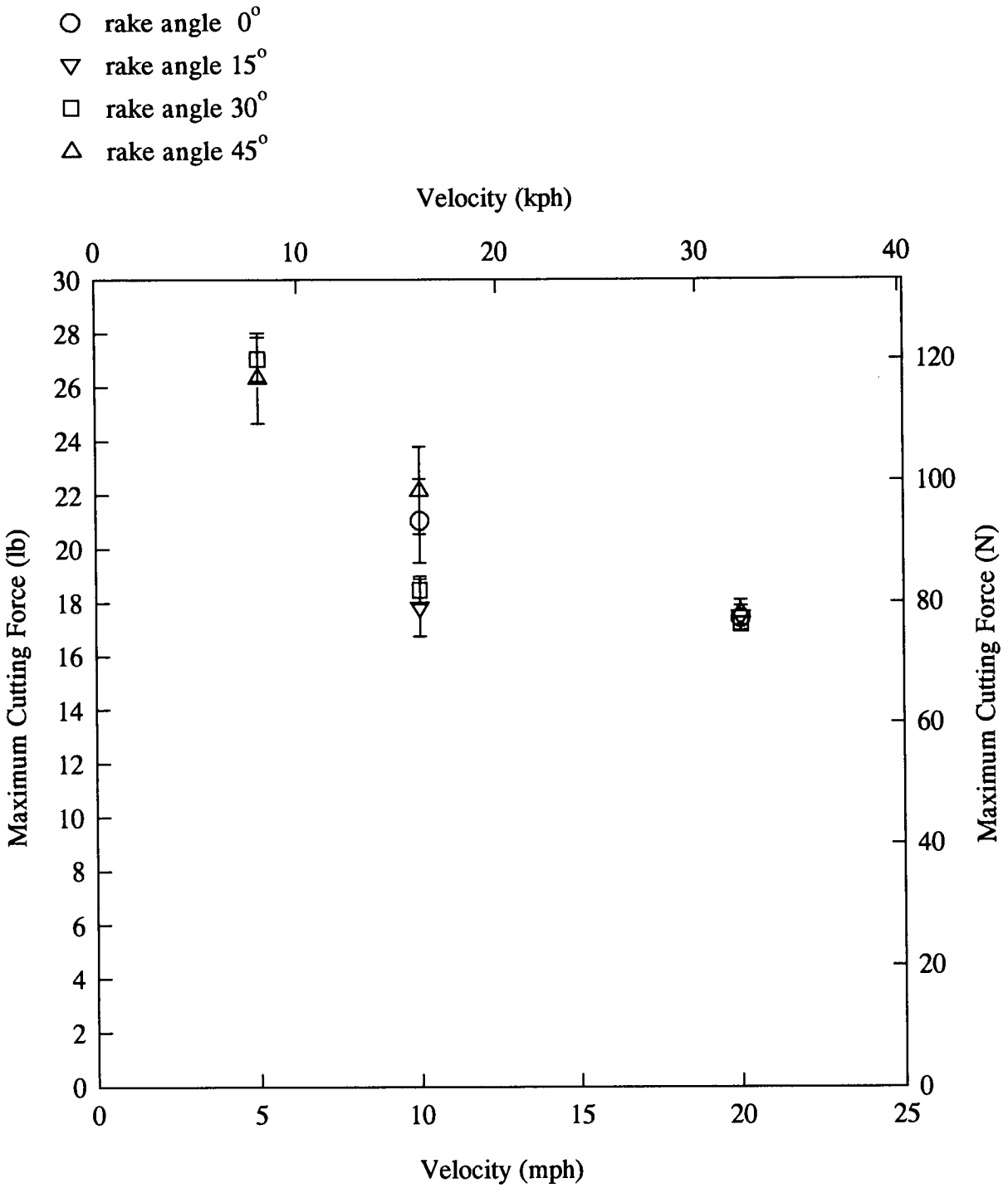

Figure 3.14. Maximum cutting force for various levels of cutting velocity

4

Discussion of Results

4.1 Introduction

Discussed herein are the implications of the test results. These results were used in the design process for the prototype blade, which was subsequently tested in the field (Chapter 5).

4.2 Base Line Tests

Baseline tests were conducted at four rake angles with fixed 5° clearance angle, 0° attack angle, 5 in. blade width, and 0 in. flat width. As can be seen in Figure 3.5, the maximum scraping forces decreased from 0° to 15° rake angle, then increased as the rake angle increased. A cubic regression to the data in Figure 3.5, shows that the optimal rake angle for baseline tests occurs between 15° and 30° angle of rake (about 18°). However, the differences observed from Table 3.1 are not significant at the 99% confidence level. Therefore, it can be stated that scraping force does not vary significantly with rake angle. This may appear somewhat surprising in that the rake angle was thought to play a significant role in clearing debris away from the cutting edge during field operations. In the laboratory, where only 12 in. (30.5 cm) of ice was cut, there was not sufficient debris generated to cause any significant force effect.

4.3 Clearance Angle and Blade Flat Tests

In clearance angle tests, blades with a rake angle of 30° and an attack angle of 0° were used. It is shown in Figure 3.6 that the maximum cutting forces increased slightly as the clearance angle increased from 2° to 5°, then was constant until a 10° clearance angle. It should be noted that tests with 0° clearance angle failed (the blade stopped on the top of the pavement sample during ice scraping and did not scrape over the whole sample) due to the very high download experienced. Thus, the maximum cutting force for the 0° clearance angle could not be obtained in this study (it might be obtained if more powerful equipment were used).

It is, however, clear that a good edge for ice cutting requires a non-zero clearance angle. Because not much difference in the cutting forces between clearance angles of 2° and 10° was observed, and because of the failure of tests for the 0° clearance angle, more tests involving clearance angles between 0° and 2° would be needed to understand this phenomenon more fully. At the 99% confidence level, there is a significant difference between 2° and 5° clearance angles. However, the change is slight and greater changes are expected from 0° to 2°.

The downforce was measured by the base load cells, which were placed under the rear supporting roller. As Figure 3.7 shows, the downforces for the 0° clearance angle were much larger than those for the other clearance angles. Furthermore, the variation observed in download between 2° and 10° clearance angle was significant at both 95% and 99% confidence levels.

The tests on the effect of flat width were performed at two speeds. Figure 3.8 shows that there was no significant variation in maximum horizontal cutting force with flat width. However, Figure 3.9 shows that the download forces differed dramatically with flat width. The maximum downloads increased with increasing flat width. Those for 3/8 in. (0.95 cm) flat width were above 100 lb (446 N) which reduced the speed of the sled significantly during cutting. When the flat width covered the whole bottom blade area (0° clearance angle), the blade could not go through the pavement sample (as discussed above). It is obvious that the download is of considerable importance. If the download in a real ice cutting situation became excessive, control over the truck or vehicle would be lost. Accordingly, further study in this area would be fruitful.

4.4 Attack Angle Tests

Only two attack angles were considered (0° and 35°). As Figure 3.10 shows, there was no significant variation in the horizontal cutting force between 0° and 35° attack angle tests. It is shown in Table 3.6 that the maximum side load experienced by the cutting edge was about 1.1 lb (4.91 N), which was very small. It cannot, however, be concluded that the intermediate attack angles have little or no effect on the cutting force. Further study might examine loads at such intermediate angles. The lack of effect observed in these tests, which is somewhat surprising when compared to the indications from common practice that a non-zero attack angle is much better at cutting ice, almost certainly arise from the fact that there was little or no debris buildup during the tests. As noted above for the rake angle results, the short test length almost certainly leads to this result.

4.5 Blade Width Tests

Like the attack angle tests, the blade width tests had the same geometrical parameters as the base line tests except for the two blade widths. It is evident from Figure 3.11 that variation

of the maximum scraping force between the 3 and 5 in. (7.62 and 12.7 cm) blades was not significant. However, if the force per unit width of blade in contact with the ice is considered, higher forces were experienced with the 3 in. (7.62 cm) blade. This is consistent with the somewhat more complex stress state the narrow blade would cause at its ends, implying more force per unit width to scrape.

4.6 Pretreatment Tests

Pretreatment tests were conducted at both 23°F and -4°F (-5°C and -20°C) using a cutting edge with a 30° rake angle, a 5° clearance angle, and a 0° attack angle. Five quantities of salt (sodium chloride) were used in the tests. There was no significant difference of the maximum scraping forces for these quantities of salt (Figure 3.12).

This result is very surprising, since salt is generally considered an excellent anti-icing agent. Undoubtedly, further work is required in this area, but it is possible that the diffuse and uniform manner of applying the salt had a strong influence on the results. In the field, salt is applied in the form of pellets or granules, which provides a locally high concentration of salt far above the levels tested here. These local concentrations may be the way in which salt acts effectively to weaken ice on the pavement. There is a strong probability that the sample preparation technique affected the results.

4.7 Temperature and Cutting Velocity Tests

Although testing has only been performed at 23°F and -4°F (-5° and -20°C), there was little observable difference between the results obtained, as shown in Figure 3.13. This is an encouraging practical result, in so far as it suggests that there is little reason to consider developing different approaches for removing ice at different temperatures. Obviously, as temperatures increase above 23°F (-5°C), the ice problem will diminish somewhat due to melting and sublimation.

As can be seen from Figure 3.14, cutting force diminished with increasing velocity. This variation was significant at the 95% confidence level, and has the same trend as found at lower velocities by Nixon, DeJong and Chung (1993). However, the trend should not be extrapolated to high velocities.

4.8 Ice Cutting Model

From the observations made in the tests described herein, it is possible to develop a tentative model for the failure of ice under cutting. The tests show that ice is fractured into very small particles during cutting. It appears that the ice is crushed by compressive forces

generated ahead of and beneath the cutting edge. Figure 4.1 shows a truck cutting ice, the same truck used in the field tests (Chapter 5). This picture shows that ice fragments are ejected both before and behind the blade, which suggests that there are two zones of failed ice Figure 4.2. Ice in zone 1 is ejected upwards, before the blade. Because the ice is so finely fractured, there is relatively little friction between the blade and ice and thus rake angle has a minimal effect on the force. The ice in zone 2 is also fractured, but in order to clear, it must pass underneath the cutting edge. Upon fracturing, the ice takes up more volume than in its unfractured state, and thus requires some clearance in order to pass beneath the edge. If this clearance is not available the broken ice fragments must be recompressed by the edge, resulting in a high downforce. This model is obviously very preliminary, and requires significant examination, both by way of testing and also by some finite element modeling.

4.9 Summary

The tests performed show the importance of clearance angle and flat width. They also show that rake angle, attack angle, and temperature have minimal effect on the force required to cut ice from pavements. While further work is need in a number of areas, these results indicate several areas in which current technology can be improved.

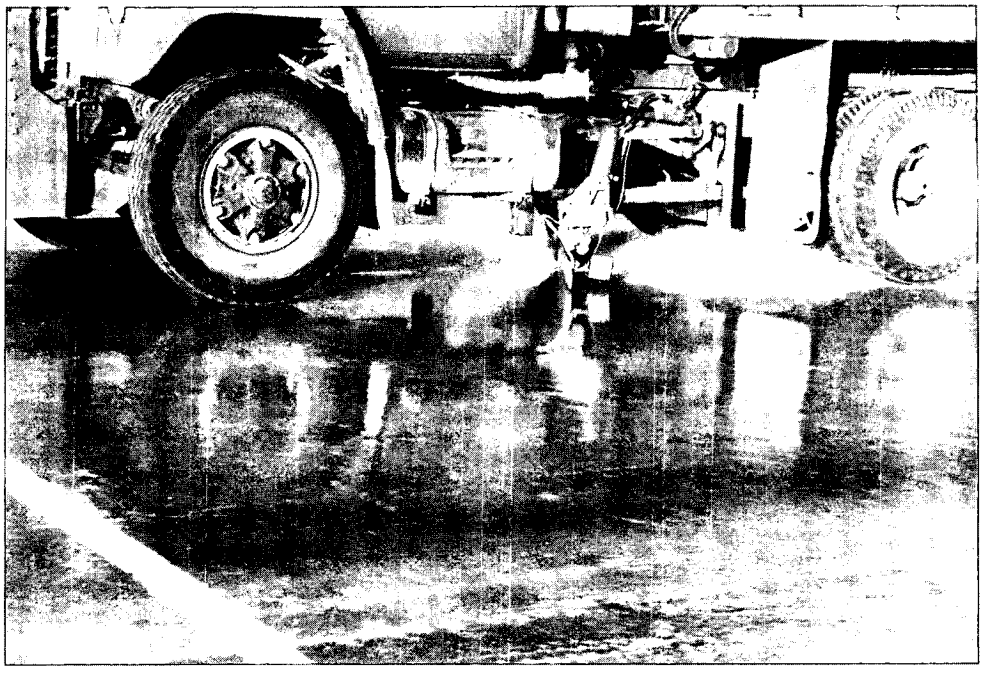

Figure 4.1. A truck cutting ice

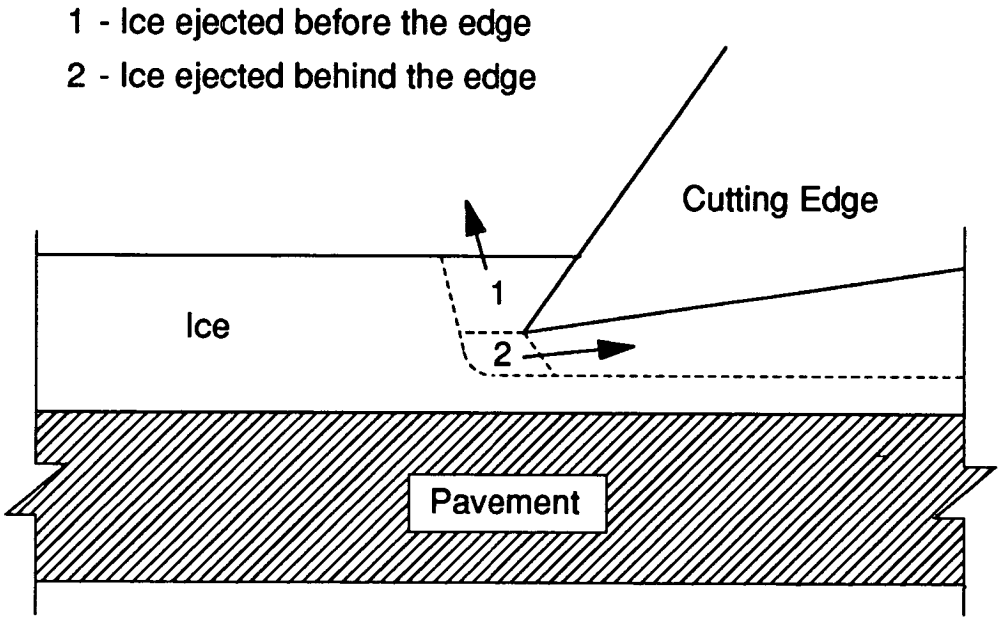

Figure 4.2. Tentative model of ice cutting

5

Field Tests of Prototype Blade

5.1 Blade Design Methodology

In developing the design for the prototype blade, two concerns were paramount. First, the blade had to make the best use of the results found in the laboratory study. In particular, some way of maintaining a non-zero clearance angle was required, since this appeared to be the key parameter from the laboratory study. The second concern was ensuring that the cutting edge could withstand the shock loading common to ice removal (when, for example, a pavement joint is encountered). Other concerns, such as wear characteristics and cost, were not given great weight in the design process. Studies in these areas were beyond the scope of this study.

The prototype cutting edge is different in a number of ways from existing cutting edges. In particular, the carbide insert is mounted flush with the front face, so that carbide is exposed to the ice directly (Figure 5.1). The insert is somewhat softer than typical carbide inserts for cutting edges, so as to obtain better shock resistance. Specifically, the insert has a Rockwell A hardness in the range 83.7 - 84.7, compared with 87.6 - 89.0 for regular carbide inserts. The non-zero clearance angle (shown in Figure 5.1), should remain in place during the life of the blade. No estimate of blade lifetime was determined, for reasons indicated above. Four identical cutting edges of this type (each 4 ft. (1.22 m) long) were obtained from Kennametal Inc., Latrobe, PA. One of these edges is shown in Figure 5.2.

5.2 Field Test Apparatus

Tests were conducted using a 25 ton (22.7 t) truck with an underbody plow blade, supplied by the Iowa Department of Transportation (IDoT) for use in their project HR-334. The truck is shown in Figure 5.3. The underbody blade can be adjusted to a variety of orientations. The vertical position and down pressure can be controlled for the left and right sides of the blade by means of a hydraulic cylinder located on each side of the blade. The blade angle (the angle the cutting edge makes with the pavement) is controlled by a hydraulic cylinder on each end of the blade. These two cylinders are connected in parallel so the blade angle is

uniform across the full length of the blade. Blade angle and down pressure can be adjusted independently. Further, it should be noted that the blade angle referred to in this chapter is different from the rake angle referred to previously. The rake angle refers spefically to the geometry at the tip of the cutting edge. The blade angle refers to the whole blade. It is also possible to adjust the attack angle of the blade from perpendicular to the direction of travel to an angle up to 30° from perpendicular. These angles are shown in Figure 5.4.
The cutting edge is attached to the blade support as seen in Figure 5.5. This allows for easy replacement of the cutting edge with different geometries so that the effectiveness of different cutting edges can be compared. For this series of tests three different cutting edges were used. The first is the standard mild steel blade 0.75 x 5 x 96 in. (1.9 x 12.7 x 244 cm) which came with the truck. The second is a commercially available blade with a carbide insert. The third cutting edge is the prototype described above. The three blades are shown in Figure 5.6.

The loads that the blade experiences during scraping were recorded by 0-3000 psi (0-20 MPa) pressure transducers (International Pressure Products ST-420) connected by a T section to the hydraulic supply lines of the cylinders. A transducer is located in each of the vertical motion cylinders to measure the downward pressures applied to each side of the blade. Another transducer is located in the supply hose for the cylinders which rotate the blade angle. This gauge records the pressures applied to the blade in the horizontal direction. The angle that the cutting edge makes with the pavement is measured with an inclinometer, a Schaevitz Angle Star Protractor System. The inclinometer is located on the left side of the blade in a box that can be seen in Figure 5.7. The velocity of the truck is determined by a fifth wheel located at the rear of the truck. It uses a DC tachometer generator that provides a linear relationship of speed to voltage which allows the speed to be determined with an accuracy of 0.1 mph (0.045 m/s).

Also on the truck is a load cell to measure the force required to pull a weighted sled behind the truck. This provides information about the friction changes in the ice after it had been cut by the blade. The sled (Figure 5.8) weighed 330 lb (149 kg) and was pulled at a constant velocity across the ice both before and after a test.

Data from the sensors are collected on a portable computer, a Kontron IP Lite, chosen because it is shock rated for operation up to 5 G (Figure 5.9). This shock rating is needed to guarantee normal data acquisition because the truck bounced a lot during testing. A Metrabyte DAS-8 analog-to-digital board was used with CODAS data acquisition software by Dataq Instruments. Data are written to the computer's hard drive during testing and are examined and analyzed after testing at the IIHR ice laboratory. Power for the computer and sensors is obtained from the truck batteries through a power inverter and filter system built at IIHR.

A 750 gallon tank of water in the truck is used to create the ice necessary for the testing. A 3 hp pump at the back of the tank delivers the water at 60 psi (0.4 MPa) to a spray nozzle located on a boom offset from the truck (Figure 5.10). The spray nozzle allows the water to

be sprayed uniformly over 20 ft. (6.1 m) of pavement.

5.3 Experimental Method

Testing took place at the spillway apron of the Coralville Reservoir, north of Iowa City, Iowa, when weather conditions were favorable. The temperature records for Iowa City over the last 100 years showed that testing conditions would be most suitable from mid-November hrough mid-March. Water from the Iowa River was obtained at the University of Iowa water treatment plant. Water and air temperatures were measured at the testing site. The water then was sprayed on the concrete, using the previously mentioned system, by driving back and forth over the testing area. The area covered was approximately 20 x 180 ft (6.1 x 55m). The truck travels at approximately 1 ft/sec (.305 m/s) during the spraying process. The water generally froze within 2 min., and the entire 750 gal (2840 l) was sprayed in 40 minutes. The ice hardened overnight and the testing took place the next morning. Sunny days with highs in the mid- to upper 20s (-5°C to -2°C) melted post-test ice by sunset. Temperatures then usually dropped below 20°F (-7°C) after 10:00 pm, at which time a new sheet was prepared. Warmer days pushed spraying time back as late as 3:00 am. After 3:00 am, there was not enough time for the ice sheet to harden, and if tests were performed, they might have provided erroneous results.

Water temperature affected the hardening time for the ice. For much of the winter it ranged from 33°F to 35°F (1°C to 2°C), which allowed for fast hardening times for the ice throughout most of the testing season. Near the beginning and end of the testing season, however, the river temperature could be as high as 50°F (+10°C). Water this warm caused very long hardening times for the ice, and could prevent testing altogether.
To improve traction of the tires during testing, the space around the tank in the truck bed was filled with gravel and the tank was filled with water. This gave the truck a total weight of 22 tons (19.98 t). Before testing, the air temperature, concrete temperature, ice thickness and ice condition were recorded, and the sled was pulled across the ice to measure friction. The angle of the blade was set. As the truck approached the ice sheet, the down pressure was applied to the blade. The tests were performed at approximately 15 mph (6.7 m/s) over the entire length of the ice sheet.

The ice sheet was examined and photographs were taken after each test. The overall effectiveness of the blade was determined by the thickness of ice that the cutting edge removed from the pavement as measured on site. The sled was again pulled across the ice sheet and the data from the load cell recorded by the computer. Tests were also videotaped to provide a visual record of the cutting edge performance during the test.
The testing parameters were the cutting edge, down pressure, and the angle of blade (different from the rake angle, as discussed above). For each of the three cutting edges previously described, tests were conducted at two values of down pressure, termed low (500 psi (3.33 MPa)) and high (1200 psi (8 MPa)) pressure. These values were set on the blade by increasing the down pressure to get within these ranges as displayed on the computer

screen in the cab. Blade angles were 0°, 15°, or 30°, measured back from the vertical. These values were set by using the display of the inclinometer in the cab and adjusting for the desired value. Because the angle of the cutting edge changed when the truck moved forward, it was set low, and, as the truck pulled ahead with the desired down pressure, the angle adjusted to the correct value.

The gauges were calibrated by means of a set of hydraulic jacks. The blade was first set in position, then the jacks were used to push against the blade in 500 psi (3.33 MPa) increments and the voltage of each gauge was recorded by the computer at each increment. The known pressures of the jacks could then be used to relate the voltage directly to a force and the calibration coefficient calculated. This was performed for both horizontal and vertical components of the blade.

Calibration of the inclinometer required measuring the blade angle with a protractor level for various angles and determining the calibration coefficient. The fifth wheel was calibrated by recording the time it took the truck to travel a known distance at different constant velocities and thus determining the calibration coefficient. The load cell for the friction sled was calibrated using a load cell calibration stand at IIHR.

5.4 Field Test Results

Tests performed with the standard blade showed that there were only a few places where the ice was completely removed from the pavement. Much of the ice was only partially removed or not removed at all. From measurements it appears that more ice was removed with a high down pressure and a 0° blade angle for this blade. At the high down pressure it was more difficult to maintain a constant velocity due to a loss of traction. A typical data output of the gauges for a test is shown in Figure 5.11.

Because the second and third cutting edges were not of the same geometry as the first, the 0° case could not be achieved and only the 15° and 30° cases could be studied. As with the standard blade, the second and third blades performed best at the smallest blade angle and highest down pressure. The second blade appeared to remove more ice than the first blade, and maintained its edge much better due to the carbide insert.

The prototype blade was tested last. The blade was able to remove up to half of the ice thickness (determined by measuring the ice thickness before and after cutting) across the entire 8 ft (2.44 m)length of the blade at a down pressure of 500 psi (3.33 MPa). At high down pressure the cutting edge removed nearly all the ice except for a small residual layer across the entire length of the blade.

In reviewing data from the tests, it is apparent that the loads do not provide the full story. Indeed, it appears that the higher the horizontal load is during a test, the more ice is removed. The horizontal load correlates very well with the depth of ice removed, though it

should be noted that no direct measurements have been made of cutting force as a function of depth of ice removed either in the laboratory or in the field. In addition to the horizontal force correlating with depth of cut, the vertical force also gives a good indication of the difficulty of the cut. The higher the vertical force, the harder it will be to control the vehicle, and the greater the likelihood of damage to the pavement. The tests show that two factors are important: the depth of cut, as indicated by the horizontal load; and the ratio of the vertical to horizontal load. If the latter is low, the truck is easily controlled. If the former is high, much ice is scraped.

Figures 5.12 through 5.17 show the horizontal and vertical loads for the three blades in the low pressure configuration at two angles (15° and 30°). From these test results it is apparent that the prototype blade gives the greatest depth of cut, has the best factor of controllability (ratio of vertical to horizontal forces), and provides significantly better ice scraping than either of the other two blades. Questions remain to be answered: What is the optimum blade angle and how does horizontal force correlate with depth of cut? Additional tests will be necessary to provide answers.

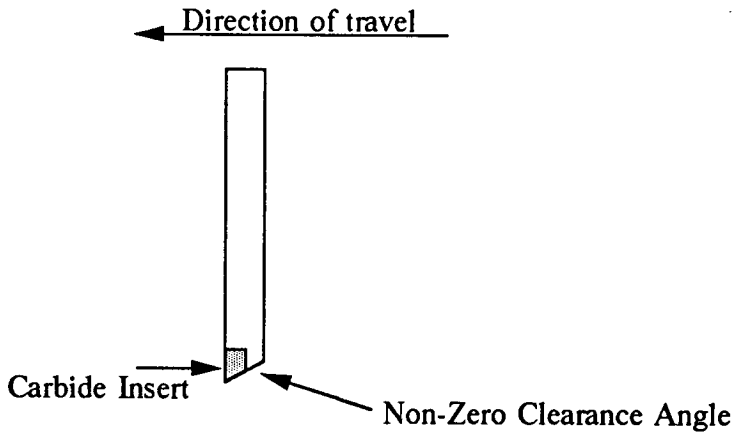

Figure 5.1. Design of prototype cutting edge

Figure 5.2. Prototype cutting edge

Figure 5.3. IDoT instrumented plowing truck

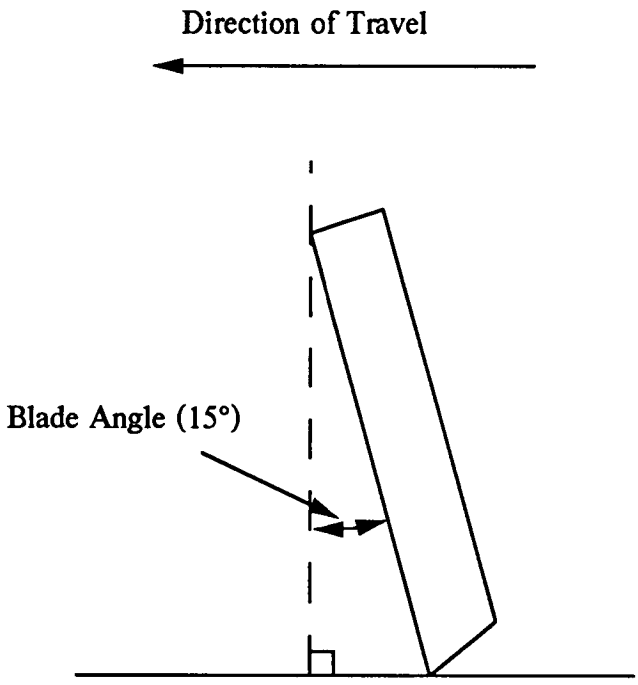

Side View of Cutting Edge.

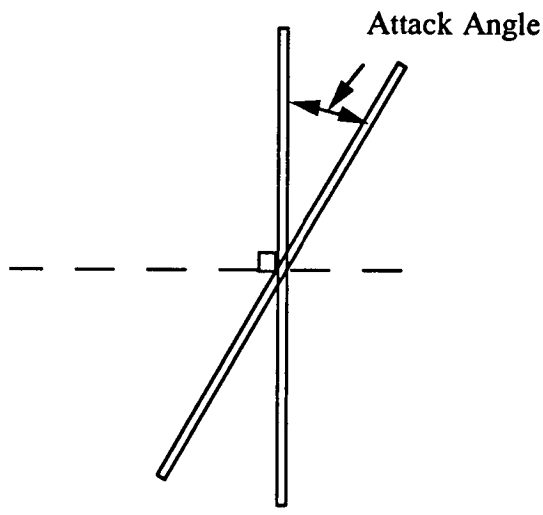

Top View of Cutting Edge.

Figure 5.4 Definition of blade angle and attack angle

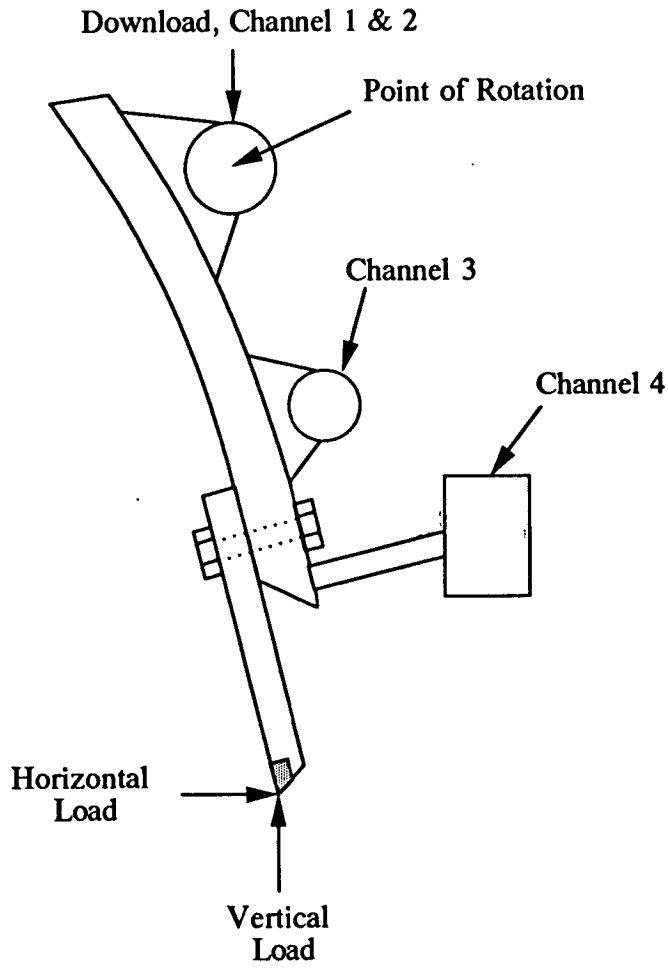

Figure 5.5. Attachment of cutting edge to blade support

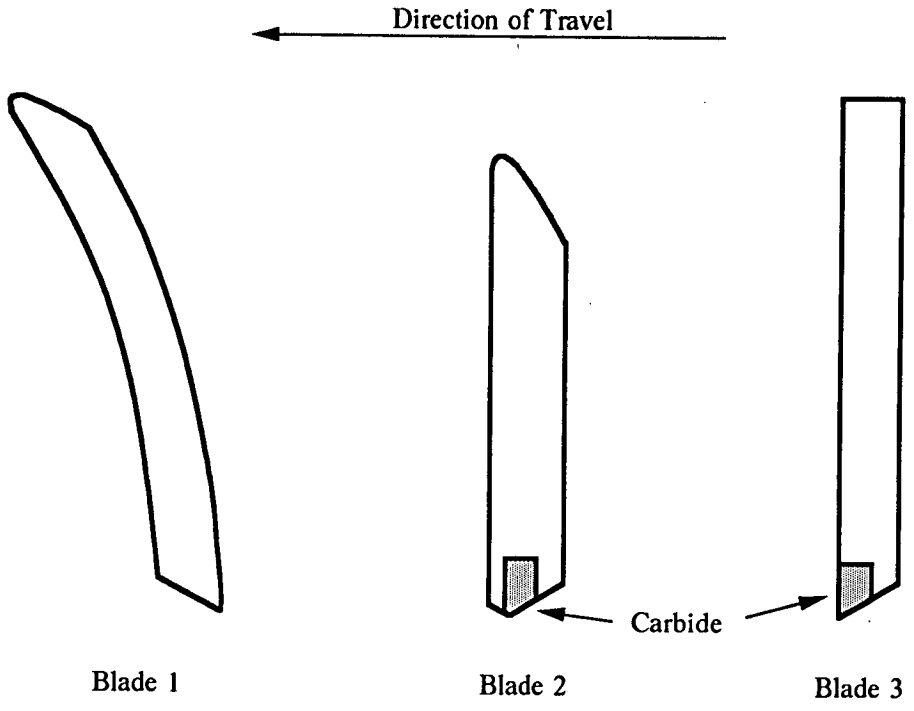

Figure 5.6. Schematic representation of three cutting edges

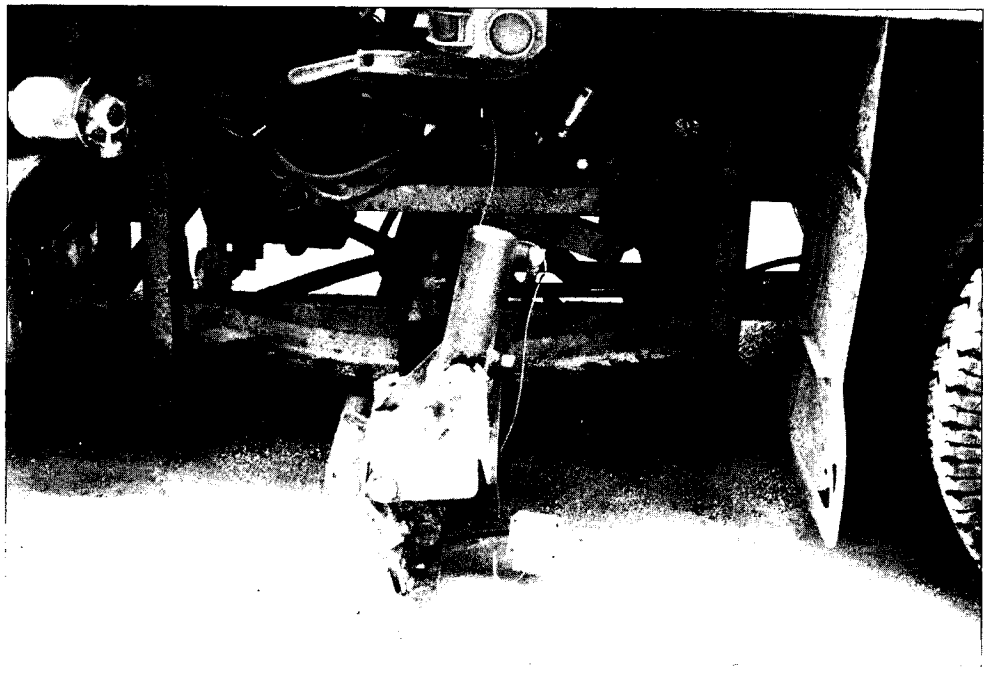

Figure 5.7. Cutting edge instrumentation

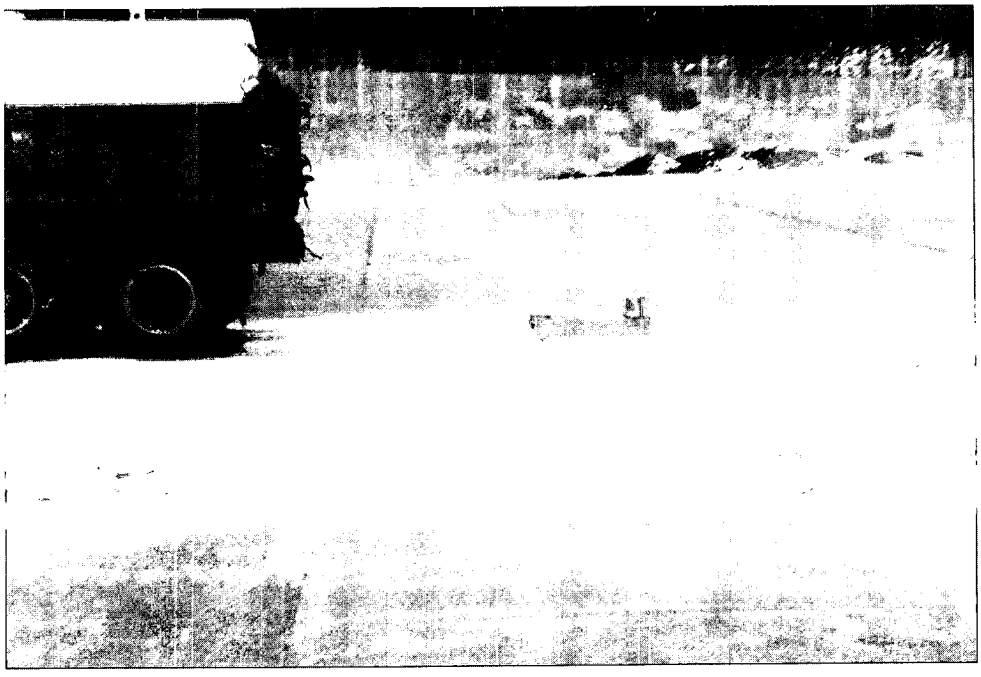

Figure 5.8. Friction sled

Figure 5.9. Test truck data acquisition system

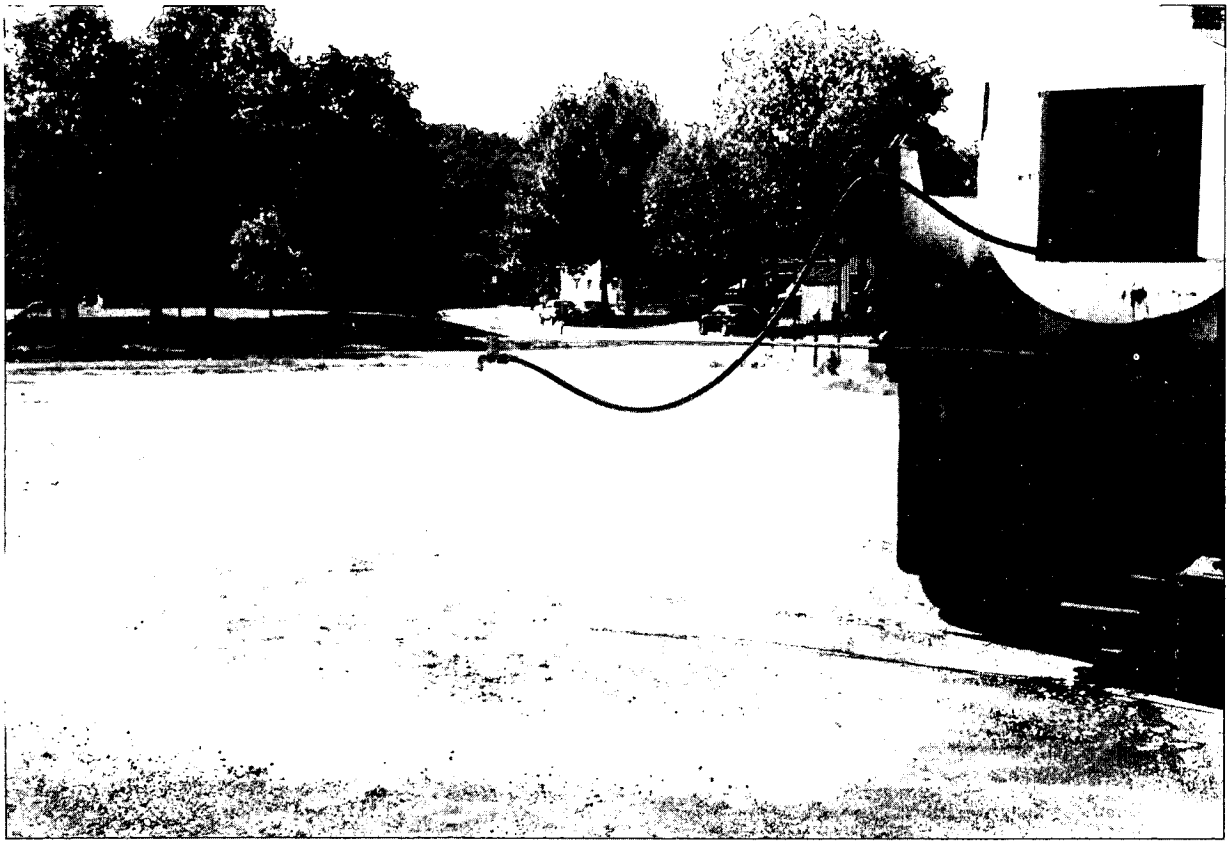

Figure 5.10. Test truck spray system

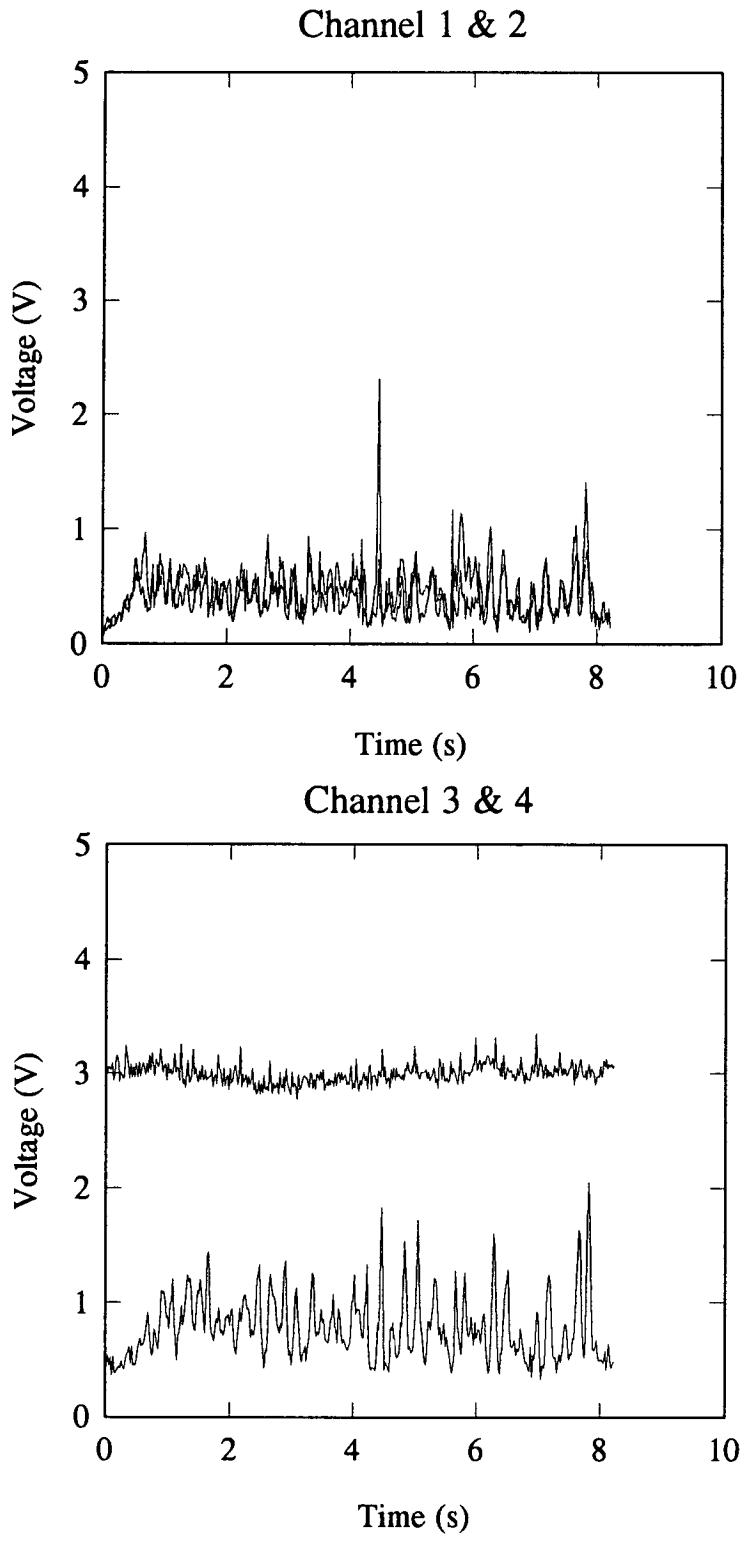

Figure 5.11. Raw data output from test of Jan 28, 1992

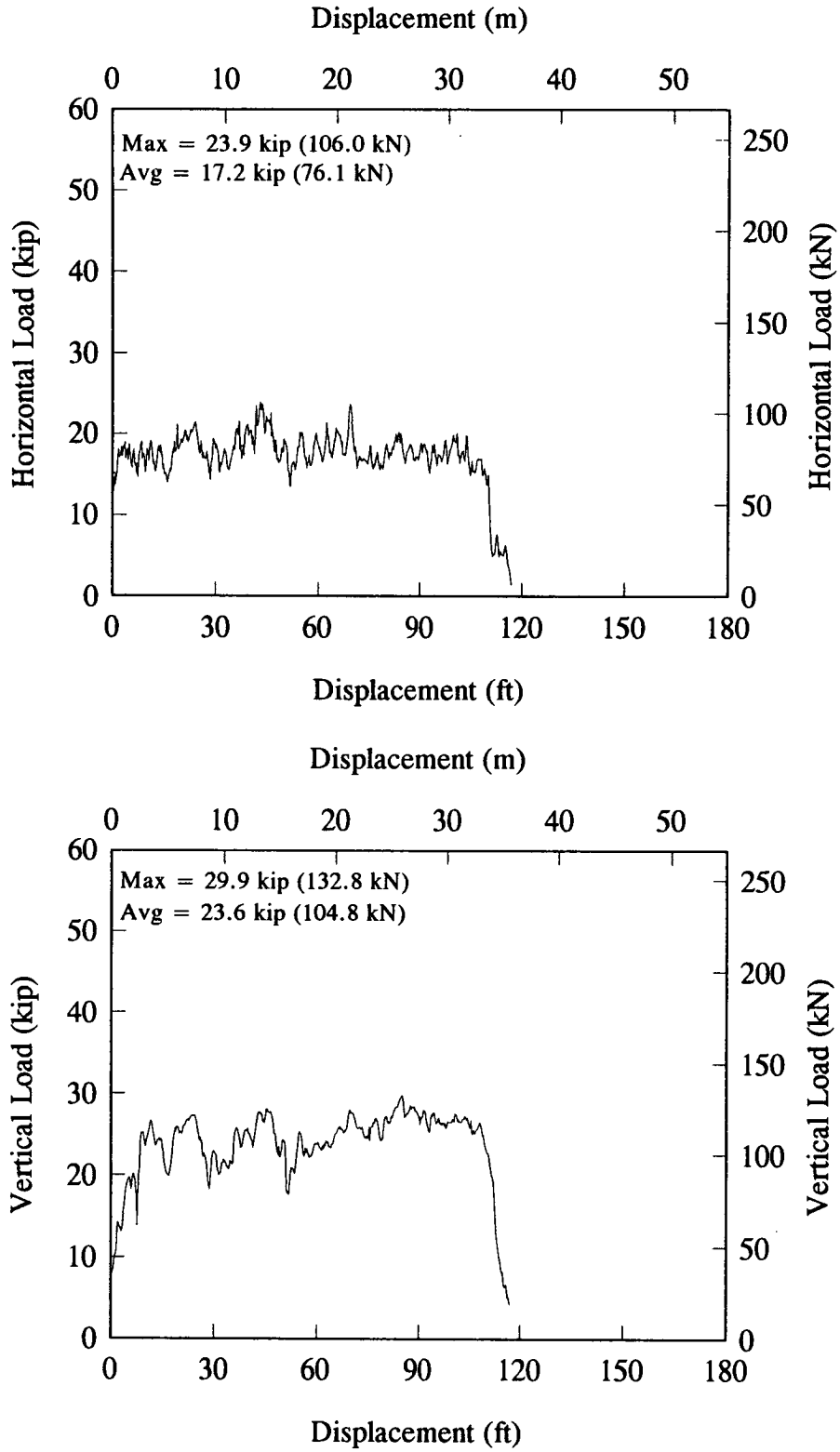

Figure 5.12. Horizontal and vertical force, cutting edge # 1, low pressure, 15° angle Test of Dec 4, 1991

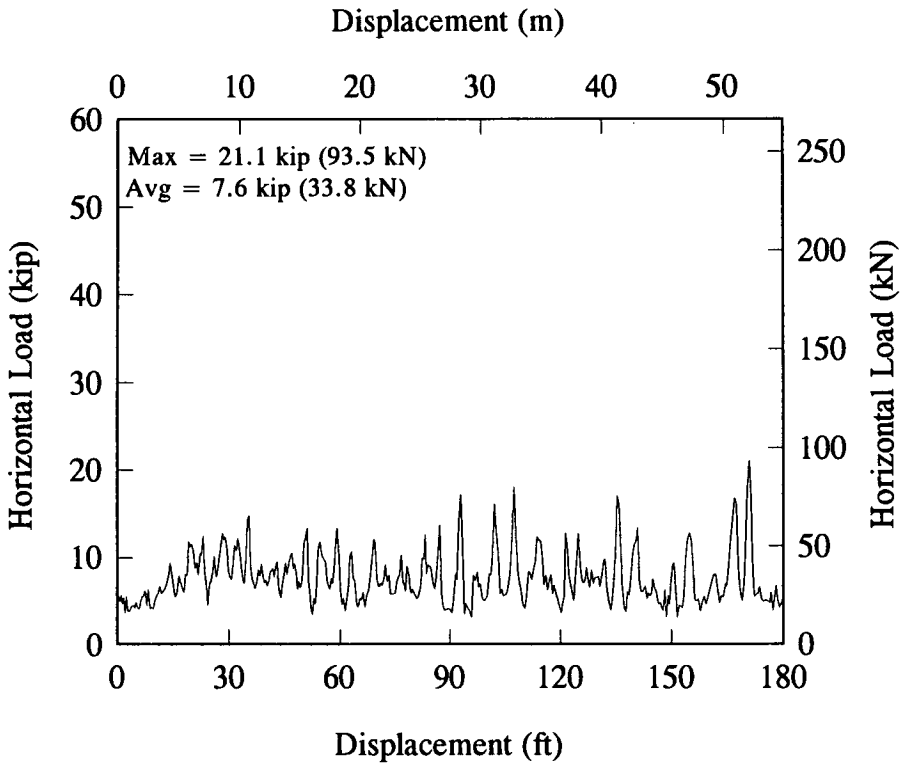

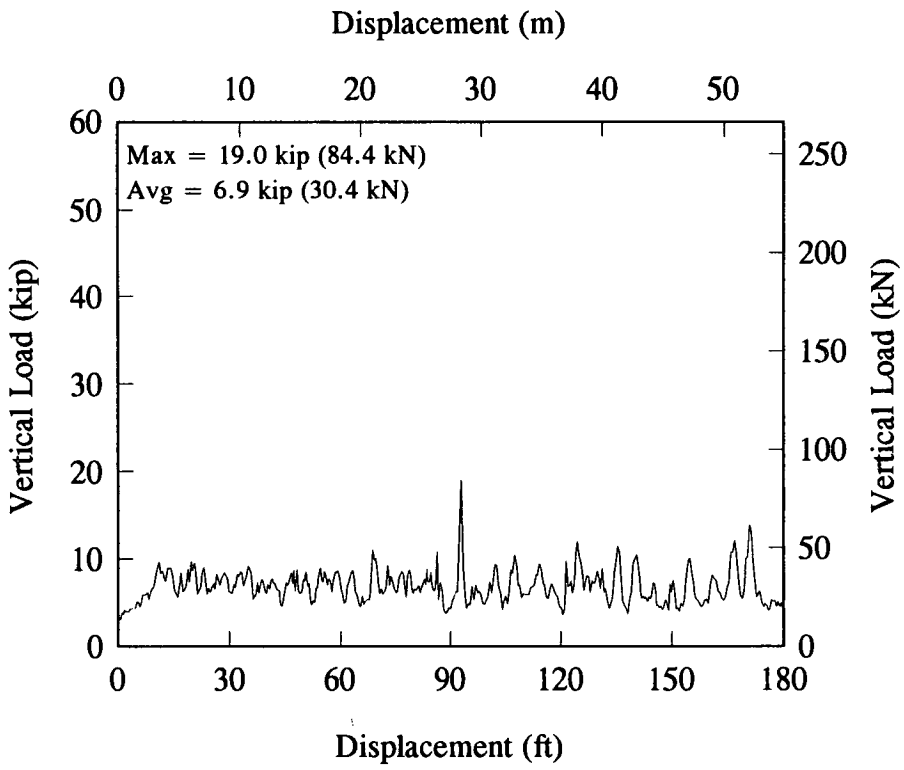

Figure 5.13. Horizontal and vertical force, cutting edge # 2, low pressure, 15° angle Test of Jan 28, 1992

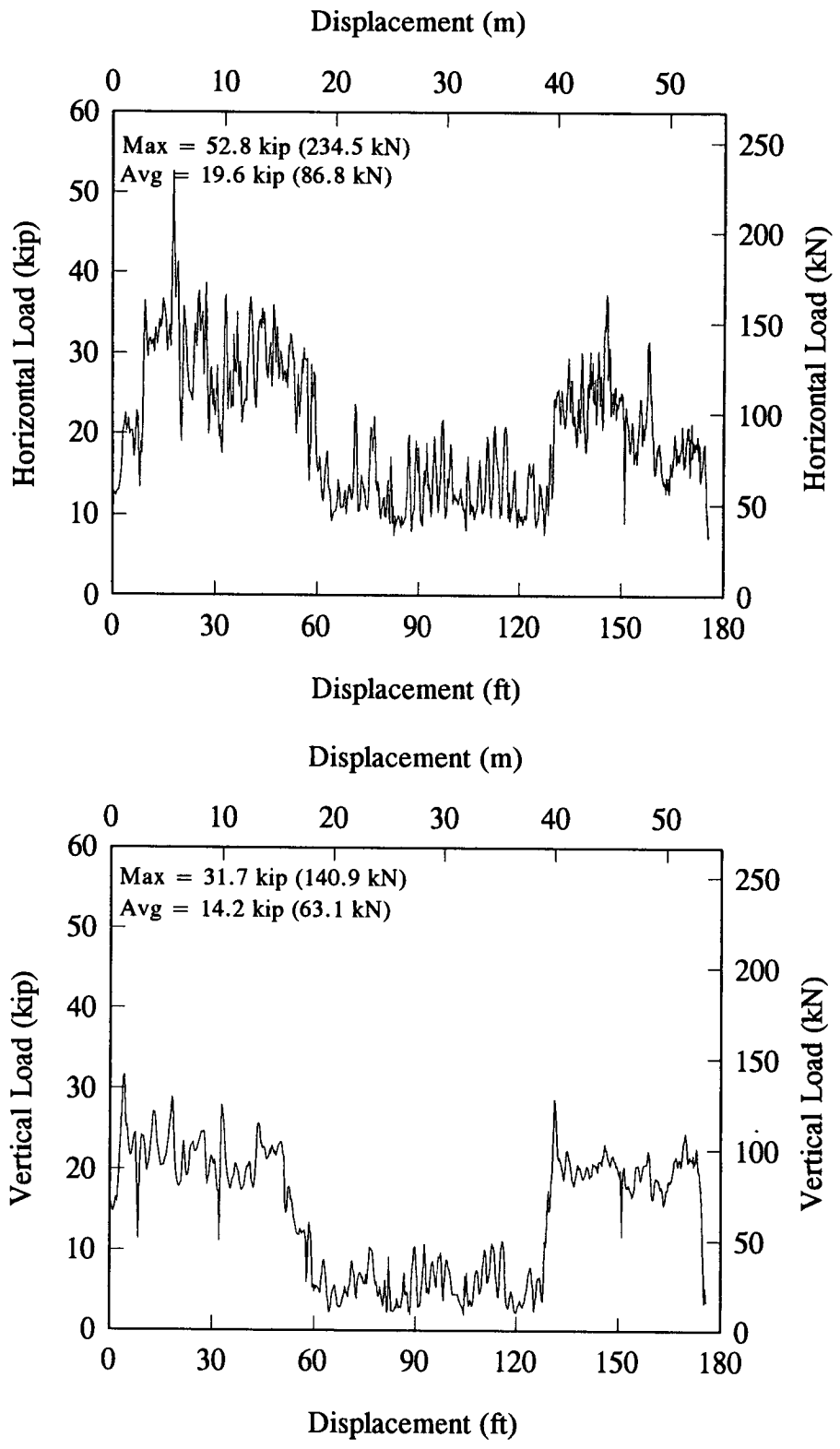

Figure 5.14. Horizontal and vertical force, cutting edge # 3, low pressure, 15° angle test of March 11, 1992

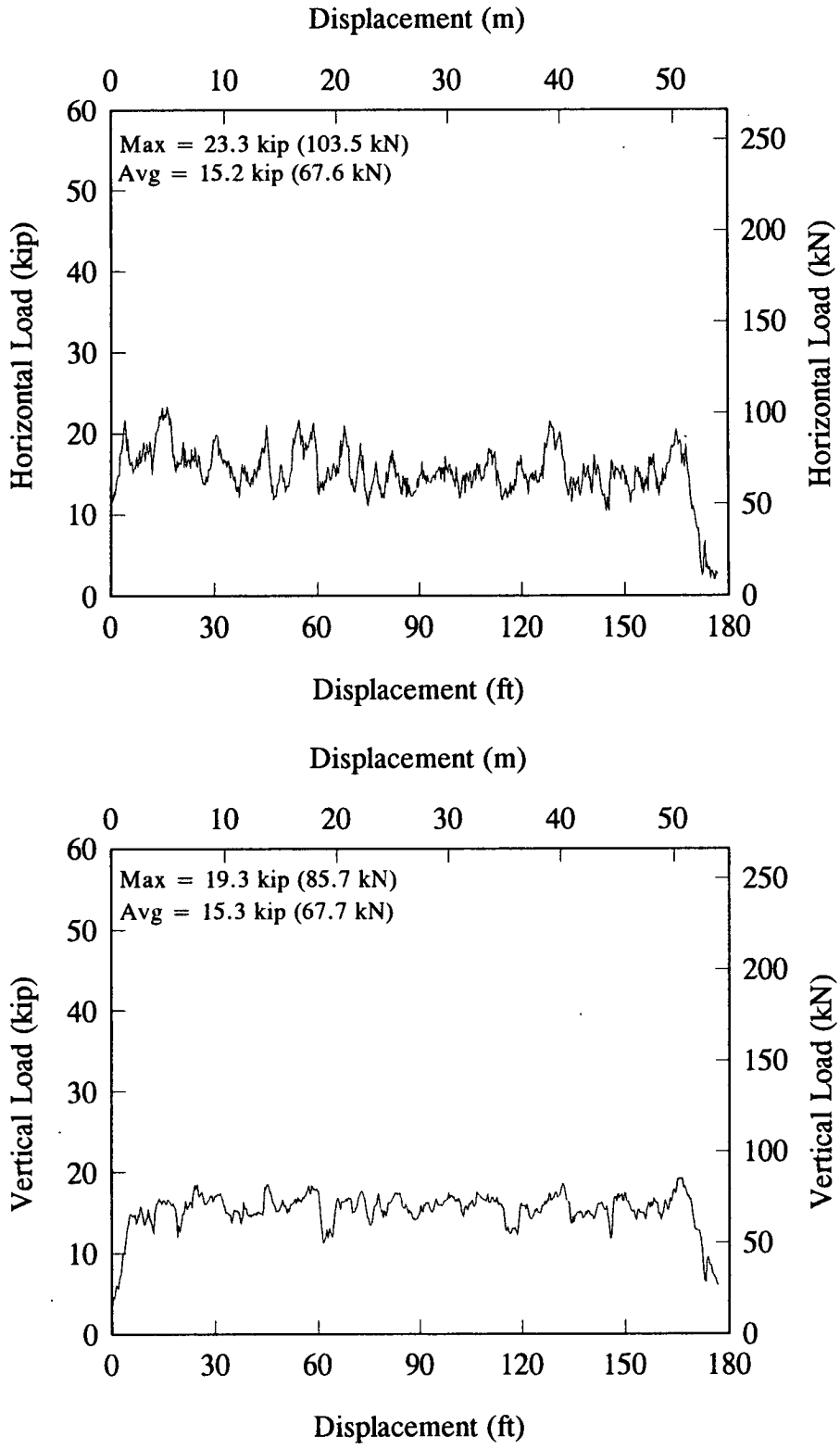

Figure 5.15. Horizontal and vertical force, cutting edge # 1, low pressure, 30° angle test of Dec 4, 1991

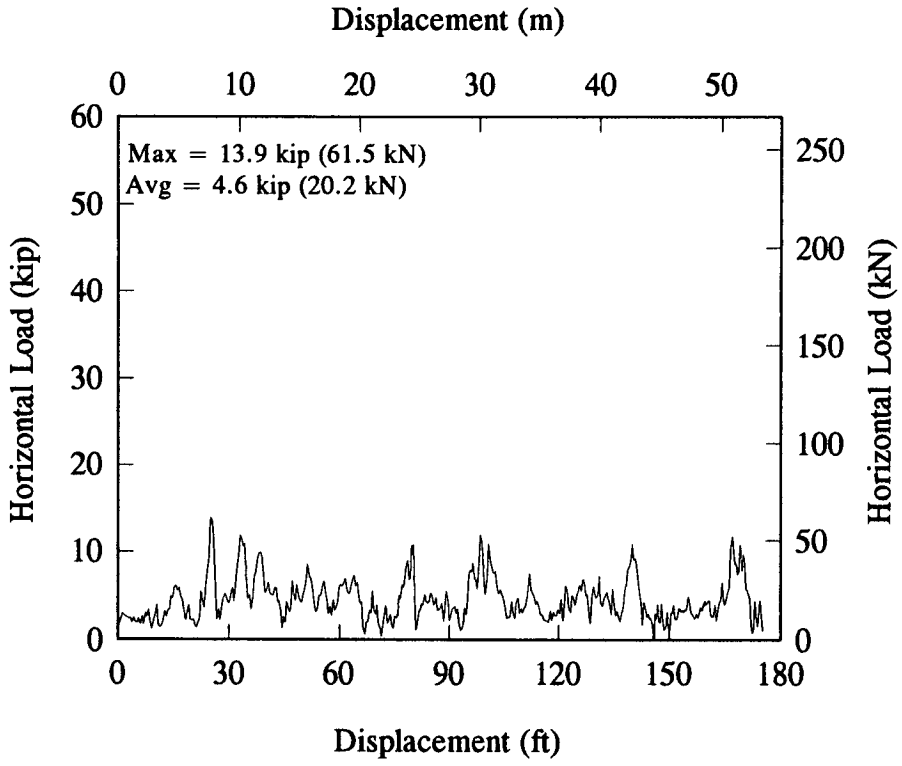

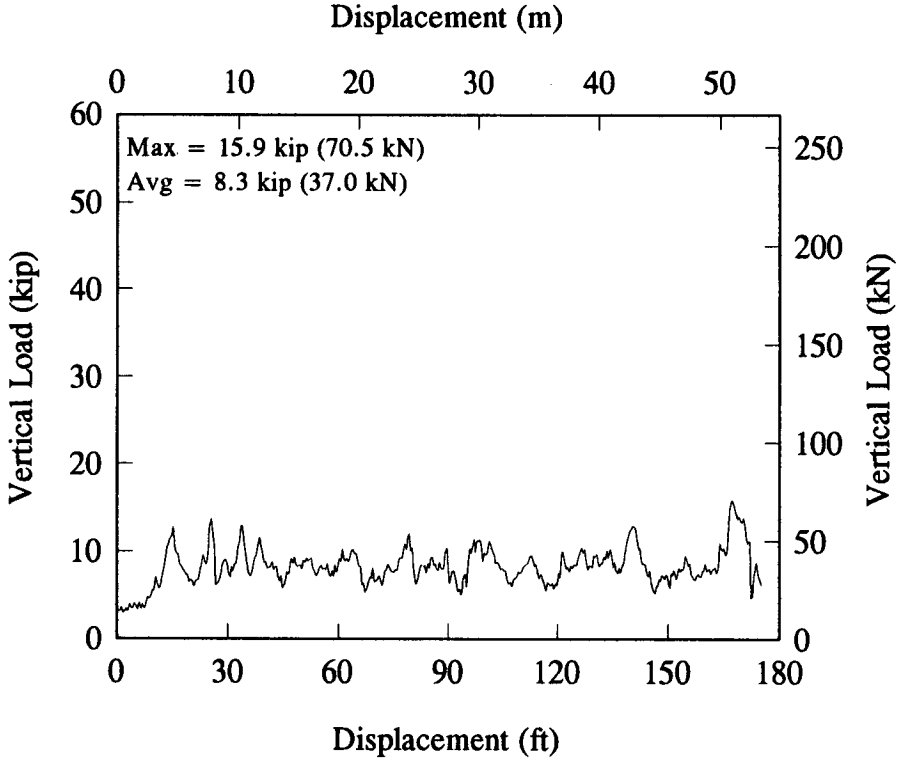

Figure 5.16. Horizontal and vertical force, cutting edge # 2, low pressure, 30° angle test of Jan 28, 1992

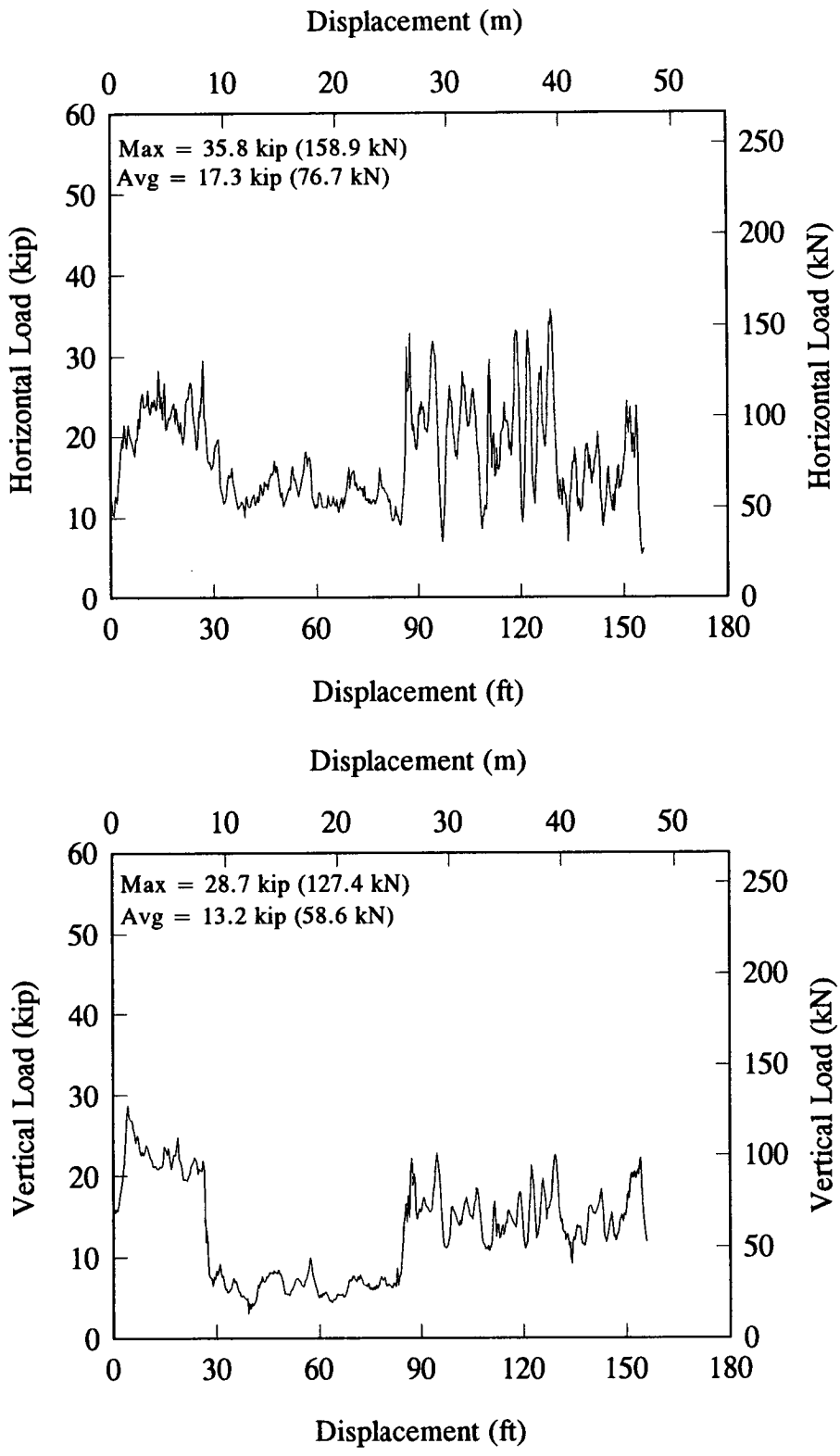

Figure 5.17. Horizontal and vertical force, cutting edge #3, low pressure, 30° angle test of March 13, 1992

6

Conclusions

As discussed previously in Section 2.3, not all possible combinations of tests in Table 2.1 have been performed. Ideally, all possible combinations of tests would be performed so that all interactions could be studied in detail. In this case, the number of test conditions would be over 2000, and three tests at each condition would require a total of over 6000 tests. The fractional factorial design was used (194 tests were conducted). These results show that rake angle has little effect on the scraping force. This effectively allows rake angle to be discarded in future tests as a variable, except for a few cases to ensure that no dependence has unexpectedly emerged.

The fact that the blade with the 0° clearance angle could not scrape the ice is also significant. Otherwise, there is no significant effect of clearance angle on the horizontal cutting force. Clearance angle has a strong effect on the download. Conversely, velocity has been observed to have a very clear effect on the scraping force. In future experiments this should continue to be a variable. The effect of temperature is less significant than the velocity effect.

Although the effect of flat width on the horizontal cutting force is not significant for widths less than 3/8 in. (0.95 cm), again a clear effect on the download was observed, which is consistent with the 0° clearance angle result. In many respects, these are the key results from the study. Their practical implication is that the current method of removing ice, which ensures a 0° clearance angle, must be changed to provide some clearance, either by designing new cutting edges or by changing scraping methods.

The prototype blade (blade # 3 in Chapter 5) designed with these results in mind was tested in the field, and found to perform significantly better than conventional blades. This tends to confirm the laboratory results and suggests further testing of the prototype blade in field situations is well warranted.

With regard to further work, there are clearly questions regarding the effects of pretreatment which need to be addressed. It would also be of value to simplify the current load-cell setup, perhaps by mounting the cutting edge to a three-axis load cell on the ram. The clearance angle and blade flat width effects would benefit from further study to determine at which

point these parameters cause significant changes in download on the cutting edge. There is a need to correlate the effect of the depth of cut through the ice with the horizontal force experienced by the cutting edge, starting in the laboratory and eventually going to the field. In addition, other, more complex geometries have not been tested yet, including serrated blades.

This study produced a prototype blade design, which was tested under idealized field conditions and performed significantly better than existing blades. The effects of various cutting-edge geometry parameters have been studied and some understanding has been forthcoming. A tentative model for how ice fractures when removed from pavement has been proposed. This model, and a number of other factors, require further laboratory study. The prototype cutting edge also requires more extensive field testing to assess its wear characteristics.

Appendix A

The Ice Cutting Equipment

A.1 The Hydraulic Ice-cutting Machine

The ice-cutting machine (Figures A.1 and A.2) incorporated a sled supported by four rails on which the cutting edge was mounted (Figures A.3 and A.4). The sled was accelerated by a hydraulic ram to the desired velocity of 20 mph (8.94 m/s) in about 15 in. (38.1 cm). The cutting edge scraped over a 12 in. x 4 in. x 8 in. (30.5 x 10.2 x 20.3 cm) pavement sample, mounted on rollers and anchored to two heavy fixed plates. A load cell on each plate (Figures A.1 and A.5) measured the loads on the pavement sample during the ice-scraping process.

A.1.1 The Hydraulic System

The schematic of the hydraulic system is shown in Figure A.6. A two-position, four-way directional control valve directs flow through selected passages. Four flow control valves (needle valves) control the rate of flow. Needle valves B and C were left fixed after adjustment for optimum flow characteristics. Needle valves A and D controlled the flow speed and were set fully open or fully closed, depending on the speed modes. Two speeds (high and low) were designed into the hydraulic system. For slow speed, flow control valve A was set fully open and flow was controlled by valve D. For high speed, valve D was set fully shut and flow was controlled by valve A.

In the initial status (power on and pump on), the four-way valve was in the neutral position (Figures A.6 and A.7) and the fluid flowed through the hydraulic pump to the relief valve and then back to the reservoir. For low speed, when the forward button on the control box was pushed, the four-way valve was shifted to the downward position (Figures A.7 and A.8) and fluid flowed through the four-way valve through pipe A to push the hydraulic ram forward. The fluid in the cylinder moved through pipe B and back to the reservoir. When the sled hit a trigger fixed on the machine (Figure A.9), the four-way valve was shifted back to the neutral position and the hydraulic ram was stopped. Similarly, when the retract button on the control box was pushed, the four-way valve was shifted to the upward position

(Figures A.7 and A.10) and fluid flowed across the four-way valve through pipe B to push the hydraulic ram backward. The fluid in pipe A then returned to the reservoir. Again when the sled hit a trigger fixed on the machine (Figure A.9), the four-way valve was shifted back to the neutral position and the hydraulic ram was stopped.

For high speed, when the forward button was pushed, fluid flowed through the four-way valve through pipe A to push the hydraulic ram forward (Figure A.11). The fluid in the cylinder moved through pipe B to the high-flow capacity valve (or "regen" valve) and back to the cylinder to increase the flow speed. When the sled hit a trigger, the hydraulic ram was stopped. The retract operation was the same as for slow speed.

The machine was inherently safer in the slow speed mode because the system stopped by terminating the flows in both pipe A and pipe B. In contrast, in the high speed mode, the sled kept moving forward after hitting the trigger, because the ram was stopped by the termination of the flow in pipe A only. For safety reasons, a shock absorber was installed at the end of the sled rail to stop the sled (Figure A.12). Tests with speeds below 8 mph (3.58 m/s) were executed in the slow speed mode, and those with higher speeds were run in the high speed mode.

In slow speed, the highest velocity of the sled was about 13 mph (5.81 m/s). In high speed, the machine could repeatedly achieve velocity of 20 mph (8.94 m/s) and occasionally up to 30 mph (13.4 m/s), though such speeds could not be attained repeatedly and appeared to result in excessive wear to the seals on the ram. An accumulator would be needed to obtain such higher speeds reliably and repeatedly, but was not installed.

A.1.2 Safety Features

In order to limit the system pressure, a relief valve was set in the hydraulic system to establish a working pressure. The adjustable spring (Figure A.6) was set to limit the maximum pressure that could be attained within the system. When the pressure exceeded the spring setting, the poppet was forced off its seat and excess fluid was bypassed to the reservoir. When system pressure dropped to or below the established set value, the valve automatically reseated. Typically, the relief valve was set at a pressure of 1,200 psi (8.27 MPa).

Two microswitches were set on either side of the door (Figure A.13) to ensure operator safety. Unless both doors were fully closed and locked, the hydraulic system was inoperative. The shock absorber used to stop the sled at the end of its run was also installed for safety reasons.

A.1.3 Machine Instrumentation

The primary instrumentation used in this study comprised five load cells, a velocity measuring device, and requisite signal conditioners.

A.1.3.1 Load Cells

Load cells were calibrated by applying known weights to each load cell and measuring the voltages. Experimental data, in general, have some noise, or error, the magnitude of which depends on the instrumentation and the arrangement employed for the measurements. Using the calibration curves above, a function was derived that provided a best fit to the given data by minimizing the difference between the given values of the dependent variable and those obtained from the approximating curve (i.e., by performing a linear regression on the data). The load cells had maximum load capabilities (equal in both tension and compression) of between 100 and 500 lb (45.4 and 227 kg), depending on the location at which the cell was to be used. The cells are excited by a 10 v power supply, and provide an output of $\pm$ 10 v from peak to peak.

A.1.3.2 Velocity Measuring

Velocity was calculated by differentiating the output from a position-measuring device with respect to time. Position was determined by means of two overlapping metal plates (Figure A.14). As the amount of overlap between the plates changed, the capacitance between the two plates changed, which in turn gave rise to a voltage change. This system had its own internal sampling rate somewhat slower than that used for the whole system, and thus the position voltage output was stepped (Figure 3.3). Nonetheless, a good measure of velocity was obtained with this system. Data were collected using a computer-based data acquisition system, using Labtech Notebook software, and a DAS 20 data acquisition card as well as a FORTRAN program (available upon request from TRB). The sampling rate was between 300 and 1000 Hz, depending on test velocity.

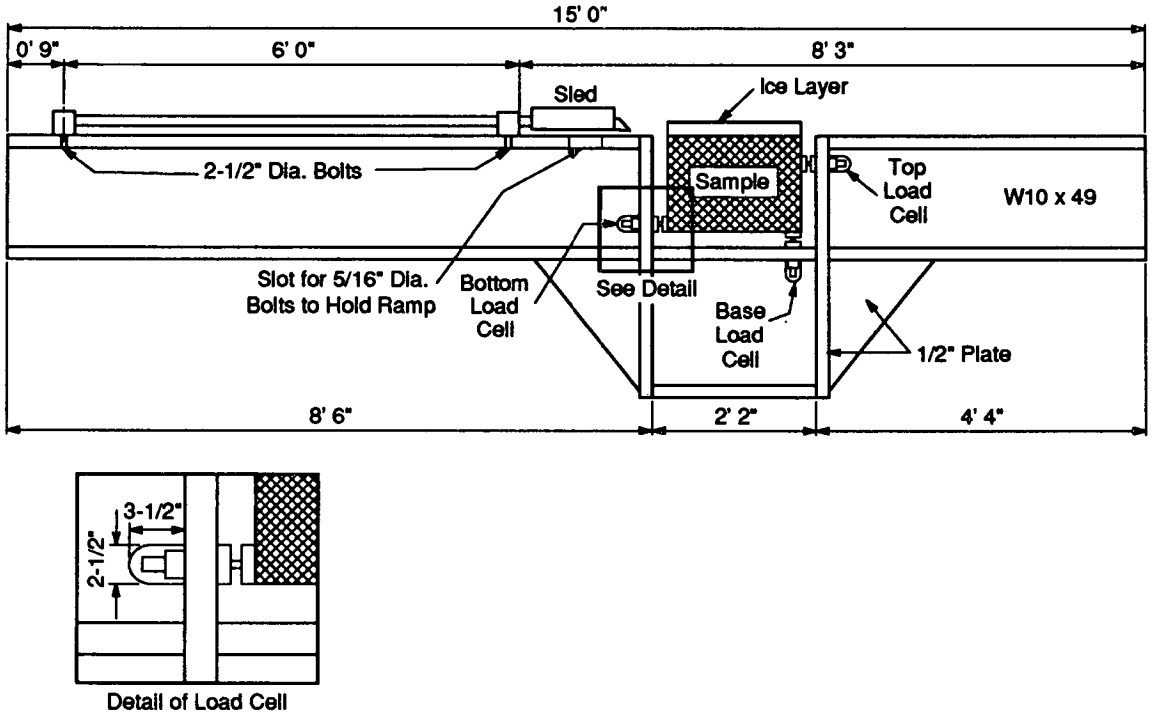

Figure A.1. Schematic of the ice-scraping machine

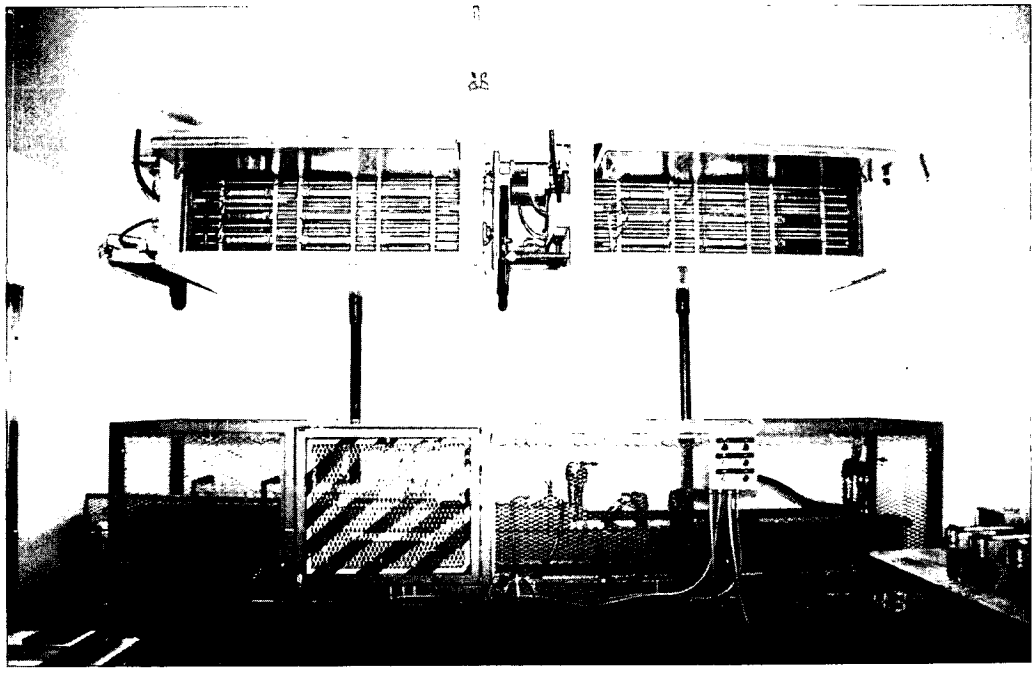

Figure A.2. Ice-scraping machine

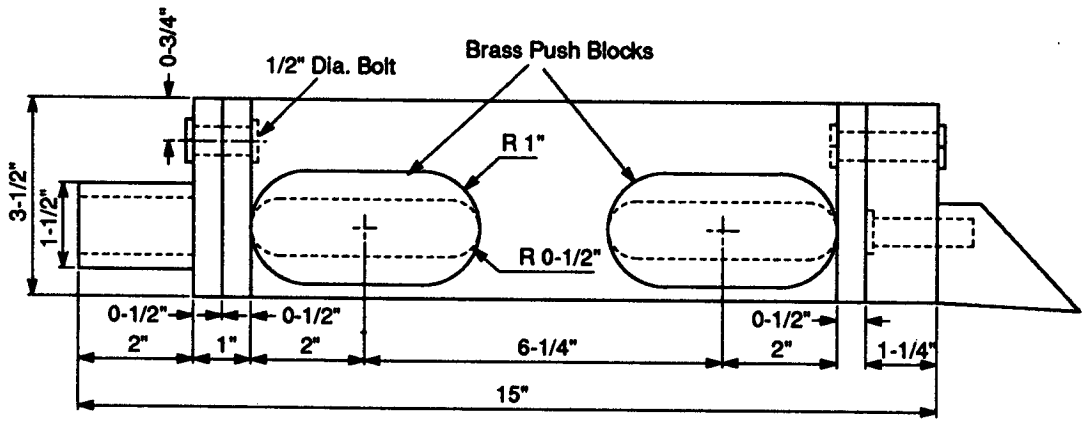

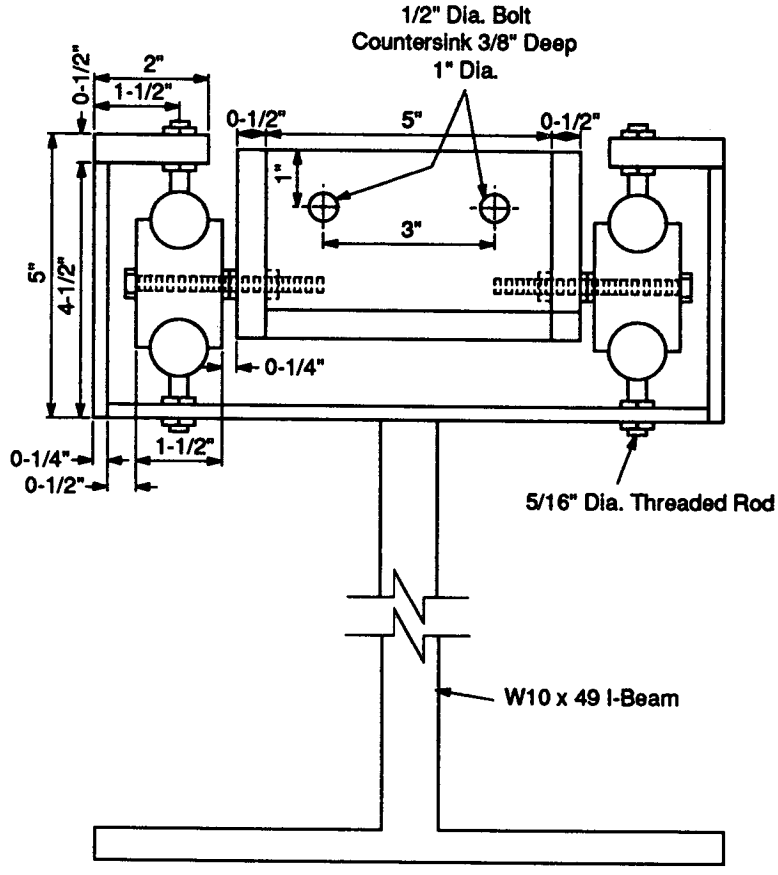

Figure A.3. Sled of the ice-cutting machine

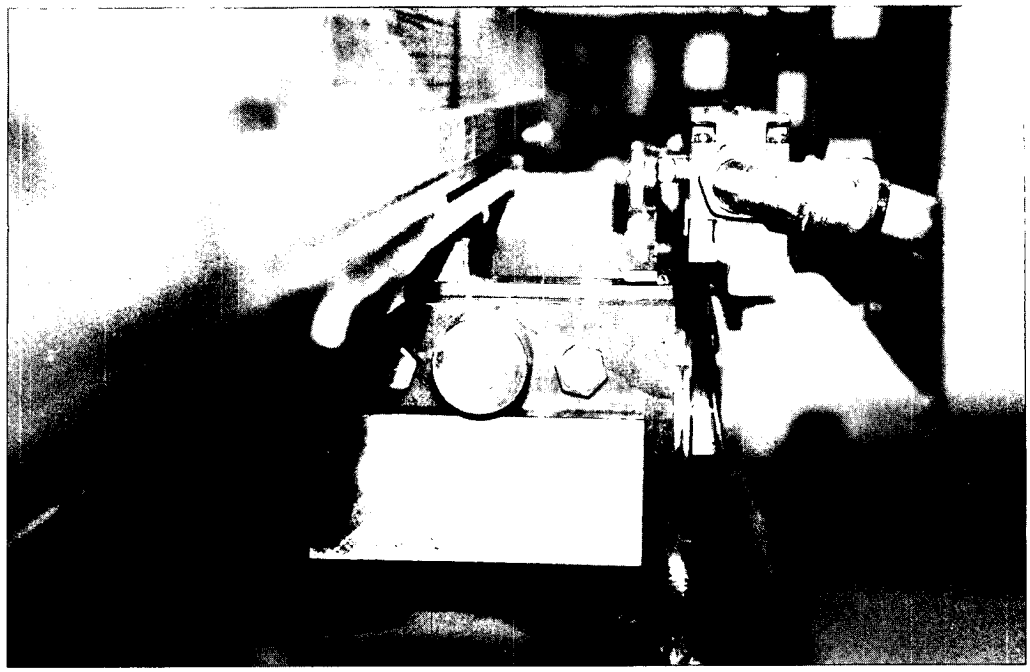

Figure A.4. Sled of the ice-scraping machine

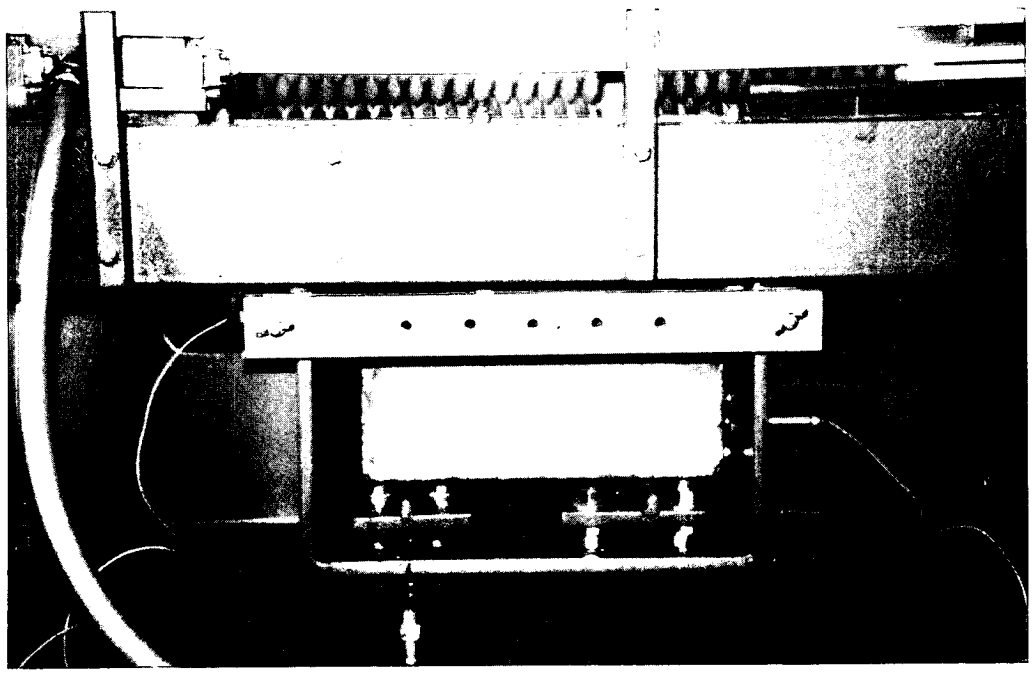

Figure A.5. Pavement sample anchored to two fixed plates

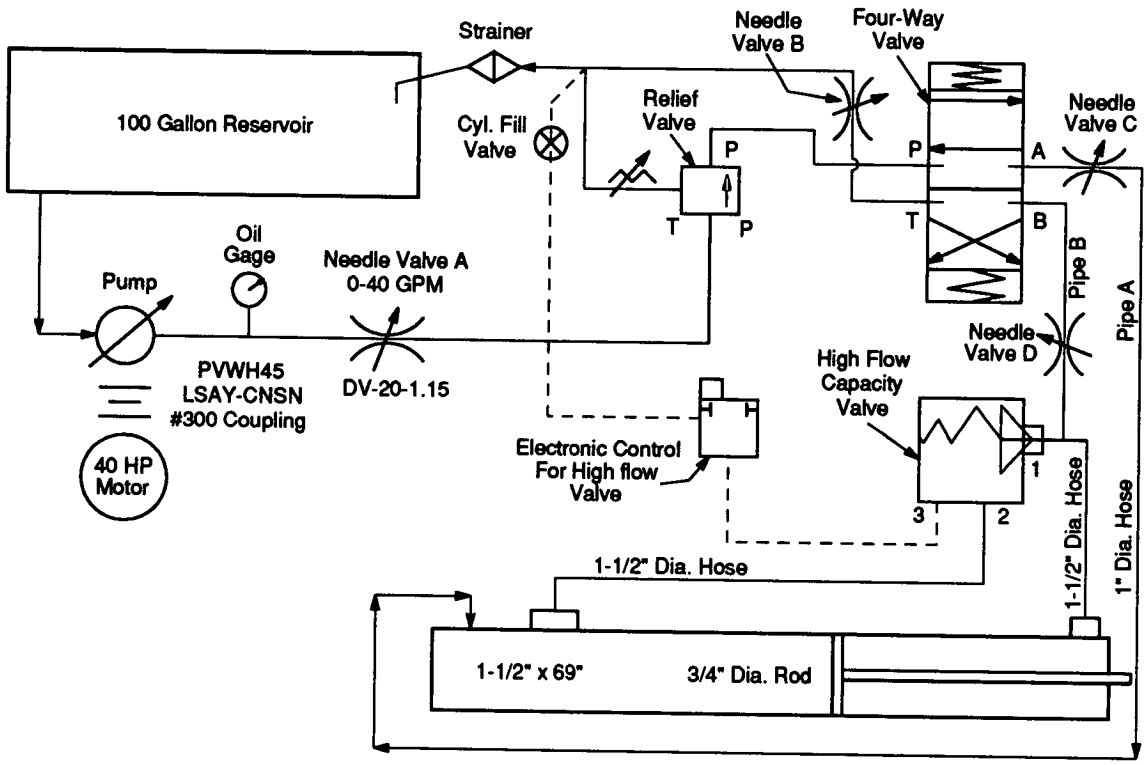

Figure A.6. Schematic of the hydraulic system

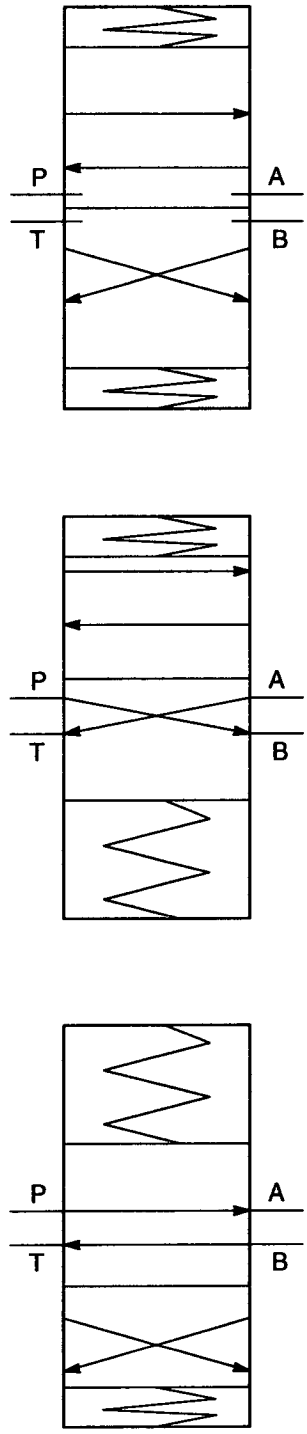

Figure A.7. The three positions of the four-way valve

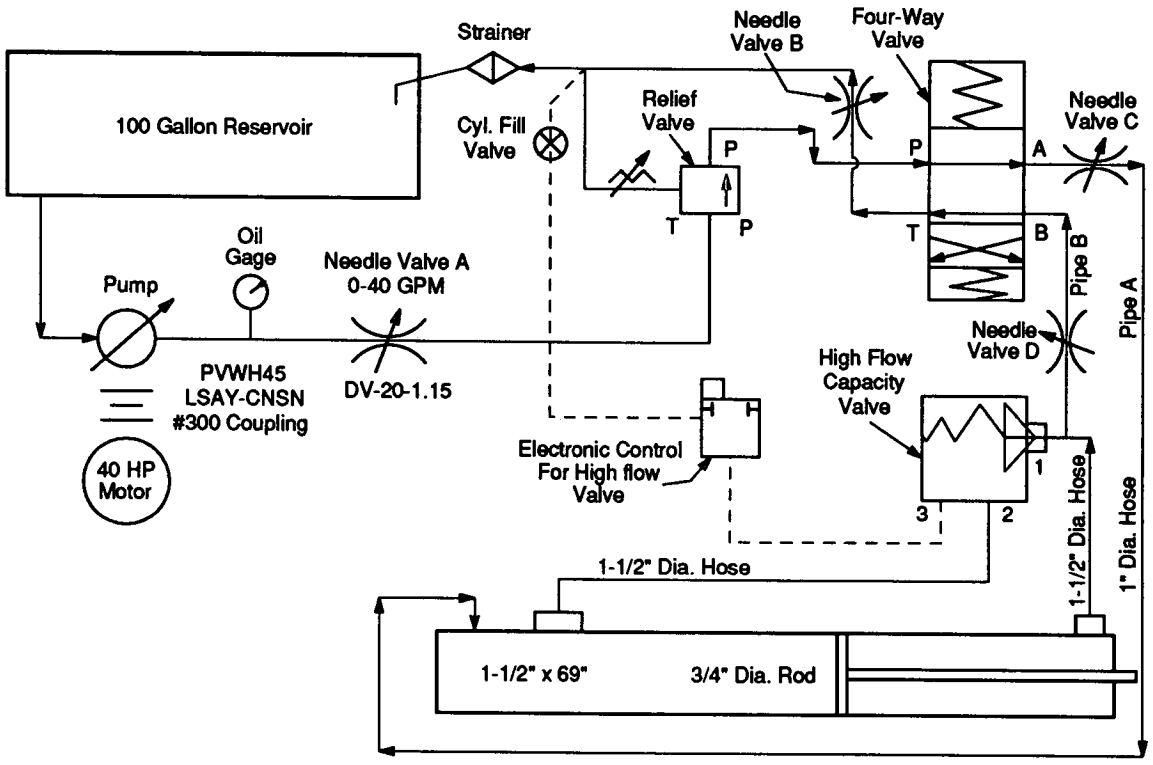

Figure A.8. Direction of fluid flow in slow speed mode when forward button was pushed

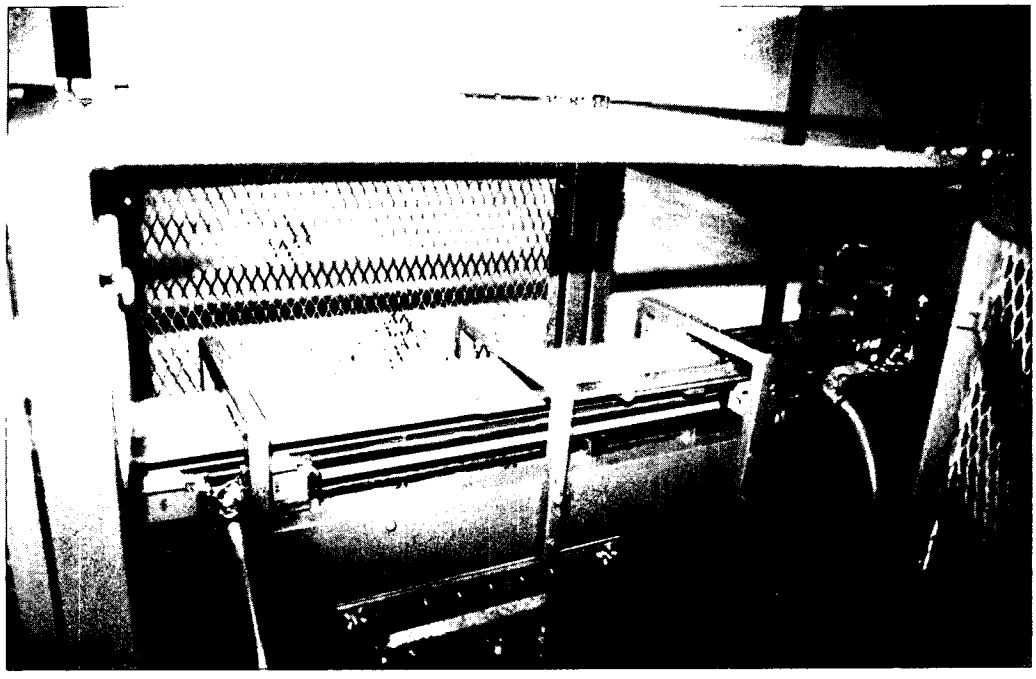

Figure A.9. Trigger on the ice-cutting machine

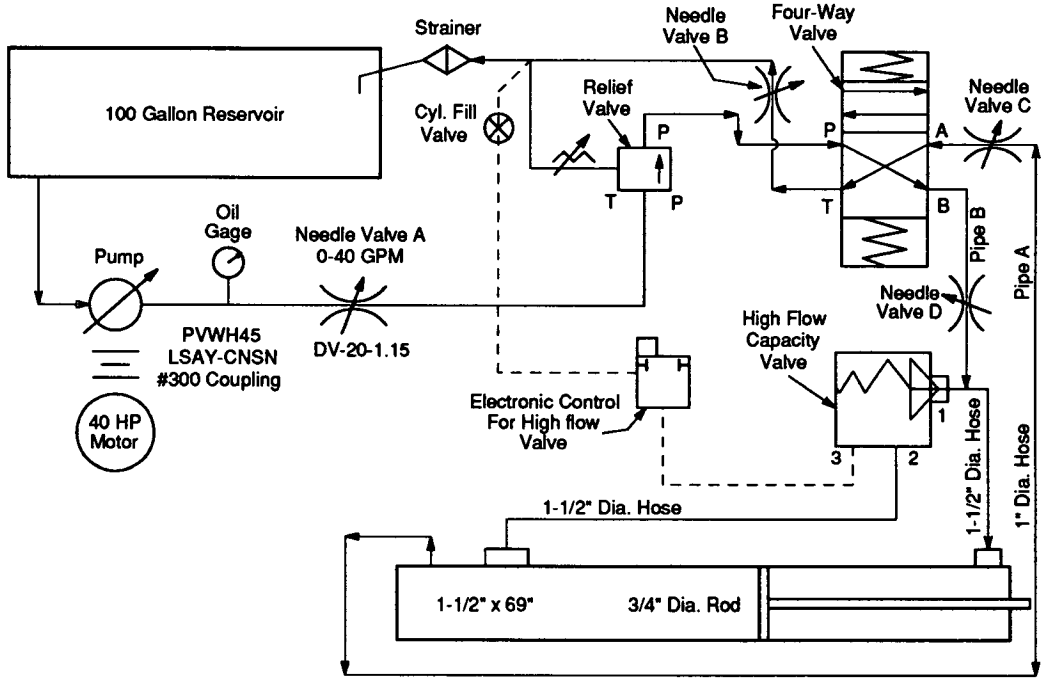

Figure A.10. Direction of fluid flow when retract button was pushed

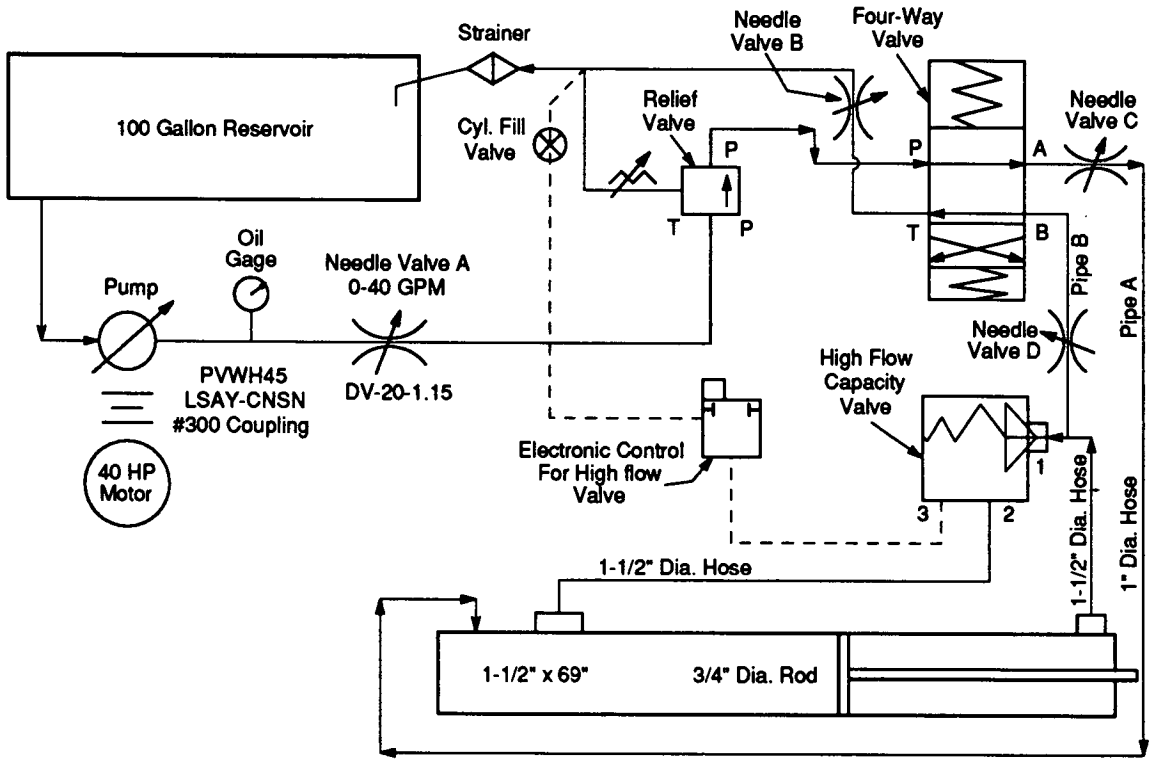

Figure A.11. Direction of flow in high speed mode when forward button was pushed

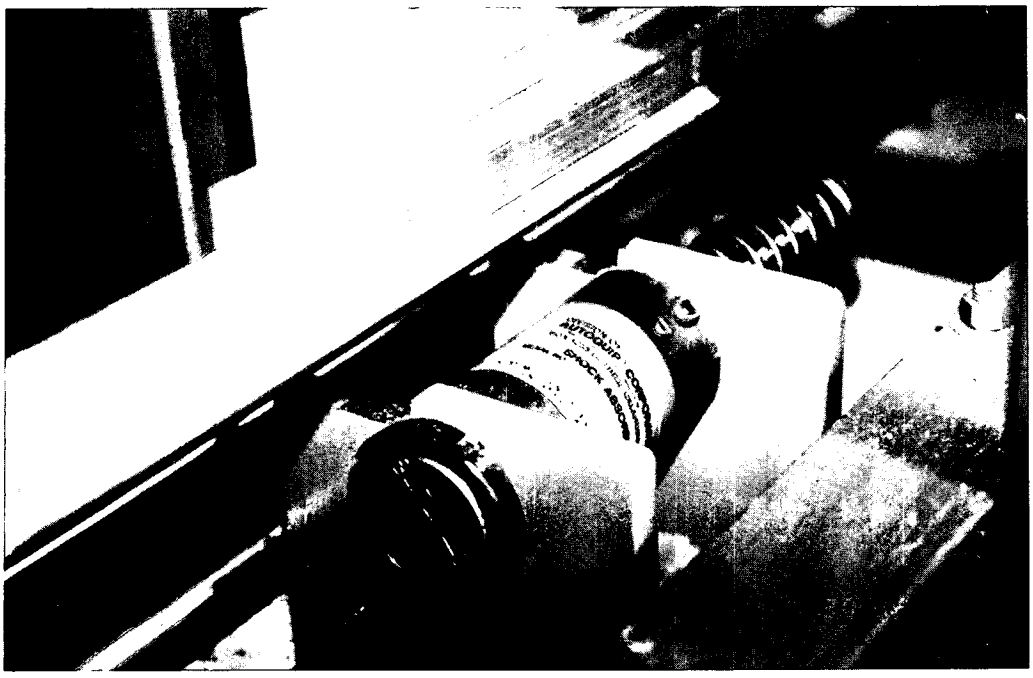

Figure A.12. Shock absorber

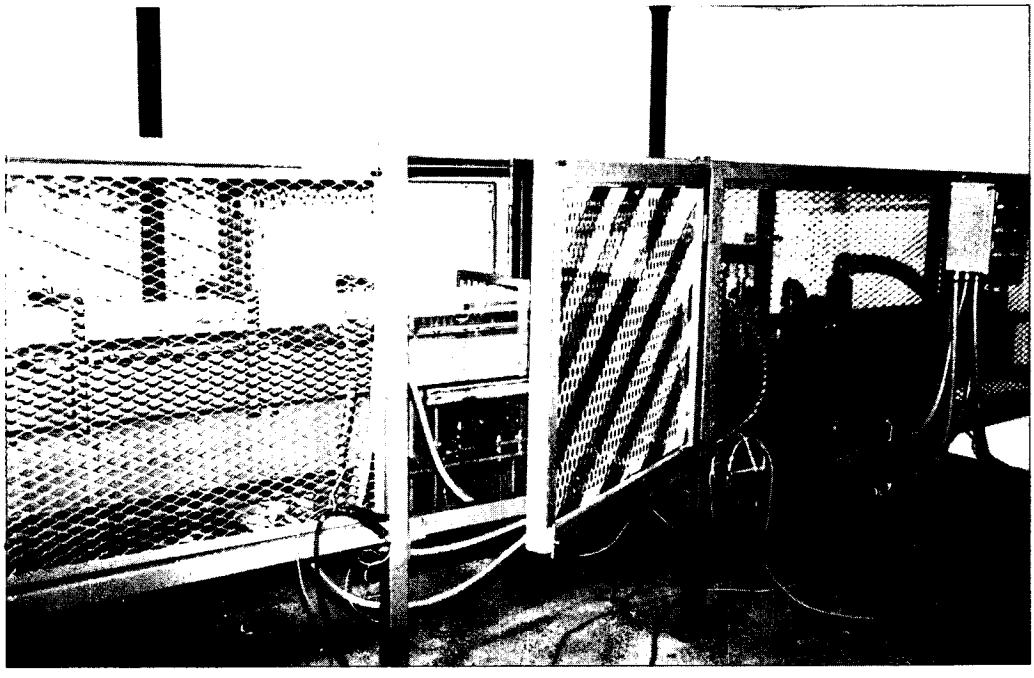

Figure A.13. Switches on the doors for safety

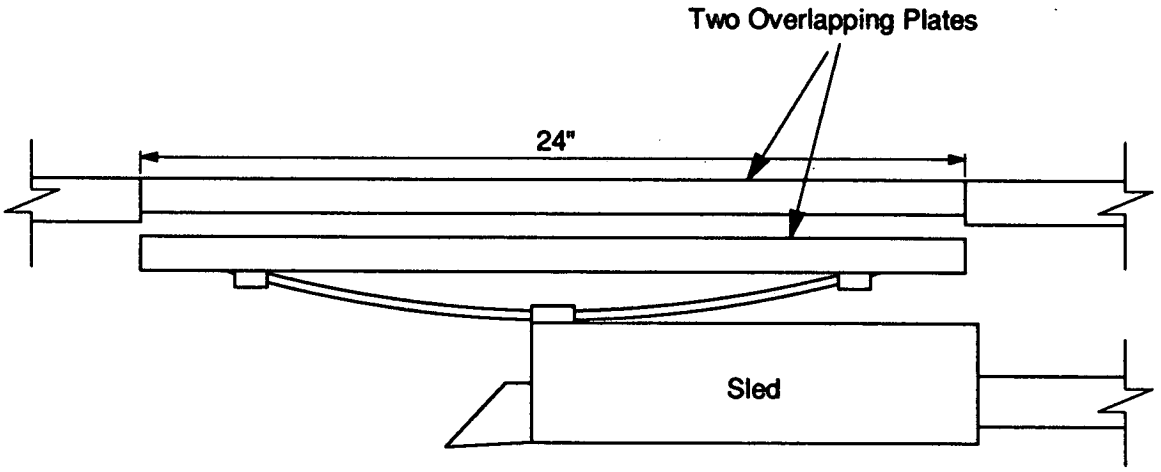

Figure A.14. Position measuring device

Appendix B

A Proof of the Validity of Ignoring Horizontal Translation During the Ice-Cutting Process

The motion of the pavement sample during ice-cutting was considered as a general plan motion, which could be treated as the sum of a translation and a rotation.
Denoting, respectively, by $d(A)_T$ and $d(A)_R$ the horizontal displacements of point A due to translation and to rotation, and by dA the total horizontal displacement, dA was written as:

$$\delta A = \delta(A)_T + \delta(A)_R \tag{B.1}$$

From Figure B.1, $d(A)_R$ could be expressed as:

$$\delta(A)_R = dl \times \delta\theta \sin\theta \tag{B.2}$$

where dl is the distance from A to B, $\delta\Theta$ the maximum rotation during the ice-cutting process, and Θ the acute angle between AB and the horizontal line.

Combining equations B.1 and B.2, dA could be written as:

$$\delta A - \delta(A)_T = dl \times \delta\theta \sin\theta \tag{B.3}$$

Similarly, the total horizontal displacement of point C, δC, due to translation and rotation could be expressed as:

$$\delta C-\delta(C)_T=d2\times\delta\theta\sin\phi \tag{B.4}$$

where $d2$ is the distance from B to C, ϕ the acute angle between BC and the horizontal line. Because the pavement sample was considered as a rigid body in this study, the horizontal displacement due to translation for all points (including A, B, and C) in the pavement sample during ice-scraping process were the same, i.e.:

$$\delta(A)_T=\delta(C)_T=\delta_T \tag{B.5}$$

where d_T is the horizontal displacement of the pavement sample due to translation.

Letting $dA = \beta dC$, and substituting into equations B.3 and B.4, δA and δC could be solved as a function of δ_T.

$$\delta A=(1+\frac{(1-\beta)d1\sin\theta}{\beta d2\sin\phi-d1\sin\theta})\delta_T \tag{B.6}$$

$$\delta C=(1+\frac{(1-\beta)d2\sin\phi}{\beta d2\sin\phi-d1\sin\theta})\delta_T \tag{B.7}$$

It should be noted that the second terms in the parentheses of equations B.6 and B.7 are the ratios of $\delta(A)_R$ to $\delta(A)_T$ and $\delta(C)_R$ to $\delta(C)_T$ and that those ratios are functions of β. Denoting, respectively, by $R_A(\beta)$ and $R_C(\beta)$ the ratios of $\delta(A)_R$ to $\delta(A)_T$ and $\delta(C)_R$ to $\delta(C)_T$, $R_A(\beta)$ and $R_C(\beta)$ can be expressed as:

$$R_A(\beta)=\frac{(1-\beta)d1\sin\theta}{\beta d2\sin\phi-d1\sin\theta} \tag{B.8}$$

$$R_C(\beta)=\frac{(1-\beta)d2\sin\phi}{\beta d2\sin\phi-d1\sin\theta} \tag{B.9}$$

The values of $d1$, $d2$, ϕ, and Θ are given below.

$$\theta=\tan^{-1}\frac{5.25}{1.875} \tag{B.10}$$

$$\phi=\tan^{-1}\frac{1.375}{10.125} \tag{B.11}$$

$$d1=\sqrt{5.25^2+1.875^2} \tag{B.12}$$

$$d2=\sqrt{10.125^2+1.375^2} \tag{B.13}$$

The parameter β was determined from experiment and its value for base line tests was about 5. For the case $\beta = 5$, the result of $R_A(5)$ being 12.92, the effect of the translation to the total displacement was less than 10%, which was small enough to be ignored.

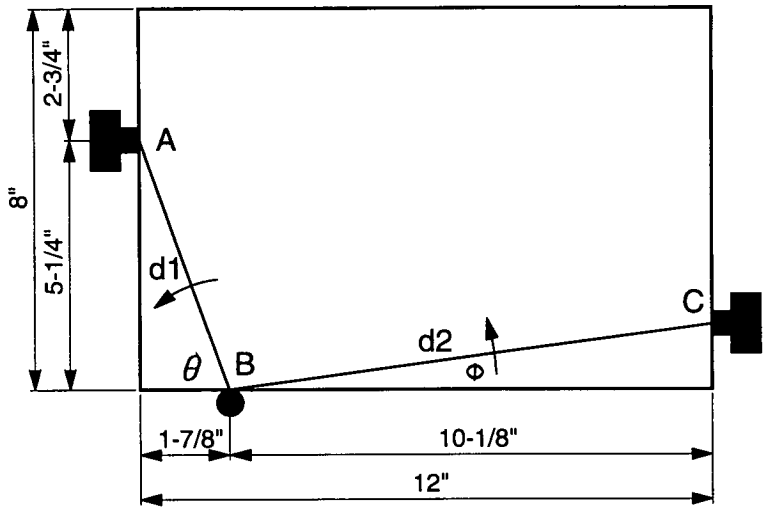

Figure B.1. Geometry of the pavement sample

Appendix C

Experimental Results

The data in the following table are presented with the following key:

Cut:	The mean cutting force experienced (lb)
Rake:	The rake angle of the cutting edge (°)
Clr:	The clearance angle of the blade (°)
Attk:	The attack angle of the blade (°)
Bld:	The width of the blade (in.)
Flat:	The width of the flat on the blade (in.)
Speed:	The cutting speed (mph)
Temp:	The test temperature (°C)
Pre:	The amount of salt applied pretest (g)
BSE1:	The load from the first base load cell (lb)
BSE2:	The load from the second base load cell (lb)
SIDE:	The sideways load (lb)
Test:	The ID # of the test being reported

Table C.1. Experimental results

Scrp	Rake	Clr	Attk	Bld	Flat	Speed	Temp	Pre	BSE1	BSE2	SIDE	Test
27.63	30	5	0	5	0	5	-5	0	x	x	x	23
26.46	30	5	0	5	0	5	-5	0	x	x	x	28
26.74	0	5	0	5	0	5	-5	0	x	x	x	30
31.72	0	5	0	5	0	5	-5	0	x	x	x	33
36.20	0	5	0	5	0	5	-5	0	x	x	x	34
25.53	0	5	0	5	0	5	-5	0	x	x	x	39
26.87	45	5	0	5	0	5	-5	0	x	x	x	50
29.17	45	5	0	5	0	5	-5	0	x	x	x	51
24.59	45	5	0	5	0	5	-5	0	x	x	x	52
26.97	45	5	0	5	0	5	-5	0	x	x	x	53
25.05	45	5	0	5	0	5	-5	0	x	x	x	54
25.38	45	5	0	5	0	5	-5	0	x	x	x	56
20.37	45	5	0	5	0	10	-5	0	x	x	x	59
20.47	45	5	0	5	0	10	-5	0	x	x	x	60
20.09	45	5	0	5	0	10	-5	0	x	x	x	61
22.53	45	5	0	5	0	10	-5	0	x	x	x	62
23.66	45	5	0	5	0	10	-5	0	x	x	x	63
24.33	45	5	0	5	0	10	-5	0	x	x	x	64
24.01	45	5	0	5	0	10	-5	0	x	x	x	65
18.88	30	5	0	5	0	10	-5	0	x	x	x	66
18.40	30	5	0	5	0	10	-5	0	x	x	x	68
18.31	30	5	0	5	0	10	-5	0	x	x	x	69
17.84	30	5	0	5	0	10	-5	0	x	x	x	70
19.90	0	5	0	5	0	10	-5	0	x	x	x	73
21.71	0	5	0	5	0	10	-5	0	x	x	x	74
22.72	0	5	0	5	0	10	-5	0	x	x	x	75
22.69	0	5	0	5	0	10	-5	0	x	x	x	76

Table C.1. Continued

Scrp	Rake	Clr	Attk	Bld	Flat	Speed	Temp	Pre	BSE1	BSE2	SIDE	Test
20.28	0	5	0	5	0	10	-5	0	x	x	x	78
18.97	0	5	0	5	0	10	-5	0	x	x	x	79
17.46	15	5	0	5	0	10	-5	0	x	x	x	80
17.09	15	5	0	5	0	10	-5	0	x	x	x	81
17.27	15	5	0	5	0	10	-5	0	x	x	x	82
20.20	15	5	0	5	0	10	-5	0	x	x	x	83
17.46	15	5	0	5	0	10	-5	0	x	x	x	84
17.46	15	5	0	5	0	10	-5	0	x	x	x	85
17.27	15	5	0	5	0	10	-5	0	x	x	x	87
17.09	15	5	0	5	0	10	-5	0	x	x	x	91
19.36	15	5	0	5	0	10	-5	0	x	x	x	92
17.39	15	5	0	5	0	10	-5	0	x	x	x	93
21.94	45	5	0	5	0	10	-5	0	x	x	x	117
28.06	45	5	0	5	0	5	-5	0	x	x	x	118
18.81	30	10	0	5	0	10	-5	0	x	x	x	120
18.02	30	10	0	5	0	10	-5	0	x	x	x	121
18.86	30	10	0	5	0	10	-5	0	x	x	x	122
19.23	30	5	0	5	0	10	-5	0	x	x	x	124
17.16	30	2	0	5	0	10	-5	0	x	x	x	126
17.21	30	2	0	5	0	10	-5	0	x	x	x	127
17.27	30	2	0	5	0	10	-5	0	x	x	x	128
18.72	30	5	0	5	0	10	-5	0	x	x	x	132
17.86	30	5	0	5	0	10	-5	0	x	x	x	133
22.11	45	5	0	5	0	10	-5	0	x	x	x	135
17.18	45	5	0	5	0	15	-20	0	x	x	x	138
17.01	45	5	0	5	0	15	-20	0	x	x	x	139
20.18	45	5	0	5	0	15	-20	0	x	x	x	140
17.15	30	5	0	5	0	15	-20	0	x	x	x	141

Table C.1. Continued

Scrp	Rake	Clr	Attk	Bld	Flat	Speed	Temp	Pre	BSE1	BSE2	SIDE	Test
17.10	30	5	0	5	0	15	-20	0	x	x	x	142
17.18	30	5	0	5	0	15	-20	0	x	x	x	143
16.92	15	5	0	5	0	15	-20	0	x	x	x	144
17.50	15	5	0	5	0	15	-20	0	x	x	x	145
17.04	15	5	0	5	0	15	-20	0	x	x	x	146
17.11	0	5	0	5	0	15	-20	0	x	x	x	147
17.47	0	5	0	5	0	15	-20	0	x	x	x	148
17.16	0	5	0	5	0	15	-20	0	x	x	x	149
17.10	0	5	0	5	0	20	-5	0	x	x	x	150
17.20	0	5	0	5	0	20	-5	0	x	x	x	151
17.95	0	5	0	5	0	20	-5	0	x	x	x	152
17.33	15	5	0	5	0	20	-5	0	x	x	x	153
17.75	15	5	0	5	0	20	-5	0	x	x	x	154
17.30	15	5	0	5	0	20	-5	0	x	x	x	155
17.23	30	5	0	5	0	20	-5	0	x	x	x	156
17.10	30	5	0	5	0	20	-5	0	x	x	x	157
17.19	30	5	0	5	0	20	-5	0	x	x	x	158
18.12	45	5	0	5	0	20	-5	0	x	x	x	159
17.59	45	5	0	5	0	20	-5	0	x	x	x	160
17.16	45	5	0	5	0	20	-5	0	x	x	x	161
18.27	30	5	0	5	0.125	10	-5	0	x	x	x	162
17.28	30	5	0	5	0.125	10	-5	0	x	x	x	163
17.55	30	5	0	5	0.125	10	-5	0	x	x	x	164
17.27	30	5	0	5	0.125	10	-5	0	x	x	x	165
17.46	30	5	0	5	0.375	10	-5	0	x	x	x	169
17.43	30	5	0	5	0.375	10	-5	0	x	x	x	170
17.37	30	5	0	5	0.375	10	-5	0	x	x	x	171
18.32	30	5	0	3	0	10	-5	0	x	x	x	172

Table C.1. Continued

Scrp	Rake	Clr	Attk	Bld	Flat	Speed	Temp	Pre	BSE1	BSE2	SIDE	Test
17.64	30	5	0	3	0	10	-5	0	x	x	x	173
18.11	30	5	0	3	0	10	-5	0	x	x	x	174
17.62	30	5	0	5	0.375	10	-5	0	x	x	x	175
17.15	30	5	0	5	0.375	10	-5	0	x	x	x	176
17.24	30	5	0	5	0.25	10	-5	0	x	x	x	178
17.29	30	5	0	5	0.25	10	-5	0	x	x	x	179
17.24	30	5	0	5	0.25	10	-5	0	x	x	x	180
17.37	30	5	0	5	0.25	15	-5	0	x	x	x	181
17.59	30	5	0	5	0.25	15	-5	0	x	x	x	182
17.21	30	5	0	5	0.25	15	-5	0	x	x	x	183
17.13	30	5	0	5	0.125	15	-5	0	x	x	x	184
17.31	30	5	0	5	0.125	15	-5	0	x	x	x	185
17.26	30	5	0	5	0.125	15	-5	0	x	x	x	186
17.59	30	5	0	5	0.375	15	-5	0	x	x	x	187
17.31	30	5	0	5	0.375	15	-5	0	x	x	x	188
17.98	30	5	0	5	0.375	15	-5	0	x	x	x	189
17.83	30	5	0	3	0	15	-5	0	x	x	x	190
17.98	30	5	0	3	0	15	-5	0	x	x	x	191
18.08	30	5	0	3	0	15	-5	0	x	x	x	192
19.10	30	5	0	5	0	15	-5	0	x	x	x	193
18.90	30	5	0	5	0	15	-5	0	x	x	x	194
18.74	30	5	0	5	0	15	-5	0	x	x	x	195
17.55	30	5	0	5	0.125	15	-5	0	7.04	20.08	x	196
17.44	30	5	0	5	0.125	15	-5	0	8.59	16.07	x	197
17.14	30	5	0	5	0.125	15	-5	0	6.52	4.02	x	198
17.29	30	5	0	5	0.25	15	-5	0	22.26	15.04	x	199
17.81	30	5	0	5	0.25	15	-5	0	4.55	17.61	x	200
17.30	30	5	0	5	0.25	15	-5	0	8.59	25.65	x	201

Table C.1. Continued

Scrp	Rake	Clr	Attk	Bld	Flat	Speed	Temp	Pre	BSE1	BSE2	SIDE	Test
17.14	30	5	0	5	0.375	15	-5	0	1.97	5.56	x	204
18.26	30	5	0	3	0	15	-5	0	0	0.51	x	206
17.55	30	5	0	3	0	15	-5	0	0	0	x	207
18.07	30	5	0	3	0	15	-5	0	0.52	0.51	x	208
18.07	30	5	35	5	0	10	-5	0	0.52	1.55	x	209
18.31	30	5	35	5	0	10	-5	0	1.47	5.97	x	210
17.42	30	5	35	5	0	10	-5	0	1.97	9.06	x	211
18.51	30	5	35	5	0	10	-5	0	1.45	5.97	x	212
17.10	30	5	0	5	0	15	-5	0	0	0.51	x	213
17.44	30	5	0	5	0	15	-5	0	2.48	0.42	x	214
17.39	30	5	0	5	0	15	-5	0	1.55	2.47	x	215
18.04	30	5	35	5	0	10	-5	0	1.04	8.55	0.94	216
17.16	30	5	35	5	0	10	-5	0	0.52	4.53	0.78	217
17.32	30	5	35	5	0	10	-5	0	0.93	7.52	3.68	218
18.43	30	5	35	5	0	10	-5	0	1.04	8.55	0	219
17.12	30	5	35	5	0	10	-5	0	0	2.06	1.58	220
17.41	30	5	35	5	0	10	-5	0	1.04	9.58	11.52	221
17.80	30	5	0	5	0	10	-20	0.06	2.48	5.56	x	222
17.37	30	5	0	5	0	10	-20	0.06	8.59	7.52	x	223
17.68	30	5	0	5	0	10	-20	0.06	12.63	11.54	x	224
18.48	30	5	0	5	0	10	-20	0.12	4.55	8.55	x	225
17.94	30	5	0	5	0	10	-20	0.12	6.11	9.06	x	226
17.94	30	5	0	5	0	10	-20	0.12	6.11	8.55	x	227
19.37	30	5	0	5	0	10	-20	0.24	3.52	1.55	x	228
19.37	30	5	0	5	0	10	-20	0.24	3.0	1.55	x	229
19.39	30	5	0	5	0	10	-20	0.24	3.0	1.55	x	230
18.36	30	5	0	5	0	10	-20	0.48	2.48	5.05	x	231
18.15	30	5	0	5	0	10	-20	0.48	14.7	18.13	x	232

Table C.1. Continued

Scrp	Rake	Clr	Attk	Bld	Flat	Speed	Temp	Pre	BSE1	BSE2	SIDE	Test
17.90	30	5	0	5	0	10	-20	0.48	6.11	5.97	x	233
17.77	30	5	0	5	0	10	-20	0.96	4.04	10.09	x	234
18.11	30	5	0	5	0	10	-20	0.96	9.63	10.51	x	235
18.10	30	5	0	5	0	10	-20	0.96	9.63	10.51	x	236
18.44	30	5	0	5	0	10	-5	0.06	1.45	2.99	x	237
17.40	30	5	0	5	0	10	-5	0.06	0.52	3.50	x	238
17.23	30	5	0	5	0	10	-5	0.12	1.55	2.99	x	240
19.58	30	5	0	5	0	10	-5	0.12	0	0	x	241
17.10	30	5	0	5	0	10	-5	0.12	1.04	2.99	x	242
17.79	30	5	0	5	0	10	-5	0.24	1.55	4.53	x	243
17.62	30	5	0	5	0	10	-5	0.24	5.07	8.55	x	244
17.59	30	5	0	5	0	10	-5	0.24	5.18	3.5	x	245
17.61	30	5	0	5	0	10	-5	0.48	2.48	2.99	x	246
18.01	30	5	0	5	0	10	-5	0.48	0.93	5.97	x	247
18.55	30	5	0	5	0	10	-5	0.48	7.56	2.47	x	248
18.86	30	5	0	5	0	10	-5	0.96	2.48	5.05	x	249
17.75	30	5	0	5	0	10	-5	0.96	7.04	3.5	x	250
17.12	30	5	0	5	0	10	-5	0.96	0	0	x	251
18.11	30	10	0	5	0	15	-5	0	0.52	0	x	253
18.43	30	10	0	5	0	15	-5	0	0.52	0	x	254
18.41	30	10	0	5	0	15	-5	0	0.52	0	x	255
17.38	30	10	0	5	0	15	-5	0	0.52	0	x	256
17.55	30	10	0	5	0	15	-5	0	0.52	0	x	257
17.15	30	10	0	5	0	15	-5	0	0.52	0	x	258
18.59	30	10	0	5	0	15	-5	0	0.52	0	x	261
27.29	30	10	0	5	0	15	-5	0	0.52	0	x	262
23.21	30	10	0	5	0	15	-5	0	0.52	0	x	263

Bibliography

American Public Works Association Research Foundation.(1970). "Vehicle Corrosion Caused by De-icing Salts", American Public Works Association Research Foundation, special report #34. Chicago Illinois.

Atkinson, K.E. (1989). An Introduction to Numerical Analysis. New York: Wiley.

Beer, F.P. and E. Russell (1984). Vector Mechanics for Engineers. New York: McGraw-Hill.

Blackburn, R.R. and A.D. ST. John (1977). Physical Alternatives to Chemicals for Highway Deicing, Vol. I: Phase I Results-Development of Concepts, Interim Report No. 1, May. Contract No. DOT-FH-11-9126, Midwest Research Institute.

Dickinson, W.E. (1968). "Snow and Ice Control-A Critical Look at Its Critics." Highway Research Record Number 227. Highway Research Board, National Research Council, Washington, D.C.

Donald, M.M. and M.R. Eigerman (1972). A Search: New Technology for Pavement Snow and Ice Control. EPA-R2-72-125. Office of Research and Monitoring, U.S. Environmental Protection Agency, Washington, D.C.

Dongarra, J., J. Bunch, C. Moler, and G. Stewart (1979). Linpack User's Guide. Philadelphia: SIAM Publishers.

Dudley, A.P. and J. Pippenger (1987). Basic Fluid Power, 2nd edition. New York: Prentice-Hall Inc.

EPA (1991). Guidance Document for Selecting Antiskid Materials Applied to Ice - and Snow - Covered Roadways. EPA - 450/3 - 90 -007.

Fromm, H.J. (1968). "Corrosion of Auto-Body Steel and the Effects of Inhibited De-icing Salts." Highway Research Record Number 227. Highway Research Board, National Research Council, Washington, D.C.

Hoye, W.N. (1961). "Runway Ice Removal." Canadian Aeronautical Journal. Vol. 7, No. 4.

Huang, N.C. (1981). "Mechanics of Ice-Lifting From a Flat Surface Through Penetration With a Sharp Blade." Transaction of the ASME. Vol. 48, pp 936-942.

Iowa Department of Transportation (1984). "Standard Specifications for Highway and Bridge Construction." p 224.

Jaluria, Yogesh (1988). Computer Methods for Engineering. Massachusetts: Allyn and Bacon.

Montgomery, D.C. (1984). Design and Analysis of Experiments. New York: John P. Wiley & Sons, Inc.

Nevada DOT (1990). "Roadside Erosion and Revegetation Needs Associated with the Use of De-icing Salt within the Lake Tahoe Basin, Prepared for Nevada Department of Transportation."

Nixon, W.A., D. DeJong and C.-H. Chung (1993). "Low rate scraping tests to remove ice from pavements", IIHR report forthcoming.

Shames, I.R. and C.L. Dym (1985). Energy and Finite Element Methods in Structural Mechanics. New York: McGraw-Hill.

Transportation Research Board (1991). Highway Deicing: Comparing Salt and Calcium Magnesium Acetate, Special Report 235. National Research Council, Washington DC.

Highway Operations Advisory Committee

Chairman
Dean M. Testa
Kansas Department of Transportation

Vice-Chairman
Clayton L. Sullivan
Idaho Transportation Department

Members
Ross B. Dindio
The Commonwealth of Massachusetts Highway Department

Richard L. Hanneman
Salt Institute

Rita Knorr
American Public Works Association

David A. Kuemmel
Marquette University

Magdalena M. Majesky
Ministry of Transportation of Ontario

Michael J. Markow
Cambridge Systematics, Inc.

Gerald M. Miner
Consultant

Richard J. Nelson
Nevada Department of Transportation

Rodney A. Pletan
Minnesota Department of Transportation

Michel P. Ray
The World Bank

Michael M. Ryan
Pennsylvania Department of Transportation

Bo H. Simonsson
Swedish Road and Traffic Research Institute

Leland Smithson
Iowa Department of Transportation

Arlen T. Swenson
John Deere

Anwar E.Z. Wissa
Ardman and Associates, Inc.

John P. Zaniewski
Arizona State University

Liaisons

Ted Ferragut
Federal Highway Administration

Joseph J. Lasek
Federal Highway Administration

Frank N. Lisle
Transportation Research Board

Byron N. Lord
Federal Highway Administration

Mohamed Y. Shahin
U.S. Army Corps of Engineers

Harry Siedentopf
Federal Aviation Administration

Jesse Story
Federal Highway Administration

7/23/93

Expert Task Group

Duane E. Amsler, Sr.
New York State Department of Transportation

Walter G. Bartel
Oregon Department of Transportation

Paul R. Camp
University of Maine

Brian H. Chollar
Federal Highway Administration

Frank N. Lisle
Transportation Research Board

Paul F. Miller
Michigan Department of Transportation

Rodney Pletan
Minnesota Department of Transportation

Donald M. Walker
University of Wisconsin at Madison

Anwar E.Z. Wissa
Ardaman and Associates

7/22/93